A Fourier Transforms and the Delta Function

Ultrasonic NDE involves the propagation of short, transient pulses. A pulser, for example, generates voltage pulses that drive an ultrasonic transducer. That transducer transforms the electrical pulses into mechanical pulses that travel as waves and are converted back into electrical pulses at the receiving transducer. The received electrical pulses are then often displayed on an oscilloscope as a voltage versus time signal. In order to model ultrasonic systems ultimately we must be able to describe such transient behavior. If we directly simulate these time varying signals this is referred to as modeling in the *time domain*. However, it is often more convenient to describe the ultrasonic system and its components in terms of their *frequency domain* response, which is obtained by applying the Fourier transform to the time domain signals. It is always possible to recover the time domain signal from its Fourier transform through an inverse Fourier transform, so that working in the frequency domain does not imply a loss of information. In this Appendix we will describe some of the basic properties of Fourier and inverse Fourier transforms and we will show how these transforms can be implemented numerically with Fast Fourier Transform (FFT) algorithms. We will also introduce the delta function and its Fourier transform since that function plays a key role in modeling linear systems, as shown in Appendix C.

A.1 The Fourier Transform and Its Inverse

Consider a pulse, $v(t)$, a signal that is a function of the time, t. The Fourier transform of $v(t)$, $V(f)$, is given by [A.1], [A.3],

$$V(f) = \int_{-\infty}^{+\infty} v(t) \exp(2\pi i f t)\, dt \,. \tag{A.1}$$

The variable f is the frequency. Typically in ultrasonic NDE problems f is given in MHz (millions of cycles/sec), where 1 cycle/sec = 1 Hz, and the

corresponding time, t, is given in microseconds. Although we integrate over all times in Eq. (A.1), most ultrasonic pulses are non-zero only over a finite time interval. The inverse Fourier transform, which allows us to obtain $v(t)$, is

$$v(t) = \int_{-\infty}^{+\infty} V(f) \exp(-2\pi i f t)\, df \,. \tag{A.2}$$

Equation (A.2) shows that in order to recover $v(t)$ one must integrate over both negative and positive frequencies. If the time domain function is real, however, it can be shown that its Fourier transform satisfies $V(-f) = V^*(f)$, where $(\ )^*$ denotes the complex conjugate. Thus, the negative frequency components can be obtained from the positive components and in this sense they are redundant. Later, we will show how to recover the time domain signal, $v(t)$, from only the positive frequency components.

There are other definitions of the Fourier transform and its inverse that are used in the literature so that one must be careful when comparing results, using Eqs. (A.1) and (A.2), to similar results from other authors. We will use the definitions of Eqs. (A.1) and (A.2) exclusively in this work, or their equivalent definitions given by

$$\begin{aligned} V(\omega) &= \int_{-\infty}^{+\infty} v(t) \exp(i\omega t)\, dt \\ v(t) &= \frac{1}{2\pi} \int_{-\infty}^{+\infty} V(\omega) \exp(-i\omega t)\, d\omega \end{aligned} \tag{A.3}$$

in terms of the *circular frequency*, ω, as measured in rad/sec, where $\omega = 2\pi f$. Since $v(t)$ and $V(f)$ can be obtained from each other, we can write this relationship as $v(t) \leftrightarrow V(f)$. In a similar fashion we write the corresponding relationships for a time shifted or differentiated signal as:

$$\begin{aligned} v(t - t_0) &\leftrightarrow \exp(2\pi i f t_0) V(f) \\ \frac{dv}{dt} &\leftrightarrow -2\pi i f V(f). \end{aligned} \tag{A.4}$$

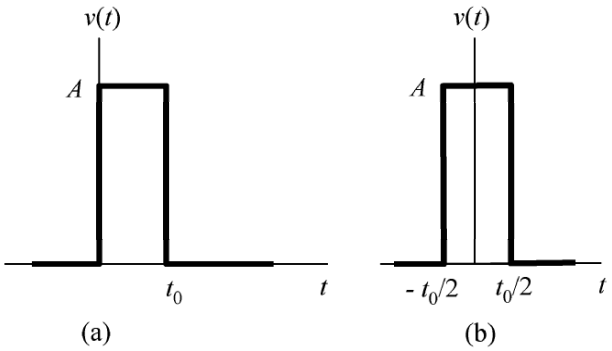

Fig. A.1. (a) An example of a simple "box" time domain function and **(b)** the same function shifted in time.

For many other relationships see [A.3] or [Fundamentals].

As an example of a Fourier transform, consider the simple "box" function shown in Fig. A.1 (a). The Fourier transform of this function can be obtained analytically as

$$\begin{aligned} V(f) &= \int_0^{t_0} A\exp(2\pi ift)\,dt \\ &= \frac{At_0\exp(i\pi ft_o)\sin(\pi ft_o)}{\pi ft_0}. \end{aligned} \tag{A.5}$$

The magnitude of this complex Fourier transform is shown in Fig. A.2 (a) and its phase is given in Fig. A.2 (b). The phase plot shows periodic jumps of π radians corresponding to the sign changes at these points of the $\sin(\pi f t_0)$ function. Otherwise the phase of the Fourier transform is a linearly increasing function of frequency due to the $\exp(i\pi f t_0)$ term in Eq. (A.5). If we shift this box function to the left by $t_0/2$, the shifting property of the Fourier transform given in Eq. (A.4) shows that for this symmetrical function (see Fig. A.1 (b)) we instead obtain a purely real Fourier transform given by

$$V(f) = \frac{At_0\sin(\pi ft_o)}{\pi ft_0}$$

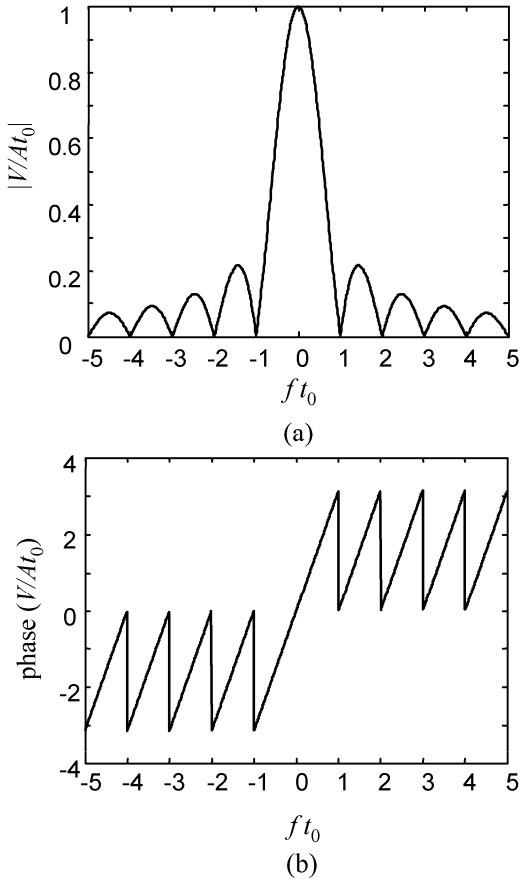

Fig. A.2. (a) The magnitude of the Fourier transform of the "box" function of Fig. A.1 (a) and **(b)** the phase of this transform.

As another example of the use of the Fourier transform, consider the following time function and its Fourier transform (also called the *Fourier spectrum* of the signal):

$$\begin{aligned} v(t) &= \cos(2\pi f_c t)\exp\left[-t^2/4A^2\right] \\ V(f) &= A\sqrt{\pi}\left\{\exp\left[-4\pi^2A^2(f-f_c)^2\right]+\exp\left[-4\pi^2A^2(f+f_c)^2\right]\right\}. \end{aligned} \tag{A.6}$$

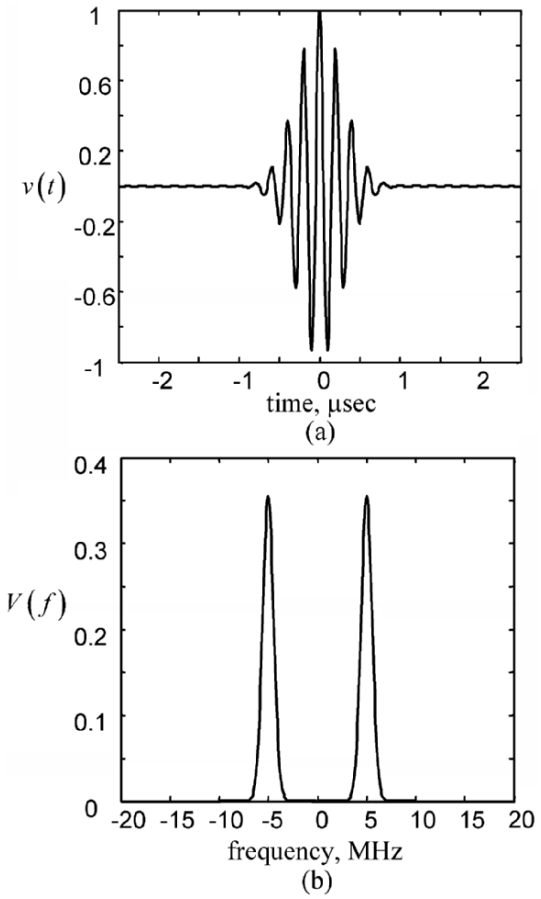

Fig. A.3. (a) The time domain function in Eq. (A.6) and **(b)** the Fourier transform of Eq. (A.6) for $A = 0.2$, $f_c = 5$ MHz.

These functions are shown in Fig. A.3 for $A = 0.2$ and $f_c = 5$ MHz. The time domain function is a transient that has a shape typical of many ultrasonic signals. The frequency domain spectrum is a pair of Gaussians whose maxima are located at the frequencies f_c and $-f_c$. The constant A controls both the amplitude of these Gaussians and their widths. Normally, one specifies the characteristics of a frequency domain spectrum as shown in Fig. A.4 by a *center frequency*, f_c, defined as the frequency at which the maximum frequency domain response occurs, and a width of the spectrum. One measure of the width that is commonly used in ultrasonic NDE is the

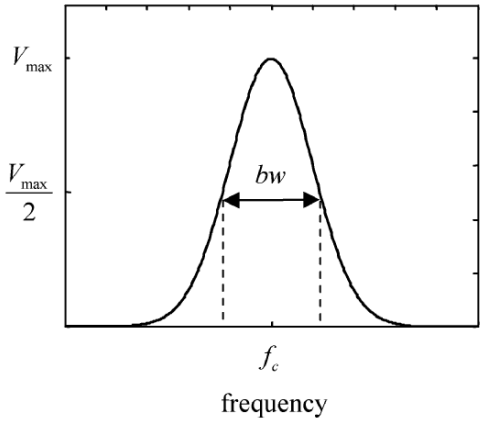

Fig. A.4. Definition of the center frequency, f_c, and −6 dB bandwidth, *bw*, of a spectrum.

−6 *dB bandwidth*, *bw*, which is defined in this case as the width of the Gaussian when the amplitude drops 6 decibels (*dB*) below its maximum at $f = f_c$, as shown in Fig. A.4. Note that an amplitude ratio V/V_r is defined in terms of decibels (*dB*) as

$$\frac{V}{V_r}(dB) = 20\log_{10}\left(\frac{V}{V_r}\right). \tag{A.7}$$

Since $20\log_{10}(1/2) = -6.02\,dB$, at −6 *dB* the amplitude has been reduced to a value of approximately one half that of the reference value, where in our case the reference value is the maximum at $f = f_c$. The parameter, *A*, can be shown to be related to the –6 *dB* bandwidth, *bw*, by the relation $A = \sqrt{\ln 2}/(\pi bw)$. Figure A.5 shows the functions in Eq. (A.6) for a center frequency $f_c = 10$ MHz and for various choices of the −6 *dB* bandwidth, *bw*. It can be seen that a narrow bandwidth results in a wide pulse with significant ringing in the time domain signal while a wide bandwidth generates a very short pulse with little ringing. Ultrasonic transducers with a large bandwidth are called wide-band, high resolution transducers because the short time domain signals they generate allow one to resolve signals that are near to one another. Ultrasonic transducers with

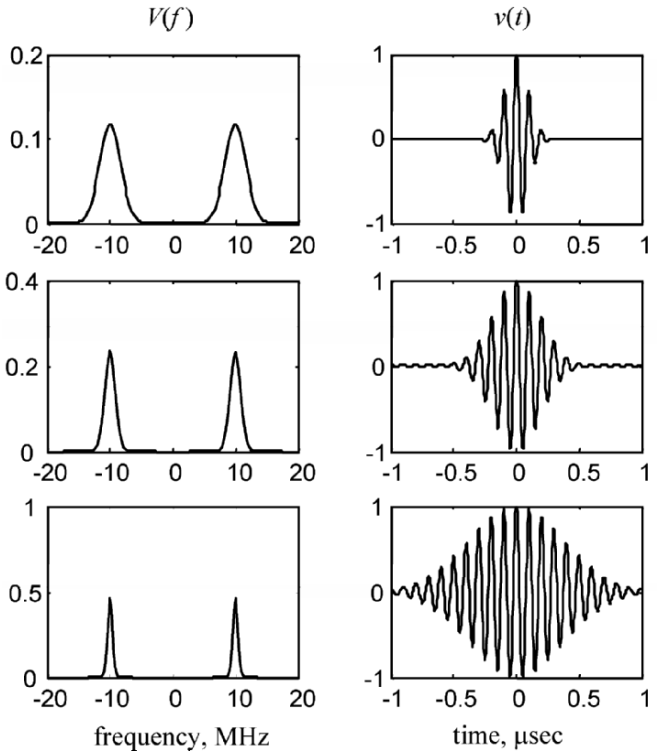

Fig. A.5. Wave forms and spectra obtained from Eq. (A.6) for f_c = 10 MHz and (from top to bottom) *bw* = 4, 2, 1 MHz, respectively. Note that the amplitudes of the spectra are getting larger and their widths narrower as the bandwidth decreases although the amplitudes appear to be decreasing with decreasing bandwidth because of the changing vertical scale.

small bandwidths are called narrow-band, high sensitivity transducers. Although they cannot as easily resolve closely separated signals, the longer duration pulses they generate normally have more energy than wide-band signals and they can therefore penetrate deeper into materials.

As a final example of a Fourier transform pair, consider a 1-D wave pressure pulse traveling along the positive *x*-direction in a fluid.

Such a pulse has the form $p(t-x/c)$ where c is the wave speed. If we take the Fourier transform of this traveling wave we find

$$\begin{aligned}&\int_{-\infty}^{+\infty} p(t-x/c)\exp(2\pi ift)\,dt\\&=\exp(2\pi ifx/c)\int_{-\infty}^{+\infty} p(u)\exp(2\pi ifu)\,du\\&=P(f)\exp(2\pi ifx/c),\end{aligned}\tag{A.8}$$

where $P(f)$ is the Fourier transform of $p(t)$. Note that we could also have obtained this result directly by using the shifting property relationship of Eq. (A.4). If we put this Fourier transform back into the inverse Fourier transform expression, we obtain

$$\begin{aligned}p(t-x/c)&=\int_{-\infty}^{+\infty} P(f)\exp(2\pi ifx/c-2\pi ift)\,df\\&=\frac{1}{2\pi}\int_{-\infty}^{+\infty} P(\omega)\exp(ikx-i\omega t)\,d\omega,\end{aligned}\tag{A.9}$$

where $k=\omega/c=2\pi f/c$ is called the *wave number*. Equation (A.9) shows that we can consider a 1-D pulse as a superposition of terms of the form $p=A\exp(ikx-i\omega t)$ which is a harmonic plane wave traveling in the positive x-direction. The amplitude, A, of the plane wave is just proportional to the spectrum of the pressure wave, i.e. $A=P(\omega)/2\pi$. The wave number is related to the *wavelength*, λ, of the wave through the relation $k=2\pi/\lambda$. To see the meaning of the terms in the exponential factor of this harmonic wave, first fix x (i.e. sit at a fixed location in space) and watch the wave go by as a function of the time, t. The pressure will go through a complete cycle (the exponential will change by 2π radians) in a time, T_p, (in seconds) called the period of the wave. Thus, over one cycle $2\pi fT_p=2\pi$. This shows that the frequency, f, (in Hz or cycles/sec) is just $f=1/T_p$. Since $\omega=(2\pi\ rad/cycle)(f\ cycles/\sec)$ we see that ω is just the rate at which the argument of the exponential term of the pressure is changing in time at a fixed location in units of rad/sec. Now, instead fix the time t and consider the pressure changes as a function of x. Physically, this would correspond to taking a "snapshot" of the wave variations at a

fixed time as a function of the distance, x. Again the pressure will go through a complete cycle over a distance, D, when $kD = 2\pi D/\lambda = 2\pi$ so that the wave length, λ, is just that distance, measured in units of length/cycle. But $k = (2\pi\ rad/cycle)/(\lambda\ length/cycle)$ so the wave number is just the rate at which the argument of the exponential term of the pressure is changing in distance at a fixed time in terms of units of rad/length.

Equation (A.9) shows that in solving wave propagation and interaction problems, we can consider the behavior of harmonic waves and then obtain the solution for a pulse by Fourier superposition. We have shown this fact here only for 1-D plane waves, but it is also true for other types of waves as well.

A.2 The Discrete Fourier Transform

In practice, experimental ultrasonic NDE signals are manipulated digitally, i.e. the analog (continuous) time domain signals are first sampled and then these sampled values are stored digitally for later processing. Thus, it is also important to be able to deal with Fourier transforms and their inverses in terms of discrete, sampled signal values. This can be done using forms similar to Eqs. (A.1) and (A.2) given by the discrete Fourier transform pair [A.2]:

$$\begin{aligned} V(f_n) &= \Delta t \sum_{j=1}^{N} v(t_j) \exp\left[2\pi i (j-1)(n-1)/N\right] \quad (n = 1,2,...,N) \\ v(t_k) &= \frac{1}{N\Delta t} \sum_{n=1}^{N} V(f_n) \exp\left[-2\pi i (n-1)(k-1)/N\right] \ (k = 1,2,...,N), \end{aligned} \tag{A.10}$$

where $v(t_k), V(f_k)$ are values of a time domain function and its Fourier transform at discrete frequency and time values, respectively, $\Delta t = t_{k+1} - t_k$ is the sampling time interval, and N is the total number of sampled points. As with the Fourier transform and its inverse, the discrete Fourier transform pair of Eq. (A.10) may appear in different forms in the literature. Here, Eq. (A.10) is the discrete transform pairs corresponding directly to Eqs. (A.1) and (A.2).

While the Fourier transform and its inverse are usually applied to non-periodic functions their discrete Fourier transform counterparts in Eq. (A.10) are always periodic functions. For example, the first sampled

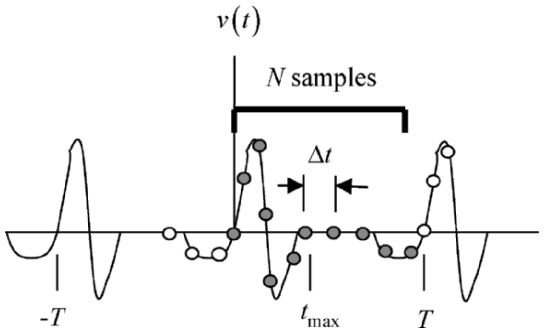

Fig. A.6. A sampled periodic time domain function showing the N sampled values used in the discrete Fourier transform (dark circles) and other sampled values (light circles). The sampling time interval is Δt, the time $t_{\max}$ is the time at which the transient signal ends, and the time $T = N\Delta t$ is the period.

value in the time domain, $v(t_1)$, is normally taken to be the value sampled at $t = 0$. There are then N sampled values from $t = 0$ to $t = (N\text{-}1)\Delta t$. The sampled value $v(t_{N+1}) = v(N\Delta t)$, however, is the same as the value at time $t = 0$ and subsequent samples $v(t_{N+2}), v(t_{N+3})$ etc. also repeat previous values. As Fig. A.6 shows the sampled time function is periodic with period $T = N\Delta t$. Similarly, in the frequency domain the first sampled value, $V(f_1)$, is the frequency component for $f = 0$ (the d.c. value) and there are then N sampled frequency components from $f = 0$ to $f = (N\text{-}1)\Delta f$, where $\Delta f = 1/T$. The sampled value $V(f_{N+1}) = V(N\Delta f)$, is again the d.c. value. The frequency domain function is therefore also periodic with period $f_s = 1/\Delta t$, where f_s is the sampling frequency (see Fig. A.7). In Appendix G a MATLAB function s_space is given that generates a sampled time or frequency axis with precisely these values needed for application of the discrete Fourier transform or its inverse. For example, s_space(0, T, N) generates a set of N evenly spaced sampled values going from 0 to T - Δt, where $\Delta t = T/N$ is the sample spacing. Note that if we used the built-in MATLAB function linspace(0, T, N) we would obtain instead a set of N evenly sampled values going from 0 to T with sample spacing $\Delta t = T/(N\text{-}1)$.

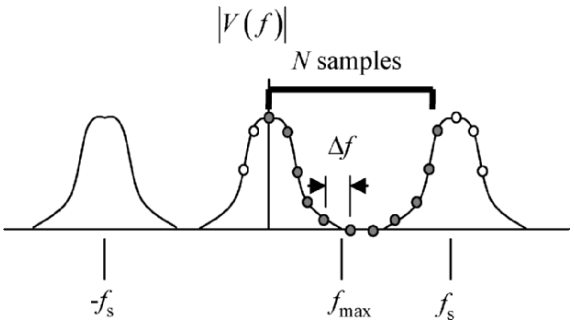

Fig. A.7. The magnitude of a sampled periodic frequency domain function showing the N sampled values use in the discrete inverse Fourier transform (dark circles) and other sampled values (light circles). The frequency sampling interval is $\Delta f = 1/T$, the frequency $f_{\max}$ is the maximum frequency contained in the signal and the sampling frequency $f_s = 1/\Delta t$ is the period.

As long as the original time domain signal is shorter than the sampling period, T, and the sampling frequency is sufficiently high to capture all the significant "wiggles" in the signal it can be seen from Fig. A.6 that the N sampled time domain components contained in the discrete Fourier transform will capture the entire signal adequately. Note that if the time signal has non-zero values before $t = 0$, those values will appear in the upper half of the N time domain samples as shown in Fig. A.6. The MATLAB function c_shift (see section G.8 in Appendix G for a code listing) can be used to shift the entire time domain function and place these negative time values back into their proper position so that the function does not appear to be split. Similarly, a MATLAB function t_shift given in Appendix G changes the time-axis appropriately.

In the frequency domain the negative frequency components in the discrete Fourier transform are also contained in the upper half of the N frequency domain samples as can be seen from Fig. A.7. Since inherently the frequency spectrum of a real time domain function must contain both negative as well as positive frequency components, Fig. A.7 shows that unless the sampling frequency, f_s, is at least double $f_{\max}$, the highest frequency contained in the signal, these periodically repeated functions will overlap and we will not recover the original spectrum of the signal. To prevent this phenomenon, which is called *aliasing,* we must therefore always choose a high enough sampling frequency. This requirement is

embodied in what is called the Nyquist criterion (or the sampling theorem) which is [A.1]:

The sampling frequency, $f_s = 1/\Delta t$*, must be at least twice the maximum significant frequency,* $f_{\max}$*, contained in the waveform being sampled.*

In ultrasonic NDE, the transducers commonly used do not produce significant frequencies above about 20 MHz and inspected materials (steel,

Code Listing A.1. The FFT corresponding to Eq.(A.10).

```
function y = FourierT(x, dt)
% FourierT(x, dt) computes forward FFT of x, with sampling time interval dt
% FourierT assumes the Fourier transform  is in terms of exp(2*pi*i*f*t)
% For NDE, frequency components are normally in MHz, dt in microseconds
% If x is a matrix, the transform is performed on the columns of x
[nr, nc] = size(x);
if nr == 1
N = nc;
else
     N = nr;
end
y = N*dt*ifft(x);
```

Code Listing A.2. The Inverse FFT corresponding to Eq.(A.10).

```
function y = IFourierT(x, dt)
% IFourierT(x, dt) computes the inverse FFT of x, for a sampling time interval dt
% IFourierT assumes the inverse transform is in terms of exp(-2*pi*i*f*t)
% For NDE, frequency components are normally in MHz, dt in microseconds
% If x is a matrix, the inverse transform is performed on the columns of x
[nr,nc] = size(x);
if nr == 1
     N = nc;
else
     N = nr;
end
y =(1/(N*dt))*fft(x);
```

aluminum, etc.) also attenuate ultrasound severely above such frequencies. Thus, a frequency of 100 MHz is normally a conservative choice for the sampling frequency that will satisfy the Nyquist criterion. This corresponds to a sampling time interval $\Delta t = 10$ nanoseconds. The number of sampling points, *N*, then determines the total length of the time record, $T = N\Delta t$, being digitized which in turn determines the sampling interval in the frequency domain, Δf, since $\Delta f = f_s / N = 1/N\Delta t = 1/T$.

To implement the discrete Fourier transform pair of Eq. (A.10) efficiently, one uses Fast Fourier Transform (FFT) algorithms, which are widely available [A.4]. Numerous books have been written on FFTs if one is interested in the details of those algorithms. To perform these discrete transforms in MATLAB, we must be aware that the built-in MATLAB FFT functions fft and ifft are defined such that the signs are exchanged in the exponentials appearing in Eq. (A.10) and the MATLAB functions do not include the sampling time constant Δt or *N* appearing in the coefficients of Eq. (A.10). Thus, we have defined a new set of MATLAB functions, FourierT and IFourierT, to implement the discrete transforms in Eq. (A.10). Those functions are defined in Code Listings A.1 and A.2. The functions FourierT and IFourierT, like fft and ifft, will perform Fast Fourier Transforms and their inverse on either vectors or matrices. If the input data is a vector, it can be a column or row vector. If the input data of these functions is a matrix, then they will perform the FFTs or inverse FFTs on the columns of the matrix. Fast Fourier Transform algorithms are often implemented with the number of samples $N = 2^m$ for some integer *m*. In fact some FFT algorithms require the number of samples be a power of two. The MATLAB functions fft and ifft do not have this restriction so that neither do the functions FourierT and IFourierT. However, these functions are also more efficient when the number of samples is a power of two.

If we give the function IFourierT only the positive frequency components of a real time domain function, then to recover that real time function we need to compute twice the real part of the output of IFourierT (which will be complex), This is necessary since if we compute the inverse Fourier transform of a function $V(f)$ using only the positive frequency components we do not obtain the function $v(t)$ but instead find the function $v_+(t)$ where [Fundamentals]:

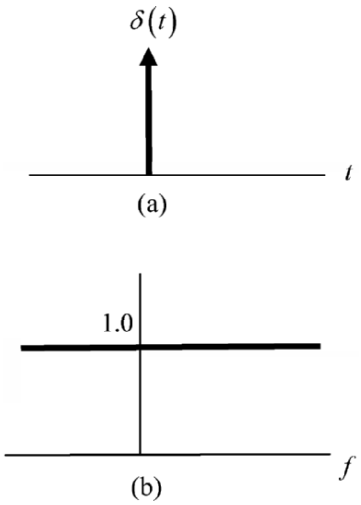

Fig. A.8. (a) A delta function, and **(b)** its Fourier transform.

$$\begin{aligned} v_+(t) &= \int_0^\infty V(f)\exp(-2\pi i f t)\,df \\ &= \frac{1}{2}v(t) + \frac{i}{2\pi}\int_{-\infty}^{+\infty}\frac{v(\tau)}{\tau - t}\,d\tau \end{aligned} \tag{A.11}$$

so that one-half of the original function v is in the real part of $v_+(t)$ and one half of the *Hilbert transform* [A.3] of v shows up in the imaginary part. [Note that if $V(f_1) = V(f)\big|_{f=0}$ is non-zero, which can happen with time functions whose average (dc) value is not zero, then one half of that value must be associated with the positive frequencies and one half with the negative frequencies, i.e. we should compute IFourierT on the positive frequencies only after first making the replacement $V(f_1) \to V(f_1)/2$].

A.3 The Delta Function

One function that plays a key role in analyzing linear systems is the *delta function* [A.1]. We can define a delta function from a limit of the "box"

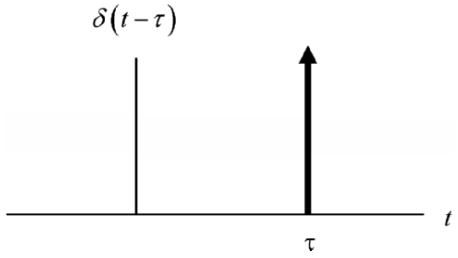

Fig. A.9. A shifted delta function.

function shown in Fig. A.1 (a). If we let $t_0 \to 0$ but keep the product $At_0 = 1$ so that the function always contains unit area, then the box function becomes an infinite spike at $t = 0$ as shown in Fig. A.8 (a), which we will denote symbolically by the delta function $\delta(t)$. In the same limit the Fourier transform of the box function becomes simply unity at all frequencies, as shown in Fig. A.8 (b) so that we have the Fourier transform pair $\delta(t) \leftrightarrow 1$. Thus, a delta function generates all frequencies equally. It is this property that makes a delta function an ideal function to serve as a system input since the output of a system with such an input will then reflect how the system modifies this uniform input at all frequencies. As discussed in Appendix C, this allows us to obtain the transfer function of a linear system. The shifted delta function $\delta(t-\tau)$ is an infinite spike at time $t = \tau$, as shown in Fig. A.9. Some important properties of $\delta(t-\tau)$ are:

$$\delta(t-\tau) = 0 \quad t \neq \tau$$

$$\int_a^b g(t)\delta(t-\tau)\,dt = \begin{cases} 0 & \tau < a \text{ or } \tau > b \\ g(\tau) & a < \tau < b \\ g(\tau)/2 & \tau = a \text{ or } \tau = b \end{cases} \tag{A.12}$$

and

$$\int_{u=-\infty}^{u=t} \delta(u-\tau)\,du = H(t-\tau) = \begin{cases} 0 & t < \tau \\ 1/2 & t = \tau, \\ 1 & t > \tau \end{cases} \tag{A.13}$$

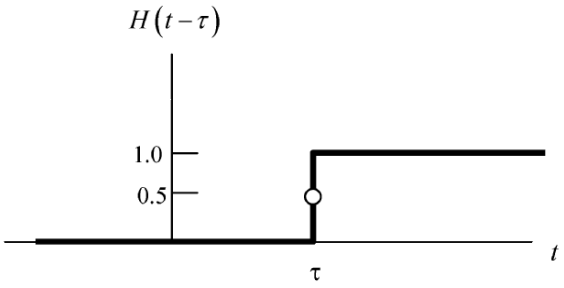

Fig. A.10. A unit step function at t = τ.

where $g(t)$ is an arbitrary function and $H(t)$ is the unit step function. Equation (A.12) shows the sampling properties of the delta function while Eq. (A.13) shows that the integral of the delta function $\delta(t-\tau)$ is the step function $H(t-\tau)$, as shown in Fig. A.10. If we examine the several Fourier transform relations of Eq. (A.4) for the delta function we find

$$\begin{aligned} \delta(t-t_0) &\leftrightarrow \exp(2i\pi f t_0) \\ \frac{d\delta}{dt} &\leftrightarrow -2\pi i f. \end{aligned} \tag{A.14}$$

A.4 References

A.1 Bracewell RN (2000) The Fourier transform and its applications, 3rd ed. McGraw-Hill, New York, NY

A.2 Burrus CS, Parks TW (1985) DFT/FFT and convolution algorithms. John Wiley and Sons, New York, NY

A.3 Sneddon IN (1951) Fourier transforms. McGraw-Hill, New York, NY

A.4 Walker JS (1996) Fast Fourier transforms, 2nd ed. CRC Press, New York, NY

A.5 Exercises

1 (a). Write a MATLAB function, spectrum1, which computes the positive frequency components of a signal given by

$$V(f) = A\sqrt{\pi}\exp\left[-4\pi^2 A^2 (f - f_c)^2\right],$$

where A is given in terms of the -6 *dB* bandwidth, *bw*, as $A = \sqrt{\ln 2}/(\pi bw)$. Spectrum1 should return sampled values of V for a set of sampled frequencies, f (in MHz), and a specified center frequency, fc , (in MHz), and bandwidth, bw, (in MHz), i.e. we should have for the MATLAB function call:

```
>> V = spectrum1(f, fc, bw)
```

Show that your function is working by evaluating the spectrum for 512 frequencies ranging from zero to 100 MHz with fc = 5 MHz, bw = 1 MHz. Generate the frequencies with the function s_space (see Appendix G), i.e. evaluate

```
>> f = s_space(0, 100, 512);
```

Plot V over a range of frequencies 0 – 10 MHz (approximately).

1 (b). Use the MATLAB function IFourierT to obtain a sampled time domain function, $v(t)$, from the sampled spectrum computed in problem 1 (a). Plot $v(t)$ by first generating a set of 512 time domain values with the function s_space, i.e.

```
>> t  = s_space(0,  512*dt, 512);
```

where dt is the time interval between samples (which in this case is dt = 1/100). Then use the t_shift and c_shift functions given in Appendix G so that the sampled values of $v(t)$ shown are not split between the first and last half of the window. Show that your results agree with the analytical result:

$$v(t) = \cos(2\pi f_c t)\exp\left[-t^2/4A^2\right]$$

if we take into account the fact that we only used the positive frequency components.

1 (c). Now apply the FourierT function to the sampled $v(t)$ obtained from part 1 (b) and plot the magnitude of the resulting spectrum $V(f)$. How is this $V(f)$ different from the one you started with?

1 (d). If you look carefully at your plot of *V*(*f*) in part 1 (a) you should see that the sampling interval, Δf, in the frequency domain is not quite small enough to give an accurate representation of the Gaussian function. Take the $v(t)$ signal obtained in 1 (b), shift it so that all the values in the second half of the time domain window are zero, and then append 512 zeros to that signal. Apply FourierT to this longer signal to obtain the spectrum. Show that this process, which is called *zero padding*, improves our resolution in the frequency domain. Note that zero padding does not affect the sampling frequency.

2. The Hilbert transform, $\mathcal{H}\left[f(t)\right]$, of a function $f(t)$ is defined as

$$\mathcal{H}\left[f(t)\right] = \frac{1}{\pi}\int_{-\infty}^{+\infty} \frac{f(\tau)d\tau}{\tau - t}.$$

When a plane traveling wave of the form $f(t - x/c)$ is reflected from a surface beyond a critical angle, as discussed in Appendix D, the Hilbert transform of the function $f(t)$ appears in the reflected wave causing the reflected waveform to be distorted from the incident wave. It can be shown [A.2] that if $F(\omega)$ is the Fourier transform of $f(t)$ then the Fourier transform of the Hilbert transform of $f(t)$, $\tilde{\mathcal{H}}(\omega)$, is given by $\tilde{\mathcal{H}}(\omega) = -i\,\mathrm{sgn}(\omega)F(\omega)$ where

$$\mathrm{sgn}(\omega) = \begin{cases} +1 & \omega > 0 \\ -1 & \omega < 0 \end{cases}.$$

We can use this fact in conjunction with the Fast Fourier transform as a convenient way to compute the Hilbert transform of a function. To see this consider the follow example:

In MATLAB, define a sampled time axis consisting of 1024 points going from $t = 0$ to $t = 10$ μsec. Over this time interval define a sampled function $f(t)$ that has unit amplitude for $4.5 < t < 5.5$ μsec and is zero otherwise. Use FourierT to calculate the Fourier transform, $F(\omega)$, of $f(t)$. Then use the relationship $\tilde{\mathcal{H}}(\omega) = -i\,\mathrm{sgn}(\omega)F(\omega)$ to find the Fourier transform of the Hilbert transform of $f(t)$ and compute the Hilbert transform itself by performing an inverse Fourier transform on this result with IFourierT. [Note that if you use only the positive frequency values to compute the inverse, then we only need to multiply those values by $-i$]. Plot your results versus time. In this case the Hilbert transform of $f(t)$ can be obtained analytically [Fundamentals]. It is

$$\mathcal{H}\left[f(t)\right] = \frac{1}{\pi}\ln\left|\frac{t-5.5}{t-4.5}\right|.$$

Using a different plotting symbol, plot this function also on the same graph. How do your results compare?

B Impedance Concepts and Equivalent Circuits

Impedance is very important concept for ultrasonic systems since it appears in a variety of contexts [B.1]. Thus, in this Appendix we will discuss briefly impedance as it appears in both electrical and acoustical components. We will also examine the concept of equivalent circuits and the use of Thévenin's theorem to represent active electrical systems such as an ultrasonic pulser.

B.1 Impedance

Impedance is a quantity that is most often associated with electrical circuits. Consider, for example, the electrical elements shown in Fig. B.1. The time varying voltage and current for these elements are related to one another through the following relations:

Resistor– $$V(t) = R\, I(t) \tag{B.1a}$$

Capacitor– $$C\frac{dV(t)}{dt} = I(t) \tag{B.1b}$$

Inductor– $$V(t) = L\frac{dI(t)}{dt}. \tag{B.1c}$$

If we assume these voltages and currents are harmonic, i.e. $V = V_0 \exp(-i\omega t)$, $I = I_0 \exp(-i\omega t)$, then for these elements we have

Resistor– $$V_0 = R\, I_0 \tag{B.2a}$$

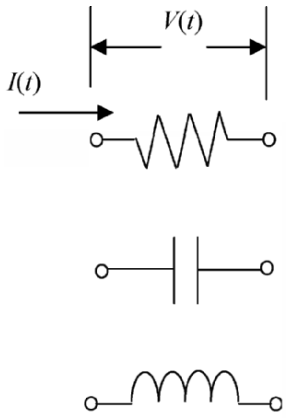

Fig. B.1. The voltage and current flowing (top to bottom) in a resistor, capacitor, and inductor, respectively.

Capacitor– $$V_0 = \frac{I_0}{-i\omega C} \tag{B.2b}$$

Inductor– $$V_0 = -i\omega L\, I_0. \tag{B.2c}$$

We could instead take the Fourier transform of all the relations in Eqs. (B.1a-c) and view Eqs. (B.2a-c) as the relations between the Fourier transform of the voltage, $V_0(\omega)$, and the Fourier transform of the current, $I_0(\omega)$, for these elements. In general, we see we can write for all these elements $V_0(\omega) = Z^e(\omega) I_0(\omega)$, where $Z^e(\omega)$ is the *complex electrical impedance*. The impedance has the dimensions of volts/amps = ohms (Fourier transforms of voltage and current will have dimensions such as volts/Hz and amps/Hz but their ratio is still ohms). We see that $V_0(\omega) = Z^e(\omega) I_0(\omega)$ is true for these simple individual circuit elements. However, we can also take a complex circuit composed of many of these elements and also replace them by an equivalent complex impedance in the same fashion.

Impedance also is associated with mechanical systems [B.1]. Consider, for example, the mechanical elements shown in Fig. B.2. The

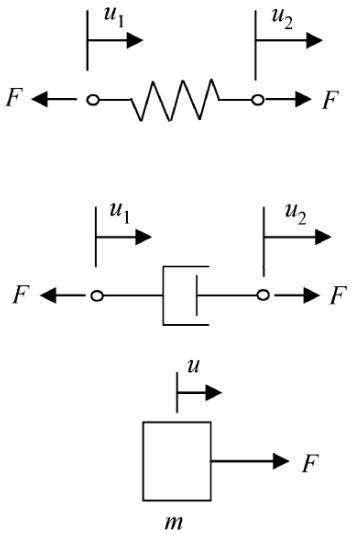

Fig. B.2. The forces and displacements acting (top to bottom) in a spring, dashpot, and mass, respectively.

time varying forces and displacements for these elements are related to one another through the following relations:

Spring– $$F = k\left(u_2 - u_1\right) \tag{B.3a}$$

Dashpot– $$F = c_d\left(\frac{du_2}{dt} - \frac{du_1}{dt}\right) \tag{B.3b}$$

Mass– $$F = m\frac{d^2u}{dt^2}. \tag{B.3c}$$

Again, if we assume these forces and displacements are harmonic so that $F = F_0 \exp\left(-i\omega t\right)$, $u = U \exp\left(-i\omega t\right)$ or take the Fourier transforms of Eq. (B.3a-c) we find

Spring– $$F_0 = k\left(U_2 - U_1\right) \tag{B.4a}$$

Dashpot– $$F_0 = -i\omega c_d\left(U_2 - U_1\right) \tag{B.4b}$$

Mass– $$F_0 = -m\omega^2 U, \tag{B.4c}$$

which also can all be expressed in terms of a *complex mechanical impedance*, $Z^m(\omega)$, where $F_0(\omega) = Z^m(\omega)\Delta U(\omega)$. In this case the dimensions of the mechanical impedance are that of stiffness, i.e. force/displacement.

Ultrasonics inherently involves the propagation of waves and the concept impedance also is an important one for wave motion [Fundamentals]. Consider, for example, a 1-D plane pressure wave in a fluid propagating in the positive *x*-direction. The pressure and *x*-component of the velocity in the wave can be expressed in the forms

$$\begin{aligned} p &= P f\left(t - x/c\right) \\ v_x &= V f\left(t - x/c\right), \end{aligned} \tag{B.5}$$

where *P*, *V* are pressure and velocity amplitudes of the waves (the function *f* is dimensionless) and *c* is the wave speed. However, the pressure and velocity in the fluid are related to one another though the equation of motion of the fluid, which is (see Appendix D)

$$-\frac{\partial p}{\partial x} = \rho\frac{\partial v_x}{\partial t}, \tag{B.6}$$

where ρ is the density of the fluid. Placing the pressure and velocity expressions of Eq. (B.5) into Eq. (B.6) then gives

$$\frac{P}{c} f'\left(t - x/c\right) = \rho V f'\left(t - x/c\right), \tag{B.7}$$

where $f' = df\left(u\right)/du$. It then follows that

$$P = \rho c V. \tag{B.8}$$

The quantity $z^a = \rho c$ is called the *specific acoustic impedance* of a plane wave. If we consider the force in the wave, *F*, generated by the pressure

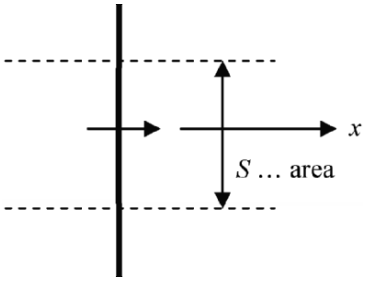

Fig. B.3. A plane wave traveling in the *x*-direction and a cross-sectional area, *S*, of the wave front.

acting on a cross-sectional area, *S*, of the wave front, as shown in Fig. B.3, then we have

$$F = PS = \rho cSV, \tag{B.9}$$

where $Z^a = \rho cS$ is called the *acoustic impedance* of the plane wave. This acoustic impedance has the dimensions in the SI system of Newtons-second/ meter (N-s/m) and the specific acoustic impedance has the dimensions N-s/m^3. For more general wave types the acoustic impedance or specific acoustic impedance is in general a complex quantity.

An ultrasonic system inherently contains electrical and electromechanical elements as well as propagating acoustic and elastic waves. Thus, the system will be described by a variety of different impedances and we need to distinguish between them. In this book we will use the symbol "*Z*" for impedances and denote electrical impedance by an "*e*" superscript and acoustical impedance by an "*a*" superscript, a notation also followed in this section. For example, in Chapter 4 the electrical input impedance of a transmitting transducer *A* is given as $Z_{in}^{A;e}$ while the same transducer's acoustic radiation impedance is given as $Z_r^{A;a}$.

B.2 Thévenin's Theorem

An ultrasonic system contains both active and passive electrical and electromechanical elements. The pulser, for example is an active electrical network since it contains the driving elements of the ultrasonic system.

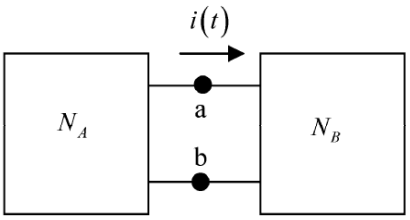

Fig. B.4. An electrical network with sources connected to a passive network.

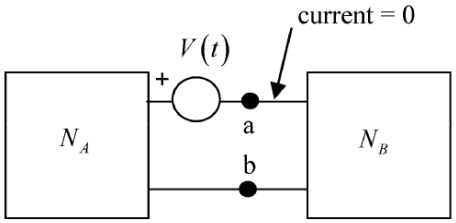

Fig. B.5. Introduction of a voltage source that makes the current flow between the two networks zero.

Cables and transducers are passive networks since they merely transfer and/or transform energy but do not generate it. To model in detail an active electrical network like a pulser would be a very challenging task since a pulser is a very complex set of circuits. If we assume the pulser acts as a linear device then Thévenin's theorem allows us to avoid this complexity and replace a pulser with a simple equivalent circuit consisting of a voltage source and electrical impedance in series. Here, we will outline briefly the proof of this important theorem [B.2].

Consider an electrical network, N_A, that contains both passive elements and sources and connect it at its terminals to a network, N_B, that is passive (no sources) as shown in Fig. B.4. Let $i(t)$ be the current flowing between two networks at terminals a-b. It is assumed here that both N_A and N_B are linear networks. Now introduce an opposing voltage source, $V(t)$, in front of the terminals a-b such that the current is driven to zero, as shown in Fig. B.5. Since now there is no current flowing between N_A and

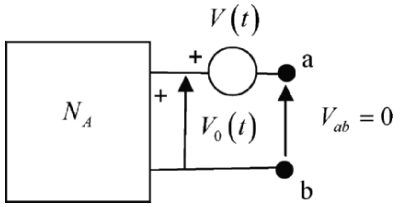

Fig. B.6. The network N_A detached from the passive network N_B .

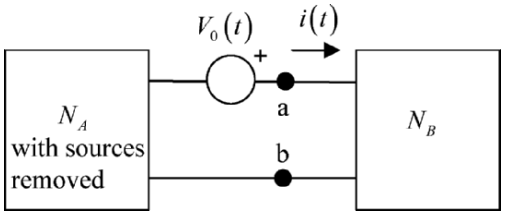

Fig. B.7. Re-attaching the network A with all the sources replaced by $V_0(t)$.

N_B , the voltage across terminals a-b, V_{ab} , is zero and we can break the circuit at a-b , as shown in Fig. B.6, without disturbing any voltages or currents. Because there is no current flowing out of the network N_A in Fig. B.6 the voltage $V_0(t)$ in that figure is the output voltage of the network N_A under open-circuit conditions and it follows that

$$V_0(t) - V(t) = V_{ab} = 0, \tag{B.10}$$

which shows that $V(t)$ is just the open-circuit voltage, $V_0(t)$, of network N_A . If we now reverse the polarity of $V(t)$ and remove all the sources in N_A (by replacing them with short circuits), when we reattach N_A to N_B the original current will be set up between N_A and N_B , as shown in Fig. B.7. Since N_B is a passive network, the voltage across terminals a-b will also be the same as in the original setup. Thus, we can say that the

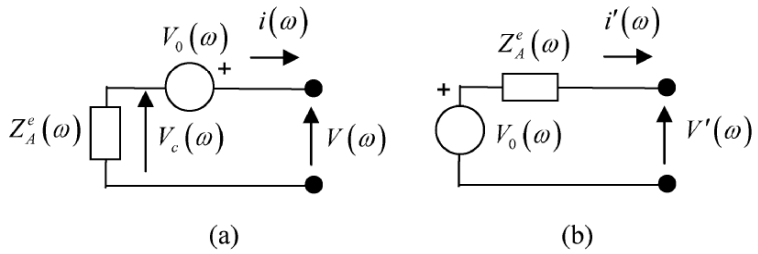

Fig. B.8. (a) The Thévenin equivalent network of Fig B.7 represented in the frequency domain by a complex source and impedance, and **(b)** the same equivalent circuit with the source and impedance exchanged.

circuit shown in Fig. B.7 is equivalent to the original circuit of Fig. B.4. This is the essence of Thévenin's theorem which states that:

A two terminal network containing sources and passive elements is equivalent (as far as its external effects are concerned) to a voltage source in series with the network with all the sources removed; the voltage of the equivalent source has the same magnitude and polarity as those of the voltage appearing across the terminals of the original network under open-circuit conditions.

If we Fourier transform all the voltages and currents appearing in these networks and work in the frequency domain, then the original network with it sources removed is equivalent to a complex electrical impedance, $Z_A^e(\omega)$, and we can replace our original network with the equivalent circuit of Fig. B.8 (a). However, from that figure we have the two equations

$$\begin{aligned} V_c(\omega) &= Z_A^e(\omega) i(\omega) \\ V(\omega) - V_c(\omega) &= V_0(\omega), \end{aligned} \tag{B.11}$$

which give

$$V(\omega) - V_0(\omega) = Z_A^e(\omega) i(\omega). \tag{B.12}$$

It is often customary to exchange the positions of the source and impedance so that the source "drives" that impedance, as shown in Fig. B.8 (b). If we let $V' = -V, i' = -i$ and $V_0 = -V_0$ in Eq. (B.12) then that equation still holds for the equivalent circuit shown in Fig. B.8 (b). Thus,

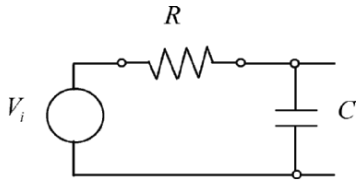

Fig. B.9. An RC-circuit and voltage source.

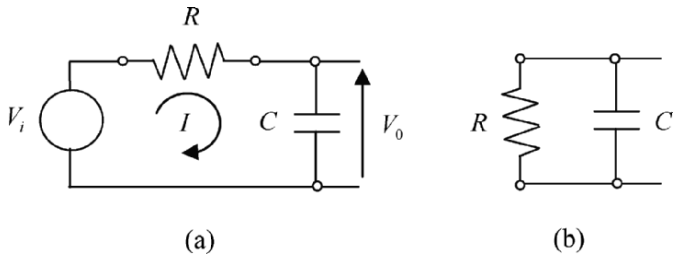

Fig.B.10. (a) The RC-circuit showing the open-circuit voltage, V_0, and the current, I, flowing in the circuit, and **(b)** the source-free circuit that must be placed in series with the open-circuit voltage to obtain the Thévenin equivalent circuit.

the complex source and impedance of Fig. B.8 (b) is the Thévenin equivalent circuit corresponding to our original network.

Example: Consider the simple circuit shown in Fig. B.9 where a voltage source with frequency components $V_i(\omega)$ is connected to a resistance, R, and a capacitance, C. Determine the Thévenin equivalent source and impedance that replaces this circuit.

Consider the open-circuit voltage, $V_0(\omega)$, and the current, $I(\omega)$, in the circuit as shown in Fig. B.10 (a). We have the relations

$$\begin{aligned} V_i - V_0 &= IR \\ V_0 &= \frac{I}{-i\omega C}. \end{aligned} \tag{B.13}$$

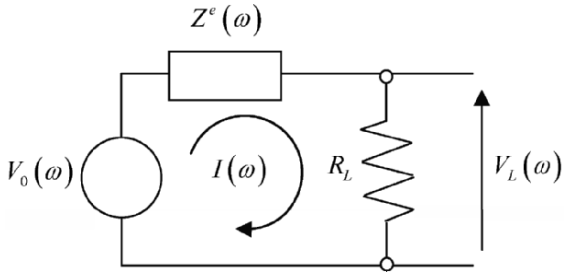

Fig. B.11. The Thévenin equivalent circuit for a pulser attached to a known external resistance, R_L, for measuring the impedance, $Z^e(\omega)$.

If we eliminate *I* from these two equations we find the Thévenin equivalent source is

$$V_0(\omega) = \frac{V_i(\omega)}{1 - i\omega RC}. \tag{B.14}$$

This circuit in series with the original circuit with the sources removed (short-circuited) is our Thévenin equivalent circuit. The source-free circuit is shown in Fig. B.10 (b) where we see that we just have the resistor and capacitor in parallel. Thus, the equivalent impedance, Z^e, of this source-free circuit is just

$$\frac{1}{Z^e(\omega)} = \frac{1}{R} + \frac{1}{(1/-i\omega C)}, \tag{B.15}$$

which gives

$$Z^e(\omega) = \frac{R}{1 - i\omega RC}. \tag{B.16}$$

B.3 Measurement of Equivalent Sources and Impedances

A pulser in an ultrasonic measurement system is an example of an electrical network containing sources. As shown in Chapter 2 if we assume

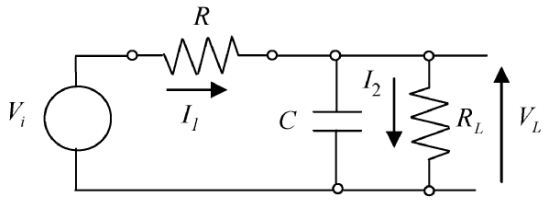

Fig. B.12. A setup for determining the impedance of the RC-circuit.

the pulser acts as a linear system we can find the Thévenin equivalent source for the pulser, $V_0(\omega)$, by measuring the open-circuit voltage, $V_0(t)$, at the output terminals of the pulser and Fourier transforming this measured voltage to obtain $V_0(\omega)$. But how do we find the equivalent impedance, $Z^e(\omega)$, of a real instrument such as a pulser since we cannot go into the instrument and physically short circuit the sources, as we did with the known circuit in the previous example? Instead, as shown in Chapter 2, we can place a known load resistance, R_L, at the output terminals of the pulser and measure the voltage, $V_L(t)$, across this load. Fourier transforming this voltage then gives $V_L(\omega)$ (see Fig. B.11). But from the Thévenin equivalent circuit of the pulser shown in Fig. B.11 (see also Chapter 2), we find that

$$\begin{aligned} V_0 - V_L &= Z^e I \\ V_L &= R_L I. \end{aligned} \tag{B.17}$$

So eliminating the current, *I*, we find

$$Z^e(\omega) = R_L\left(\frac{V_0(\omega)}{V_L(\omega)} - 1\right). \tag{B.18}$$

Equation (B.18) shows that with measurements of both $V_0(\omega)$ and $V_L(\omega)$, with the resistance, R_L, known, we can determine the Thévenin equivalent impedance, $Z^e(\omega)$. Note that this impedance does not depend on the value of the known resistance. It is only a function of the properties of the

pulser itself. We can demonstrate this method for determining the impedance for our RC-circuit example again. Figure B.12 shows that circuit and the resistance, R_L, at its output terminals. From Fig. B.12, we have

$$\begin{aligned} V_i - V_L &= I_1 R \\ V_L &= I_2 R_L \\ V_L &= \frac{(I_1 - I_2)}{-i\omega C}. \end{aligned} \tag{B.19}$$

Eliminating the currents I_1, I_2 from these equations gives

$$V_L = \frac{V_i}{(1 - i\omega RC) + R/R_L}. \tag{B.20}$$

Using Eq. (B.20) and Eq. (B.14) for the Thévenin equivalent source, we find

$$\begin{aligned} Z^e(\omega) &= R_L \left(\frac{V_0(\omega)}{V_L(\omega)} - 1 \right) = R_L \left\{ \frac{(1 - i\omega RC) + R/R_L}{(1 - i\omega RC)} - 1 \right\} \\ &= R_L \left\{ \frac{R/R_L}{(1 - i\omega RC)} \right\} = \frac{R}{(1 - i\omega RC)}, \end{aligned} \tag{B.21}$$

which is the same value for the impedance obtained earlier in Eq. (B.16) and is indeed independent of R_L.

B.4 References

B.1 Cremer L, Heckl M, Ungar EE (1973) Structure-borne sound. Springer-Verlag, Berlin, Germany

B.2 Cheng DK (1959) Analysis of linear systems. Addison Wesley, Reading, PA

B.5 Exercises

1. A propagating harmonic spherical pressure wave from a point source in a fluid is given by $p = P\exp(ikr - i\omega t)/r$, where r is the radial distance from the source (see Fig. B.13).The radial velocity can also similarly be

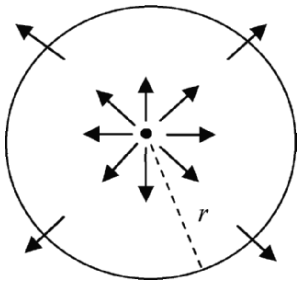

Fig. B.13. A spherical wave arising from a point source in a fluid.

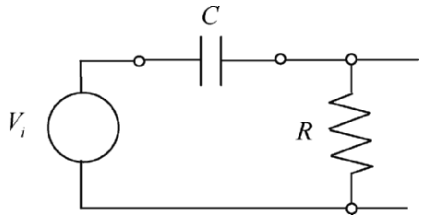

Fig. B.14. An example circuit.

written as $v_r = V\exp\left(ikr - i\omega t\right)/r$. If the equation of motion of the fluid in spherical coordinates is given by

$$-\frac{\partial p}{\partial r} = \rho\frac{\partial v_r}{\partial t},$$

determine the specific acoustic impedance P/V of this spherical wave. What happens to this impedance when the frequency, ω, is very large?

2. For the circuit shown in Fig. B.14 obtain the Thévenin equivalent source and impedance in terms of the given circuit elements.

C Linear System Fundamentals

In this book an ultrasonic system is modeled as a series of interconnected linear systems. Thus, linear system theory will be a fundamental part of all our discussions. This Appendix will outline a number of key linear systems concepts such as two port systems and linear time-shift invariant systems. We will also discuss the role that the convolution theorem plays in linear systems as well as related quantities such as impulse response functions and transfer functions.

C.1 Two Port Systems

The pulser in an ultrasonic system is an active circuit (a circuit with sources) that drives the rest of the ultrasonic system through the pulser output port. The cabling and transducer(s) in an ultrasonic system normally are passive elements (no sources) and they contain both input and output ports, as shown in Fig. C.1. In the case of a cable, it is purely an electrical system so the inputs and outputs are both of the same type (voltage, current). An ultrasonic transducer transforms voltage, V, and current, I, at its electrical port into a mechanical force, F, (arising from a pressure distribution on the face of a piezoelectric crystal as shown in Fig. C.1 (b)) and a velocity, v, (which represents the average velocity of motion of the crystal) at its acoustic port. The underlying velocity distribution is shown in Fig. C.1 (b) as being uniform at the acoustic port. A transducer with this type of velocity profile is called a *piston transducer*. [Note: piston transducer models have been shown to often be very effective for modeling real commercial ultrasonic transducers but one should be aware that this idealized model may not be suitable for all transducers. In this book we will generally assume a piston transducer model is valid].

We can represent a purely electrical two port system such as a cable schematically as shown in Fig. C.2 [C.1]. Note that it is customary to assign the currents so that they flow into the two port system on the input side and flow out on the output side, a convention that we will also follow here.

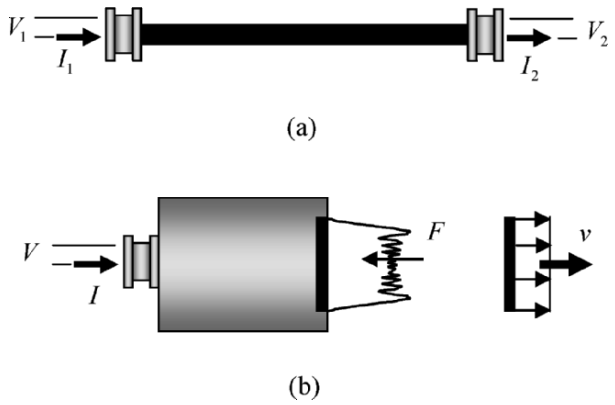

Fig. C.1. (a) Cabling as a two port electrical system, and **(b)** an ultrasonic transducer as two port system with voltage, V, and current, I, at the electrical port and force, F, and velocity, v, at the acoustic port. The force F is the net compressive force generated by the pressure distribution acting across the face of the transducer and v is the average velocity due to the velocity distribution of the transducer face. The pressure distribution is non-uniform, as shown, but the velocity distribution is taken to be the uniform velocity profile of a piston transducer.

Since we will assume this is a linear system the inputs and outputs are proportional to each other through a 2x2 transfer matrix, $[\mathbf{T}]$, where

$$\begin{Bmatrix} V_1(\omega) \\ I_1(\omega) \end{Bmatrix} = \begin{bmatrix} T_{11} & T_{12} \\ T_{21} & T_{22} \end{bmatrix} \begin{Bmatrix} V_2(\omega) \\ I_2(\omega) \end{Bmatrix}. \tag{C.1}$$

The dimensions of the elements of the transfer matrix are: T_{11}, T_{22}: dimensionless, T_{12} :ohms, T_{21} :1/ohms. Note that the voltages and currents in Eq. (C.1) are all in the frequency domain, i.e. they are the Fourier transforms of the time varying voltages and currents present at the input and output ports. Thus, the transfer matrix is also in the frequency domain. Another common way to represent a two port system is in terms of a 2x2 impedance matrix, $\left[\mathbf{Z}^e\right]$. In this case it is usual to represent the currents on both sides of the two port system as flowing into the system, as shown in Fig. C.3, and write:

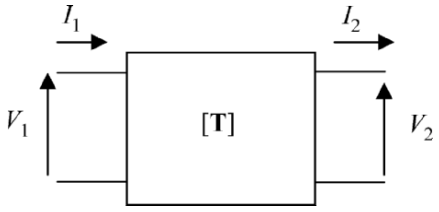

Fig. C.2. An electrical two port system represented by a transfer matrix. $[\mathbf{T}]$.

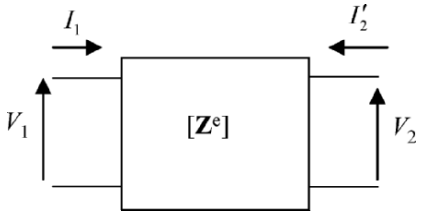

Fig. C.3. An electrical two port system represented by an impedance matrix, $\left[\mathbf{Z}^e\right]$.

$$\begin{Bmatrix} V_1(\omega) \\ V_2(\omega) \end{Bmatrix} = \begin{bmatrix} Z_{11}^e & Z_{12}^e \\ Z_{21}^e & Z_{22}^e \end{bmatrix} \begin{Bmatrix} I_1(\omega) \\ I_2'(\omega) \end{Bmatrix}, \tag{C.2}$$

where $I_2' = -I_2$. In this case the dimensions of the elements of the impedance matrix are all ohms. In addition to linearity, we will assume that a two port system is reciprocal. The meaning of reciprocity is as follows. Consider a two port system, characterized by its transfer matrix $[\mathbf{T}]$ (or, equivalently, by its impedance matrix, $\left[\mathbf{Z}^e\right]$). Let us attach this two port system to electrical networks A and B at its input and output terminals, respectively, as shown in Fig. C.4. We will call this connected set of systems state (1). Under these conditions the voltage and current at the input port are $V_1^{(1)}, I_1^{(1)}$ and the voltage and current at the output port

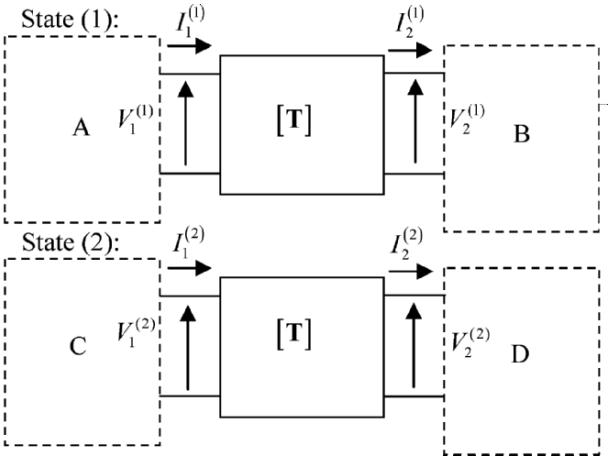

Fig. C.4. A two port system with its ports terminated differently in two states, labeled states (1) and (2).

are $V_2^{(1)}, I_2^{(1)}$. Now, attach the same two port system to two other networks C and D, as shown in Fig. C.4. Call this connected set of systems state (2). Then in this state we have $V_1^{(2)}, I_1^{(2)}$ and $V_2^{(2)}, I_2^{(2)}$ for the voltages and currents at the input and output port, respectively. Our two port system is said to be reciprocal if for any two states (1) and (2) the inputs and outputs satisfy the reciprocity relation given by

$$V_1^{(1)} I_1^{(2)} - V_1^{(2)} I_1^{(1)} = V_2^{(1)} I_2^{(2)} - V_2^{(2)} I_2^{(1)}. \tag{C.3}$$

Equation (C.3) is a rather "opaque" equation in that it is difficult to see what it really means. However, when it is applied to our two port system written in terms of its impedance matrix, one can show that reciprocity simply implies that the impedance matrix is symmetric, i.e. $Z_{21}^e = Z_{12}^e$ [C.1]. Similarly, Eq. (C.3) implies that determinant of the transfer matrix of the two port system equals one, i.e. $\det[\mathbf{T}] = T_{11}T_{22} - T_{12}T_{21} = 1$ [C.1].

For a linear, reciprocal two port system the components of the transfer matrix and the impedance matrix are obviously related. It is not difficult to show that the transfer matrix can be expressed in terms of the impedance matrix components as:

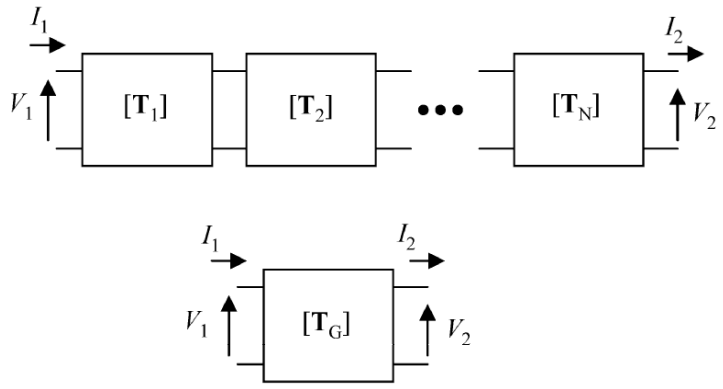

Fig. C.5. A cascade of linear, reciprocal two port systems and their replacement by a single "global" two port system.

$$[\mathbf{T}] = \begin{bmatrix} Z_{11}^e / Z_{12}^e & \left(Z_{11}^e Z_{22}^e - \left(Z_{12}^e\right)^2\right) / Z_{12}^e \\ 1/Z_{12}^e & Z_{22}^e / Z_{12}^e \end{bmatrix}. \tag{C.4}$$

From Eq. (C.4) it follows directly that $\det[\mathbf{T}] = 1$, as it should be. Similarly, the impedance matrix can be written in terms of the transfer matrix components as:

$$[\mathbf{Z}^e] = \begin{bmatrix} T_{11}/T_{21} & 1/T_{21} \\ 1/T_{21} & T_{22}/T_{21} \end{bmatrix}, \tag{C.5}$$

which shows that $Z_{21}^e = Z_{12}^e$ is automatically satisfied.

One can express impedance components in terms of transfer matrix components and vice versa so in principle it does not matter which of these representations we use for a two port system. However, when one is dealing with a series of connected two port systems, as is the case for an ultrasonic system (e.g. the cabling is attached to the transducer, both of which are two port systems) then the transfer matrix is more convenient to use since one can replace a series of connected two port systems, each characterized by their own transfer matrices $[\mathbf{T}_1],[\mathbf{T}_2],...,[\mathbf{T}_N]$ as shown in Fig. C.5, by a single global 2x2 transfer matrix , $[\mathbf{T}_G]$, where the global

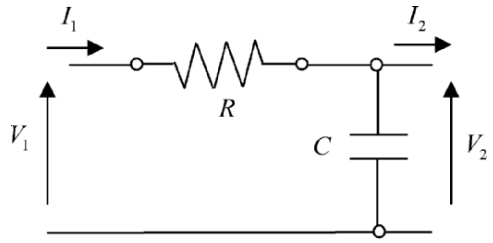

Fig. C.6. An RC-circuit modeled as a two port system.

matrix is obtained by matrix multiplication of each of the individual transfer matrices, i.e.

$$\left[\mathbf{T}_G\right] = \left[\mathbf{T}_1\right]\left[\mathbf{T}_2\right]...\left[\mathbf{T}_N\right]. \tag{C.6}$$

This global transfer matrix is also reciprocal if the individual transfer matrices are reciprocal since

$$\det\left[\mathbf{T}_G\right] = \det\left[\mathbf{T}_1\right]\det\left[\mathbf{T}_2\right]...\det\left[\mathbf{T}_N\right] = 1. \tag{C.7}$$

As a simple example of a linear, reciprocal two port system, consider the RC-circuit example used in Appendix B with the voltage source removed to form the two port system shown in Fig. C.6. To determine the transfer matrix for this circuit, consider first the voltage across the resistance and the current flowing through it. We have

$$V_1 - V_2 = RI_1. \tag{C.8}$$

Also, considering the voltage across the capacitor and the current flowing through it (which is $I_1 - I_2$ flowing downwards) we find

$$V_2 = \frac{I_1 - I_2}{-i\omega C}. \tag{C.9}$$

Equation (C.9) can be written directly in transfer matrix form (inputs in terms of outputs) as

$$I_1 = -i\omega C V_2 + I_2. \tag{C.10}$$

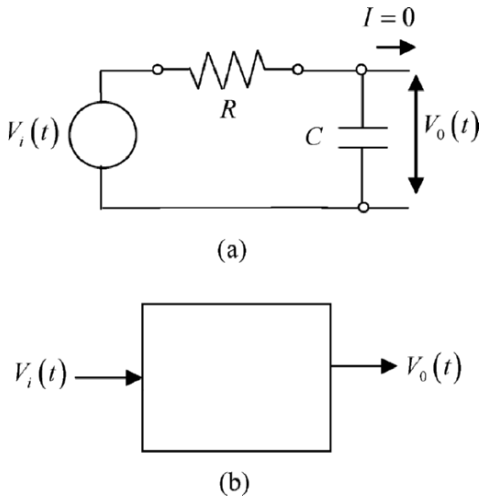

Fig. C.7. (a) An RC-circuit with a voltage source at the input and open-circuit conditions at the output, and **(b)** the representation of this terminated system as a single input-single output system.

If we now place Eq. (C.10) into Eq. (C.8), the resulting equation can also be placed in transfer matrix form as

$$V_1 = (1 - i\omega RC)V_2 + RI_2. \tag{C.11}$$

From Eqs. (C.10) and (C.11) the transfer matrix follows directly, giving

$$\begin{Bmatrix} V_1 \\ I_1 \end{Bmatrix} = \begin{bmatrix} (1 - i\omega RC) & R \\ -i\omega C & 1 \end{bmatrix} \begin{Bmatrix} V_2 \\ I_2 \end{Bmatrix}. \tag{C.12}$$

Equation (C.12) shows that $\det[\mathbf{T}] = 1$ is indeed satisfied for this system so that it is reciprocal. Using Eq. (C.5) we can also obtain the impedance matrix directly for this two port system, where

$$\begin{Bmatrix} V_1 \\ V_2 \end{Bmatrix} = \begin{bmatrix} (i\omega RC - 1)/i\omega C & -1/i\omega C \\ -1/i\omega C & -1/i\omega C \end{bmatrix} \begin{Bmatrix} I_1 \\ -I_2 \end{Bmatrix}, \tag{C.13}$$

and obviously we also have $Z_{21}^e = Z_{12}^e$.

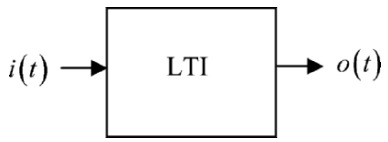

Fig. C.8. A general linear time-shift invariant (LTI) system.

C.2 Linear Time-Shift Invariant (LTI) Systems

If we have a two port linear system that is terminated in some fashion at both its ports, then this two port system reduces to a system where single inputs and outputs can be linearly related to each other [C.2], [C.3], [C.4]. As an example, consider again the RC-circuit two port system of Fig. C.6. If we attach a voltage source $V_i(t)$ at its input port and leave the output port open-circuited (Fig. C.7 (a)), we have a linear system where we can relate the open-circuit voltage, $V_0(t)$, to the input voltage, $V_i(t)$. This type of single input-single output system can be represented schematically as shown in Fig. C.7 (b). For this simple system it is easy to see that

$$\begin{aligned} V_i(t) - V_0(t) &= i(t)R \\ i(t) &= C\frac{dV_0}{dt}. \end{aligned} \tag{C.14}$$

Eliminating the current between the two equations in Eq. (C.14), we see that V_0 is related implicitly to V_i through the solution of the differential equation given by

$$\frac{dV_0(t)}{dt} + \frac{V_0(t)}{RC} = \frac{V_i(t)}{RC}. \tag{C.15}$$

We can write this relation symbolically as

$$V_0(t) = L\left[V_i(t)\right], \tag{C.16}$$

where $L[\ ]$ is a linear operator since the underlying RC-circuit is linear.

An important class of linear single input, single output systems is called a linear time-shift invariant (LTI) system, as shown schematically in

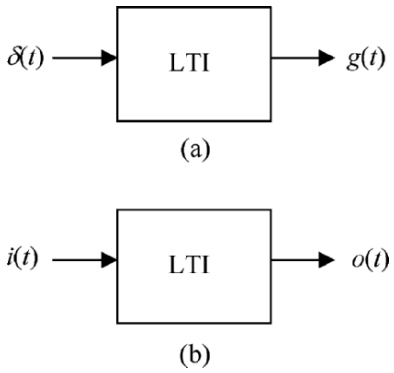

Fig. C.9. (a) An LTI system driven by a delta function input, and **(b)** driven by a general input.

Fig. C.8. for a general input, $i(t)$, and output, $o(t)$. An LTI system is defined as a linear system where a time shift of the input signal produces exactly the same time shift of the output signal. These properties can be stated mathematically as follows:

Linearity:

$$\text{If} \quad \begin{aligned} o_1(t) &= L\left[i_1(t)\right] \\ o_2(t) &= L\left[i_2(t)\right] \end{aligned} \quad \text{then} \quad \begin{aligned} o(t) &= L\left[a_1 i_1(t) + a_2 i_2(t)\right] \\ &= a_1 L\left[i_1(t)\right] + a_2 L\left[i_2(t)\right] \end{aligned} \tag{C.17}$$

Time-Shift Invariance:

$$\text{If} \quad o(t) = L\left[i(t)\right] \quad \text{then} \quad o(t - t_0) = L\left[i(t - t_0)\right] \tag{C.18}$$

It is clear that The RC-circuit example just considered is an LTI system. We expect that elements of an ultrasonic NDE system in general may also be modeled as LTI systems. LTI systems have the important property that they can be characterized completely by their response to a delta function input, $\delta(t)$. This delta function response is called the *impulse response function*, $g(t)$, of the system, and the Fourier transform of this impulse response, $G(f)$, we will call the *transfer function* of the LTI system. Figure C.9 (a) shows an LTI system being driven by a delta function input,

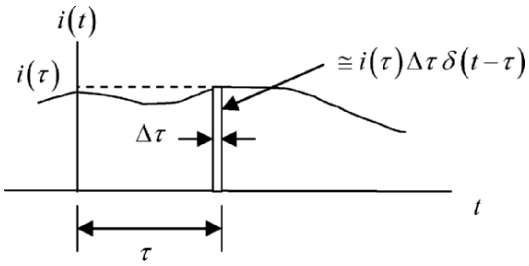

Fig. C.10. Representing a general input function as a superposition of delta function inputs.

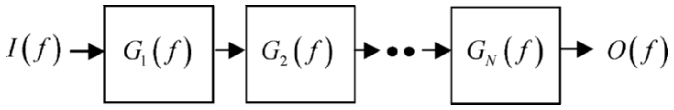

Fig. C.11. A series of LTI systems.

while Fig. C.9 (b) shows the same system under a general input. It can be shown that the output, $o(t)$, of an LTI system to a general input, $i(t)$, is given in terms of a convolution integral of that input with the impulse response function, $g(t)$, i.e.

$$\begin{aligned} o(t) &= \int_{-\infty}^{+\infty} i(\tau) g(t-\tau)\, d\tau \\ &= \int_{-\infty}^{+\infty} g(\tau) i(t-\tau)\, d\tau. \end{aligned} \tag{C.19}$$

Equation (C.19) follows directly from the properties of an LTI system since we can take a general input function and consider it as a superposition of small rectangular elements as shown in Fig. C.10. A general rectangular element at time τ of width $\Delta\tau$ and amplitude $i(\tau)$ is shown in that figure. This element, however, acts like a shifted delta function (located at $t = \tau$) a with strength (area) $i(\tau)\Delta\tau$. Thus, from the linearity and time shift invariance properties of the system, we have that the output, Δo, from this rectangular element is given by $\Delta o(t) \cong i(\tau)\Delta\tau\, g(t-\tau)$

and so by superposition over all elements, we have the total output, $o(t)$, due to the total input given by

$$\begin{aligned} o(t) &\cong \sum i(\tau)\Delta\tau g(t-\tau) \\ &= \int_{-\infty}^{+\infty} i(\tau) g(t-\tau)\, d\tau. \end{aligned} \tag{C.20}$$

The convolution integral of Eq. (C.19) is a fundamental relationship for LTI systems. If we take the Fourier transform of this relationship we obtain an even simpler result since, if we define the following Fourier transforms of the input, output, and impulse response functions, respectively:

$$\begin{aligned} I(f) &= \int_{-\infty}^{+\infty} i(t)\exp(2\pi i f t)\, dt \\ O(f) &= \int_{-\infty}^{+\infty} o(t)\exp(2\pi i f t)\, dt \\ G(f) &= \int_{-\infty}^{+\infty} g(t)\exp(2\pi i f t)\, dt \end{aligned} \tag{C.21}$$

and if the output and input are related through the convolution integral of Eq. (C.19), then it is easy to show that their Fourier transforms are related through [Fundamentals]

$$O(f) = G(f) I(f), \tag{C.22}$$

i.e. convolution in the frequency domain is just obtained by complex-valued multiplication. In a similar fashion, *deconvolution* in the frequency domain is in principle accomplished by complex-valued division. For example, we can write

$$G(f) = \frac{O(f)}{I(f)}. \tag{C.23}$$

In practice, however, such division must be done with care since noise may contaminate both the numerator and denominator and make the ratio unreliable. Often filters are used to desensitize the deconvolution process to such errors. A *Wiener filter* is a particular filter commonly used for deconvolution purposes in ultrasonic NDE. With that filter, Eq. (C.23) is replaced by

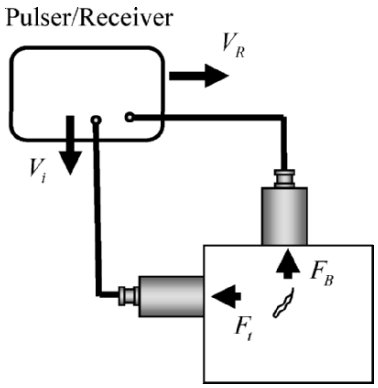

Fig. C.12. An ultrasonic flaw measurement system.

$$G(f)=\frac{O(f)I^{*}(f)}{\left|I(f)\right|^{2}+\varepsilon^{2}\max\left\{\left|I(f)\right|^{2}\right\}}, \tag{C.24}$$

where $(\ )^{*}$ denotes the complex conjugate and ε is a small constant that is used to represent the noise level present. The quantity $\max\left\{\left|I(f)\right|^{2}\right\}$ is a constant. It is the maximum value of the magnitude squared of the values of $I(f)$ present. In this form ε gives a measure of the noise as a fraction of the size of the signals present. Generally, small values such as $\varepsilon=0.01$ to 0.05 work well for many ultrasonic problems. When $\varepsilon\to 0$, Eq. (C.24) reduces to Eq. (C.23). Code listing C.1 gives a MATLAB function for implementing the Wiener filter of Eq. (C.24).The use of transfer functions such as $G(f)$ is very convenient, particularly when we have a series of connected LTI systems as shown in Fig. C.11 since the input and output of the entire system can be related through simply a product of the transfer functions of each subsystem, i.e.

$$O(f)=G_1(f)G_2(f)\cdots G_N(f)I(f). \tag{C.25}$$

In the time domain, the relationship equivalent to Eq. (C.25) would be a series of nested convolution integrals. By working in the frequency domain we can avoid having to deal with multiple integrations and instead we need

Code Listing C.1. A MATLAB function for the generation of a Wiener filter.

```
function Y = Wiener_filter( O, I, e)
% WIENER_FILTER provides a 1-D filter for desensitizing
% division in the frequency domain (deconvolution) to noise.
% The filter takes a sampled output spectrum ,O, and an
% input spectrum, I, and computes Y = O*conj(I)/(|I|^2 + e^2*M^2)
% where M is the maximum value of |I| and conj(I) is the
% complex conjugate of I. The constant e is generally taken as
% a constant to represent the noise level. Small values of e
% such as e = 0.01 often work well for ultrasonic systems.
%The calling sequence is:
%Y = Wiener_filter(O,I,e);
%
M = max(abs(I));
Y = O.*conj(I)./((abs(I)).^2 + e^2*M^2);
```

only a series of complex multiplications to obtain $O(f)$ from the input. The time domain output, $o(t)$, can then be obtained by an inverse Fourier transform.

As an example of such a cascade of LTI systems, consider an ultrasonic pitch-catch flaw measurement system, as shown in Fig. C.12. Let $V_i(f)$ be the frequency components of the Thévenin equivalent input voltage of the pulser. This input then travels through the sending cable and drives the sending transducer which outputs a mechanical force, $F_t(f)$ at its acoustic port. This force launches a wave into the specimen which then interacts with a flaw and in turn produces a driving force, $F_B(f)$, on the receiving transducer. This driving force is converted into electrical energy which is transmitted by the receiving cable back to the receiver, where it is amplified and output as the received flaw signal, $V_R(f)$. If we treat this entire measurement system as a series of LTI systems, then we can write:

$$\begin{aligned} V_R(f) &= \frac{V_R(f)}{F_B(f)}\frac{F_B(f)}{F_t(f)}\frac{F_t(f)}{V_i(f)}V_i(f) \\ &= t_R(f)t_A(f)t_G(f)V_i(f), \end{aligned} \tag{C.26}$$

where $t_G(f)$ is the transfer function for the sound generation process (containing properties of the pulser, cabling, and sending transducer), $t_R(f)$ is the transfer function for the sound reception process (containing properties of the receiving transducer, cabling, and receiver), and $t_A(f)$ is the transfer function describing the acoustic/elastic processes (wave propagation to the flaw, scattering from the flaw, and propagation from the flaw to the receiving transducer). We will see that it is possible to model and/or measure all of these transfer functions so that through Eq. (C.26) we have an *ultrasonic measurement model* of our entire ultrasonic system. The challenge, of course, is to obtain explicit expressions for the transfer functions in Eq. (C.26). Much of this book is devoted to just that task.

C.3 References

C.1 Pozar DM (1998) Microwave engineering, 2nd ed. John Wiley and Sons, New York, NY
C.2 Cheng DK (1959) Analysis of linear systems. Addison Wesley, Reading, PA
C.3 Gaskill JD (1978) Linear systems, transforms, and optics. McGraw-Hill, New York, NY
C.4 Papoulis A (1968) Systems and transforms with applications in optics. McGraw-Hill, New York, NY

C.4 Exercises

1. Consider a two port electrical system where

$$\begin{Bmatrix} V_1(\omega) \\ I_1(\omega) \end{Bmatrix} = \begin{bmatrix} T_{11} & T_{12} \\ T_{21} & T_{22} \end{bmatrix} \begin{Bmatrix} V_2(\omega) \\ I_2(\omega) \end{Bmatrix}.$$

We wish to measure the transfer matrix components (as a function of frequency). This is easy to do if we first measure the inputs and outputs under open-circuit conditions at the output port since $I_2 = 0$. Thus, if we let the voltages and currents be $\left(V_1^{oc}, I_1^{oc}\right)$ and $\left(V_2^{oc}, I_2^{oc} = 0\right)$ we have

$$T_{11} = \frac{V_1^{oc}}{V_2^{oc}}, T_{21} = \frac{I_1^{oc}}{V_2^{oc}}.$$

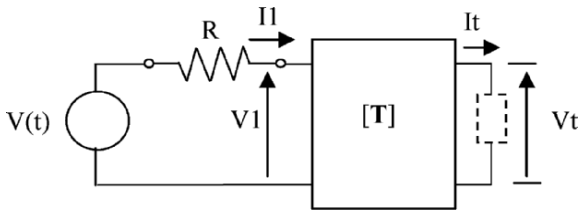

Fig. C.13. A measurement setup for obtaining the transfer matrix components of a two port system using different output terminations.

Similarly, if under short- circuit conditions at the output port ($V_2 = 0$) we measure the voltages and currents $\left(V_1^{sc}, I_1^{sc}\right)$, $\left(V_2^{sc} = 0, I_2^{sc}\right)$ we have

$$T_{12} = \frac{V_1^{sc}}{I_2^{sc}}, T_{22} = \frac{I_1^{sc}}{I_2^{sc}}.$$

Now, perform these "measurements" in MATLAB for an unknown two port system, two_portX, which is written in terms of a MATLAB function which has the calling sequence:

```
>> [ v1, i1, vt, it] = two_portX( V, dt, R, 'term');
```

The input arguments of two_portX are as follows. V is a sampled voltage source versus time, where the sampling interval is dt. R is an external resistance (in ohms). This source and resistance are connected in series to one end of the two port system as shown in Fig. C.13. The other end of the system can be either open-circuited or short-circuited. The string 'term' specifies the termination conditions. It can be either 'oc' for open-circuit or 'sc' for short-circuit. The function two_portX then returns the "measured" sampled voltages and currents versus time: v1, i1, vt, it (Note: for open-circuit conditions the function returns it = 0 and for short-circuit conditions vt = 0).

As a voltage source to supply the V input to two_portX use the MATLAB function pulserVT. For a set of sampled times this function returns a sampled voltage output that is typical of a "spike" pulser. Make a vector, t, of 512 sampled times ranging from 0 to 5 μsec, and call the pulserVT function with the following call sequence:

```
>> V = pulserVT(200, 0.05, 0.2, 12, t);
```

For the resistance, take R = 200 ohms. Using Eq. (C.14), determine the four transfer matrix components and plot their magnitude and phase from zero to approximately 30 MHz. Note that the outputs of two_portX are all time domain signals but the quantities we wish to measure are all in the frequency domain.

2. It is not physically possible to generate a delta function as the input of an LTI system to obtain its impulse response. However, it is possible to obtain the transfer function of an LTI system by deconvolution of a measured output with a known input as shown in Eq. (C.23). Consider a MATLAB function LTI_X that represents a "black box" LTI system. It can be evaluated in the form

```
>> O =LTI_X(I, dt)
```

Where I is a sampled time domain input (with sampling interval dt) and O is the time domain output. Use as an input for this LTI system the voltage output of the pulserVT function of problem 1 and obtain the transfer function of this system as a function of frequency by deconvolution. Plot the magnitude and phase (in degrees) of this transfer function from zero to approximately 30 MHz. To obtain the impulse response function from this transfer function we would have to compute its inverse Fourier transform. Is that possible with this function?

3. Consider an LTI system which has as its transfer function

$$G(f)=\begin{cases}\cos(\pi f/40) & 0<f<20MHz\\ 0 & otherwise\end{cases}.$$

Also, consider an input spectrum to this system given by

$$I(f)=\begin{cases}1-f/20 & 0<f<20MHz\\ 0 & otherwise\end{cases}.$$

We expect the output of this system will then have the spectrum

$$O(f)=G(f)I(f).$$

However, if we add noise to these functions then given *O* and *I* it may not be possible to reliably obtain G by simple division and we must use some filter instead such as the Wiener filter. The MATLAB function noisy will

generate noisy sampled versions of both the *O* and *I* given previously over a range 0-40 MHz. The function call is:

```
>> [O, I] = noisy(  ) ;
```

Plot both *O* and *I* from 0 to 40 MHz to verify those functions are correct (the noise you will see is very small) and then attempt to obtain *G* by direct division, i.e. compute

$$G(f) = \frac{O(f)}{I(f)}$$

and plot your results 0-40 MHz. Then use a Wiener filter instead to find *G* and plot your results. Take ε = 0.01. Are the results sensitive to ε? Is there any other way (besides using the Wiener filter) that you can get the "right" answer?

D Wave Propagation Fundamentals

D.1 Waves in a Fluid

In immersion testing the waves are generated by a transducer radiating sound into a fluid. Sound propagation in the fluid can be modeled by considering the fluid to be an ideal (viscous-free) compressible fluid. In this case, an element of the fluid only has pressures (compressive normal stresses) acting on its surfaces. If a wave in the fluid generates pressure changes in the x_1-direction, as shown in Fig. D.1, then we can relate those changes to the motion of the fluid by simply applying Newton's third law to a small element as shown in Fig. D.1 [Fundamentals], [D.1]. We find from

$$\sum F_x = ma_x \tag{D.1a}$$

that

$$pdx_2dx_3 - \left(p + \frac{\partial p}{\partial x_1} dx_1 \right) dx_2dx_3 + f_1 dx_1 dx_2 dx_3 = \rho dx_1 dx_2 dx_3 \frac{\partial^2 u_1}{\partial t^2}, \tag{D.1b}$$

which gives the equation of motion of the fluid in the x_1-direction as

$$-\frac{\partial p}{\partial x_1} + f_1 = \rho \frac{\partial^2 u_1}{\partial t^2}, \tag{D.1c}$$

where p is the pressure, ρ is the density of the fluid, u_1 is the displacement in the x_1-direction and f_1 is the body force (force/unit volume) acting on the fluid. Similarly, if we consider the pressure changes in the x_2, x_3 directions we find the equations of motion:

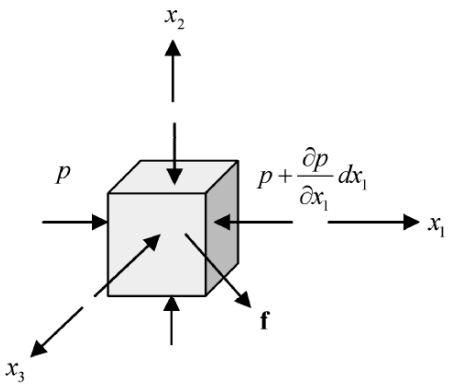

Fig. D.1. The pressures and body force acting on an element of an ideal, compressible fluid. Only the pressure changes in the x_1-direction are shown explicitly.

$$\begin{aligned} -\frac{\partial p}{\partial x_2} + f_2 &= \rho \frac{\partial^2 u_2}{\partial t^2} \\ -\frac{\partial p}{\partial x_3} + f_3 &= \rho \frac{\partial^2 u_3}{\partial t^2}. \end{aligned} \tag{D.2}$$

These three equations of motion of the fluid can also be written in vector form as

$$-\nabla p + \mathbf{f} = \rho \frac{\partial^2 \mathbf{u}}{\partial t^2} = \rho \frac{\partial \mathbf{v}}{\partial t}, \tag{D.3}$$

where $\mathbf{v} = \partial \mathbf{u} / \partial t$ is the velocity of the fluid. If we assume that the fluid is an ideal compressible fluid, then the pressure is related to the relative volume changes, dV/V, occurring in the fluid through the constitutive equation

$$p = -\lambda \frac{dV}{V}, \tag{D.4}$$

where λ is the *bulk modulus* of the fluid. For water, for example, the bulk modulus is approximately 2 GPa. These relative volume changes can be written in terms of the displacements, so we also have

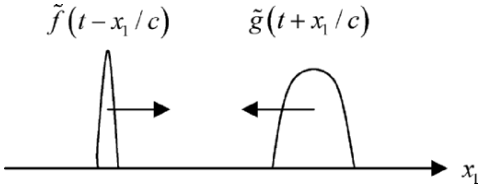

Fig. D.2. 1-D waves traveling in a fluid.

$$p = -\lambda \nabla \cdot \mathbf{u} = -\lambda \left(\frac{\partial u_1}{\partial x_1} + \frac{\partial u_2}{\partial x_2} + \frac{\partial u_3}{\partial x_3} \right). \tag{D.5}$$

To place this constitutive equation in the equations of motion, we first take the divergence ($\nabla \cdot$) of Eq. (D.3) which gives

$$-\nabla^2 p - f_b = \rho \frac{\partial^2 (\nabla \cdot \mathbf{u})}{\partial t^2}, \tag{D.6}$$

where $f_b = -\nabla \cdot \mathbf{f}$ and $\nabla^2 = \partial^2 / \partial x_1^2 + \partial^2 / \partial x_2^2 + \partial^2 / \partial x_3^2$ is the Laplacian operator. We then can place Eq. (D.5) into Eq. (D.6) to obtain the inhomogeneous wave equation for the pressure given by

$$\nabla^2 p - \frac{1}{c^2} \frac{\partial^2 p}{\partial t^2} = -f_b, \tag{D.7}$$

where $c = \sqrt{\lambda / \rho}$ is the wave speed of compressional waves (also called P-waves) in the fluid. For water, for example, c = 1480 m/sec, approximately. In NDE tests the ultrasonic waves that are generated are freely traveling so that they must satisfy the homogeneous wave equation, i.e. where $f_b = 0$.

D.2 Plane Waves in a Fluid

If we consider 1-D disturbances of the fluid where $p = p(x_1, t)$, then these disturbances must satisfy the 1-D homogeneous wave equation:

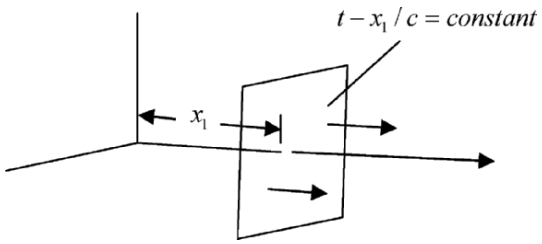

Fig. D.3. A plane wave traveling along the x_1-direction.

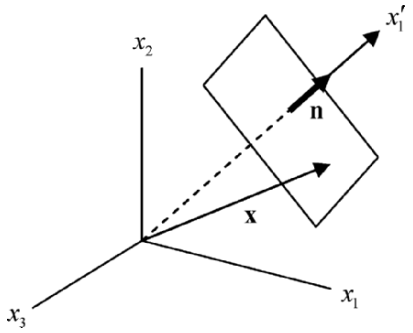

Fig. D.4. A plane wave traveling in a general direction, **n**, in three dimensions.

$$\frac{\partial^2 p}{\partial x_1^2} - \frac{1}{c^2}\frac{\partial^2 p}{\partial t^2} = 0, \tag{D.8}$$

which has general solutions of the form $p = \tilde{f}\left(t - x_1 / c\right) + \tilde{g}\left(t + x_1 / c\right)$. The $\tilde{f}$ function represents a wave traveling in the plus x_1-direction while the $\tilde{g}$ function represents a wave traveling in the negative x_1-direction, as shown in Fig. D.2. Consider the pressure wave $p = \tilde{f}\left(t - x_1 / c\right)$. The pressure in this 1-D wave is constant on the moving plane $t - x_1 / c = constant$,

so this is a plane wave traveling in the fluid (see Fig. D.3). Now, consider this plane wave traveling along an x_1'-axis which is oriented along the **n** direction as shown in Fig. D.4 (**n** is a unit vector). Then this plane wave can be written as

$$\begin{aligned} p &= \tilde{f}\left(t - x_1'/c\right) \\ &= \tilde{f}\left(t - \mathbf{x}\cdot\mathbf{n}/c\right), \end{aligned} \tag{D.9}$$

which is the general expression for a plane wave traveling in the **n**-direction in three dimensions, where here $\mathbf{x} = \left(x_1, x_2, x_3\right)$. It can be easily verified that this 3-D plane wave satisfies the full 3-D homogeneous wave equation for the fluid. Plane wave solutions are important types of waves since they can be used to model many of the wave propagation and wave interaction problems we encounter in ultrasonic NDE. An important special type of plane wave solution is a harmonic plane wave. For example, we can write a 1-D harmonic wave of frequency f (measured in Hz = cycles/sec) traveling in the x-direction as

$$p = F\left(f\right)\exp\left[2\pi i f\left(x/c - t\right)\right]. \tag{D.10}$$

As discussed in Appendix A, such harmonic wave solutions can be used to synthesize an arbitrary traveling plane wave since we have the Fourier transform relationship

$$\tilde{f}\left(t - x/c\right) = \int_{-\infty}^{+\infty} F\left(f\right)\exp\left[2\pi i f\left(x/c - t\right)\right]df, \tag{D.11}$$

where $F\left(f\right)$ is the Fourier transform of the function $\tilde{f}\left(t\right)$. Thus, there is no loss in generality in considering harmonic plane wave solutions. We can write such 1-D harmonic plane waves in a number of forms. For example, we have

$$\begin{aligned} &F\left(f\right)\exp\left[2\pi i f\left(\pm x/c - t\right)\right] \\ &= F\left(f\right)\exp\left[ik\left(\pm x - ct\right)\right] \\ &= F\left(f\right)\exp\left[\frac{2\pi i}{\lambda}\left(\pm x - ct\right)\right] \\ &= F\left(\omega\right)\exp\left[i\omega\left(\pm x/c - t\right)\right], \end{aligned} \tag{D.12}$$

where $\omega = 2\pi f$ is the circular frequency (in rad/sec), $k = \omega / c$ is the wave number (in rad/length) and $\lambda = 2\pi / k = c / f$ is the wave length (in length/cycle). The plus sign is for plane waves traveling in the positive *x*-direction and the minus sign is for waves traveling in the negative *x*-direction. A harmonic plane wave traveling in the plus **n**-direction in three dimensions can also be written in a number of forms. The most commonly used forms seen in the literature are

$$\begin{aligned} &F(\omega)\exp(ik\mathbf{n}\cdot\mathbf{x} - i\omega t) \\ &F(\omega)\exp(i\mathbf{k}\cdot\mathbf{x} - i\omega t), \end{aligned} \tag{D.13}$$

where $\mathbf{k} = k\,\mathbf{n}$ is a vector wave number.

Note, however, in all our forms we have used the time dependent factor $\exp(-i\omega t)$. Other authors may assume a factor $\exp(+i\omega t)$ or $\exp(+j\omega t)$ instead ($i = j = \sqrt{-1}$) . In that case, we must also change the signs appropriately on the spatial terms as well. For example, $F(f)\exp\left[2\pi i f(-x/c + t)\right]$ represents a plane wave traveling in the positive *x*-direction.

Also note that the last form in Eq. (D.13) can alternatively be written as

$$F(\omega)\exp\left[i\left(k_x x + k_y y + k_z z - \omega t\right)\right]. \tag{D.14}$$

But we must have $k_x^2 + k_y^2 + k_z^2 = k^2 = \omega^2 / c^2$ for Eq. (D.14) to represent a plane wave solution of the wave equation so we must have $k_z = \pm\sqrt{k^2 - k_x^2 - k_y^2}$ where the plus sign would represent a plane wave traveling in three dimensions in the positive *z*-direction while the minus sign would give a wave traveling in the negative *z*-direction. In Chapter 8 these forms arise when we discuss the use of plane waves to synthesize the wave field of an ultrasonic transducer.

D.3 Waves in an Isotropic Elastic Solid

The equations of motion for waves in an isotropic elastic solid can be obtained in the same manner as for the fluid. They are [Fundamentals], [D.1-D.3]:

$$\sum_{j=1}^{3} \frac{\partial \tau_{ji}}{\partial x_j} = \rho \frac{\partial^2 u_i}{\partial t^2} \qquad (i = 1,2,3), \tag{D.15}$$

where τ_{ij} are the stresses, u_i the displacement components in the x_i-directions, and ρ is the density of the solid. The constitutive equations for an isotropic elastic solid are more complicated than that of a fluid. They are given by generalized Hooke's law:

$$\begin{aligned}
\tau_{11} &= \lambda\Delta + 2\mu \frac{\partial u_1}{\partial x_1} \qquad & \tau_{12} &= \mu\left(\frac{\partial u_1}{\partial x_2} + \frac{\partial u_2}{\partial x_1}\right) \\
\tau_{22} &= \lambda\Delta + 2\mu \frac{\partial u_2}{\partial x_2} \qquad & \tau_{13} &= \mu\left(\frac{\partial u_1}{\partial x_3} + \frac{\partial u_3}{\partial x_1}\right) \\
\tau_{33} &= \lambda\Delta + 2\mu \frac{\partial u_3}{\partial x_3} \qquad & \tau_{23} &= \mu\left(\frac{\partial u_2}{\partial x_3} + \frac{\partial u_3}{\partial x_2}\right)
\end{aligned} \tag{D.16}$$

where λ, μ are the Lame' constants. For an isotropic elastic solid there are only two independent material constants. Some authors instead may use as the independent constants E, ν, where E is Young's modulus and ν is Poisson's ratio. In terms of these constants the Lame' constants are given by

$$\begin{aligned}
\lambda &= \frac{E\nu}{(1+\nu)(1-2\nu)} \\
\mu &= \frac{E}{2(1+\nu)}.
\end{aligned} \tag{D.17}$$

If one places the constitutive equations into the equations of motion we obtain *Navier's equations* for the displacements. In vector form we have

$$\mu\nabla^2\mathbf{u} + (\lambda + \mu)\boldsymbol{\nabla}(\boldsymbol{\nabla}\cdot\mathbf{u}) - \rho\frac{\partial^2\mathbf{u}}{\partial t^2} = 0, \tag{D.18}$$

where $\mathbf{u}$ is the displacement vector. This vector will be written in terms of its scalar components as $\mathbf{u} = (u_1, u_2, u_3) \equiv (u_x, u_y, u_z)$.

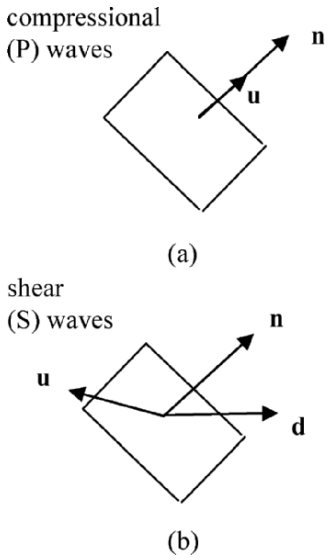

Fig. D.5. The displacements for P-waves and S-waves traveling in the **n**-direction in an isotropic elastic solid.

D.4 Plane Waves in an Isotropic Elastic Solid

Navier's equations are not wave equations, but they do have plane wave solutions. However, unlike the fluid case, there are actually two types of plane waves possible in an isotropic, elastic solid. They are called plane P-waves and plane S-waves. The P-waves are also referred to as pressure, compressional, primary, longitudinal (L), dilatational, or irrotational waves. Similarly, S-waves are also called shear, secondary, transverse (T), distortional, equivoluminal, or rotational waves. Both of these waves are *bulk waves* since they travel throughout the volume of a solid. A bulk P-wave is by far the most commonly used type of wave in NDE testing. If one places a plane wave solution of the form $\mathbf{u} = U\mathbf{n}\, f\left(t - \mathbf{x}\cdot\mathbf{n}/c_p\right)$ in Navier's equation (see Fig. D.5), that equation will be satisfied if

$$c_p = \sqrt{\frac{\lambda + 2\mu}{\rho}} = \sqrt{\frac{E(1-\nu)}{(1+\nu)(1-2\nu)\rho}}. \tag{D.19}$$

If we instead assume a plane wave solution that has the form $\mathbf{u} = U\mathbf{d} \times \mathbf{n}\, g(t - \mathbf{x}\cdot\mathbf{n}/c_s)$, where $\mathbf{d}$ is an arbitrary unit vector (see Fig. D.5(b)), in order to satisfy Navier's equations we find

$$c_s = \sqrt{\frac{\mu}{\rho}} = \sqrt{\frac{E}{2(1+\nu)\rho}}. \tag{D.20}$$

The quantities c_p, c_s are just the wave speeds for plane bulk P-waves and S-waves, respectively. For a structural material such as steel, for example, the P-wave speed is approximately 5900 m/sec while the S-wave speed is about 3200 m/sec, both of which are considerably larger than the wave speed for water (see Table D.1 for wave speeds and other properties of some selected materials). From Eqs. (D.19) and (D.20) we can see that the ratio of these wave speeds is just a function of Poisson's ratio, i.e.

$$\frac{c_p}{c_s} = \sqrt{\frac{2(1-\nu)}{(1-2\nu)}}, \tag{D.21}$$

which for many structural materials gives a ratio of about two to one.

Table D.1. Acoustic properties of some common materials.

Material	P-wave speed [m/s x 10^3]	S-wave speed [m/sx10^3]	Density [kgm/m^3x10^3]	Impedance (P-wave) [kgm/(m^2-s) x 10^6]
Air	0.33	--	0.0012	0.0004
Aluminum	6.42	3.04	2.70	17.33
Brass	4.70	2.10	8.64	40.60
Copper	5.01	2.27	8.93	44.60
Glass	5.64	3.28	2.24	13.10
Lucite	2.70	1.10	1.15	3.10
Nickel	5.60	3.00	8.84	49.50
Steel, mild	5.90	3.20	7.90	46.00
Titanium	6.10	3.10	4.48	27.30
Tungsten	5.20	2.90	19.40	101.00
Water	1.48	--	1.00	1.48

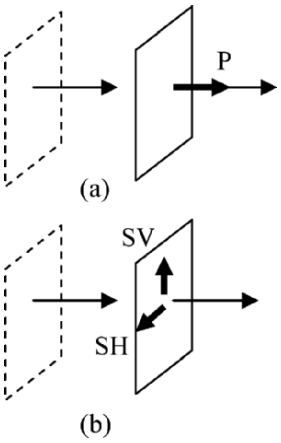

Fig. D.6. The polarizations of **(a)** P-waves, and **(b)** vertically polarized (SV) shear waves and horizontally polarized (SH) waves.

As shown in Fig. D.5 (a), the direction of the displacement in the P-wave is along the direction of propagation, **n**, while for an S-wave (Fig. D.5 (b)), the displacement lies in the plane of the wave front, i.e. perpendicular to **n**. Thus, P-waves are said to have longitudinal polarizations while S-wave are said to have transverse polarizations. Figure D.6 shows the polarizations for P-waves and S-waves and also shows that if the polarization (direction of motion) of the plane shear wave lies in a vertical plane, it is called an SV-wave (vertically-polarized shear), while if the polarization lies in a horizontal plane it is called an SH-wave (horizontally-polarized shear). In general, an S-wave may have both vertical and horizontal polarizations combined.

To solve wave propagation problems in elastic solids, many authors represent the displacement in terms of potential functions in the form

$$\mathbf{u} = \nabla\phi + \nabla \times \boldsymbol{\psi}, \tag{D.22}$$

where ϕ is a scalar potential and $\boldsymbol{\psi} = (\psi_1, \psi_2, \psi_3) \equiv (\psi_x, \psi_y, \psi_z)$ is a vector potential. The advantage of using such potentials is that in order to satisfy Navier's equations the potentials must satisfy the ordinary wave equations:

$$\begin{aligned}\nabla^2\phi - \frac{1}{c_p^2}\frac{\partial^2\phi}{\partial t^2} &= 0 \\ \nabla^2\boldsymbol{\psi} - \frac{1}{c_s^2}\frac{\partial^2\boldsymbol{\psi}}{\partial t^2} &= 0.\end{aligned} \tag{D.23}$$

Equation (D.23) shows that the scalar potential, ϕ, represents P-waves while the vector potential, $\boldsymbol{\psi}$, represents S-waves. In solving wave problems with potentials if the disturbance is two-dimensional where the displacements $\left(u_x, u_y\right)$ are the only non-zero displacements and they only depend on the *x*- and *y*-coordinates, only two potentials are needed:

$$\begin{aligned}\phi &= \phi\left(x, y, t\right) \\ \psi_z &= \psi\left(x, y, t\right), \psi_x = \psi_y = 0\end{aligned} \tag{D.24}$$

and the displacements are given by

$$\begin{aligned}u_x &= \frac{\partial\phi}{\partial x} + \frac{\partial\psi}{\partial y} \\ u_y &= \frac{\partial\phi}{\partial y} - \frac{\partial\psi}{\partial x} \\ u_z &= 0.\end{aligned} \tag{D.25}$$

In this case the stresses are also given by

$$\begin{aligned}\tau_{xx} &= \mu\left[\kappa^2\nabla^2\phi + 2\left(\frac{\partial^2\psi}{\partial x\partial y} - \frac{\partial^2\phi}{\partial y^2}\right)\right] \\ \tau_{yy} &= \mu\left[\kappa^2\nabla^2\phi - 2\left(\frac{\partial^2\psi}{\partial x\partial y} + \frac{\partial^2\phi}{\partial x^2}\right)\right] \\ \tau_{xy} &= \mu\left[2\frac{\partial^2\phi}{\partial x\partial y} + \frac{\partial^2\psi}{\partial y^2} - \frac{\partial^2\psi}{\partial x^2}\right] \\ \tau_{zz} &= \nu\left[\tau_{xx} + \tau_{yy}\right],\ \tau_{xz} = \tau_{yz} = 0\end{aligned} \tag{D.26}$$

where $\kappa = c_p / c_s$.

For a harmonic plane P-wave traveling in the positive *x*-direction, as shown in Fig. D.7 (a), we can express the wave either in terms of its potential, ϕ, displacement, u_x, velocity, v_x or stress, τ_{xx}:

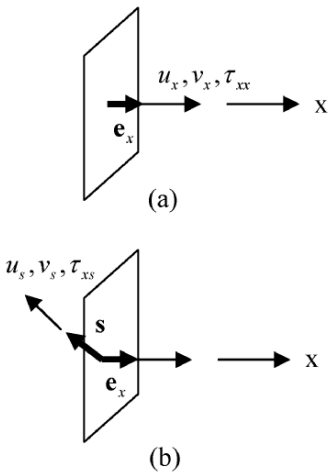

Fig. D.7. The displacement, velocity and stress **(a)** for a plane P-wave, and **(b)** for a plane S-wave, both traveling in the *x*-direction.

$$\begin{aligned} \phi &= \Phi \exp\left(ik_p x - i\omega t\right) \\ u_x &= U_x \exp\left(ik_p x - i\omega t\right) \\ v_x &= V_x \exp\left(ik_p x - i\omega t\right) \\ \tau_{xx} &= T_{xx} \exp\left(ik_p x - i\omega t\right) \end{aligned} \tag{D.27}$$

where $k_p = \omega / c_p$ is the wave number for P-waves and the amplitudes are all related:

$$\begin{aligned} U_x &= ik_p \Phi \\ V_x &= -i\omega U_x \\ T_{xx} &= -\rho c_p V_x \end{aligned} \tag{D.28}$$

For a harmonic plane S-wave we can also use the potential, ψ, displacement, u_s, velocity, v_s, or stress, τ_{xs}, to describe the wave and we have instead (Fig. D.7 (b)):

$$\begin{aligned}\boldsymbol{\psi} &= \Psi \mathbf{t} \exp\left(ik_s x - i\omega t\right)\\ \mathbf{u} &= U_s \mathbf{s} \exp\left(ik_s x - i\omega t\right)\\ \mathbf{v} &= V_s \mathbf{s} \exp\left(ik_s x - i\omega t\right)\\ \tau_{xs} &= T_{xs} \exp\left(ik_s x - i\omega t\right)\end{aligned} \tag{D.29}$$

where $\mathbf{t}$ is an arbitrary unit vector, $\mathbf{e}_x$ is a unit vector in the x-direction, $\mathbf{s} = \left(\mathbf{e}_x \times \mathbf{t}\right)/\left|\mathbf{e}_x \times \mathbf{t}\right|$ is a unit vector in the plane of the wave front, and $k_s = \omega / c_s$ is the wave number for shear waves. In this case the amplitude relations are

$$\begin{aligned}U_s &= ik_s \Psi\\ V_s &= -i\omega U_s\\ T_{xs} &= -\rho c_s V_s\end{aligned} \tag{D.30}$$

To obtain these relations in the P-wave case we have used the fact that u_x is the only non-zero displacement component in the wave and the only corresponding velocity component is $v_x = \partial u_x / \partial t$. In this case the constitutive equation for the solid (generalized Hooke's law) gives

$$\begin{aligned}\tau_{xx} &= \left(\lambda + 2\mu\right)\frac{\partial u_x}{\partial x} = \frac{E\left(1-\nu\right)}{\left(1+\nu\right)\left(1-2\nu\right)}\frac{\partial u_x}{\partial x}\\ &= \rho c_p^2 \frac{\partial u_x}{\partial x}.\end{aligned} \tag{D.31}$$

Similarly, in the S-wave case we have used the fact that the only non-zero displacement component in the wave is u_s, the displacement in the **s**-direction, and so the only corresponding velocity component is also $v_s = \partial u_s / \partial t$. In this case the constitutive equation gives

$$\begin{aligned}\tau_{xs} &= \mu \frac{\partial u_s}{\partial x}\\ &= \rho c_s^2 \frac{\partial u_s}{\partial x}.\end{aligned} \tag{D.32}$$

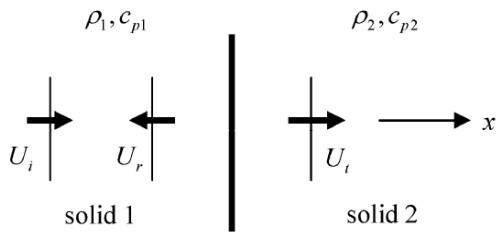

Fig. D.8. A plane P-wave incident on a planar interface between two solids.

D.5 Reflection/Refraction of Plane Waves – Normal Incidence

As a simple but important example of the use of these plane wave relations, consider the reflection and transmission of a plane harmonic P-wave that strikes a planar interface between two solids at normal incidence as shown in Fig. D.8. The density and compressional wave speed in solids one and two are $\left(\rho_1, c_{p1}\right)$, and $\left(\rho_2, c_{p2}\right)$, respectively. The displacements of the incident, reflected, and transmitted plane waves are given by

$$\begin{aligned} u_x &= U_i \exp\left(ik_1 x - i\omega t\right) \\ u_x &= -U_r \exp\left(-ik_1 x - i\omega t\right) \\ u_x &= U_t \exp\left(ik_2 x - i\omega t\right) \end{aligned} \tag{D.33}$$

where $k_1 = \omega / c_{p1}, k_2 = \omega / c_{p2}$. We have taken the reflected wave expression with a minus sign so that U_r represents the amplitude of a plane wave traveling in the –x-direction with polarization vector in the direction of propagation, i.e. the vector displacement of the reflected wave would be given by $\mathbf{u} = U_r \mathbf{e}_r \exp\left(ik_1 \mathbf{e}_r \cdot \mathbf{x} - i\omega t\right)$ where $\mathbf{e}_r = -\mathbf{e}_x$, $\mathbf{x} = x\mathbf{e}_x$. At the interface $x = 0$ the displacement u_x and the stress $\tau_{xx} = \rho c_p^2 \, \partial u_x / \partial x$ must be continuous so we find

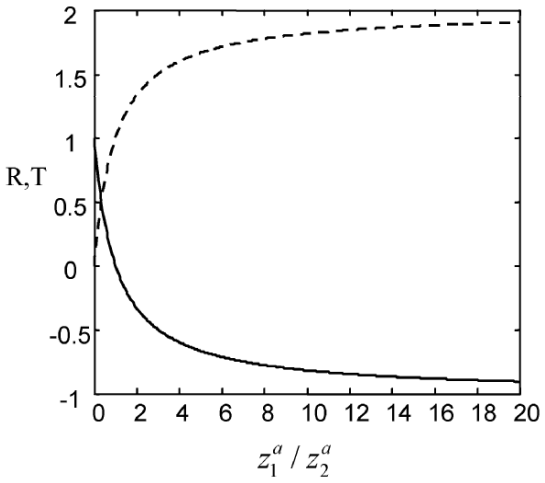

Fig. D.9. The reflection coefficient (solid line) and transmission coefficient (dashed line) versus the impedance ratio z_1^a / z_2^a.

Continuity of displacement: $$U_i - U_r = U_t \tag{D.34}$$

Continuity of stress: $$\rho_1 c_{p1} U_i + \rho_1 c_{p1} U_r = \rho_2 c_{p2} U_t \tag{D.35}$$

Solving Eqs. (D.34) and (D.35) simultaneously we find

$$\begin{aligned} T_u &= \frac{U_t}{U_i} = \frac{2\rho_1 c_{p1}}{\rho_1 c_{p1} + \rho_2 c_{p2}} \\ R_u &= \frac{U_r}{U_i} = \frac{\rho_2 c_{p2} - \rho_1 c_{p1}}{\rho_1 c_{p1} + \rho_2 c_{p2}} \end{aligned} \tag{D.36}$$

where (T_u, R_u) are the plane wave transmission and reflection coefficients (based on ratios of displacements). From Eq. (D.36) it follows that these reflection and transmission coefficients are dependent only on the specific acoustic impedances $z_1^a = \rho_1 c_{p1}, z_2^a = \rho_2 c_{p2}$. Figure D.9 plots the behavior of these coefficients versus z_1^a / z_2^a.

The limit $z_1^a / z_2^a \to \infty$ would correspond to the reflection from a free surface. In that case we see $R \to -1$ so that the total displacement $U_i - U_r$ at the interface in the first medium would be double that of the incident wave. The other limit where $z_1^a / z_2^a \to 0$ would correspond to the wave incident on a very rigid boundary. In that case $R \to 1$ so the total displacement at the interface in the first medium would be zero. For the special case where the acoustic impedances of the two solids are matched ($z_1^a / z_2^a = 1$), we see that $R = 0, T = 1$ so that there is no reflected wave and the incident wave passes through the interface with its amplitude unchanged.

These same reflection and transmission coefficients could be used for the reflection of a plane S-wave at normal incidence to a solid-solid interface if we simply replace the compressional wave speeds by the corresponding shear wave speeds, i.e.

$$\begin{aligned} T_u &= \frac{U_t}{U_i} = \frac{2\rho_1 c_{s1}}{\rho_1 c_{s1} + \rho_2 c_{s2}} \\ R_u &= \frac{U_r}{U_i} = \frac{\rho_2 c_{s2} - \rho_1 c_{s1}}{\rho_1 c_{s1} + \rho_2 c_{s2}}. \end{aligned} \tag{D.37}$$

The coefficients could also be used for a fluid-fluid or fluid-solid interface (as encountered in immersion testing) by appropriately replacing the densities and wave speeds in Eq. (D.36) or Eq. (D.37). However, note that these coefficients are based on displacement ratios and if we want to use the ratios of other quantities we may have to make appropriate adjustments. To use velocity ratios, for example, we do not need to make any changes since

$$\begin{aligned} R_v &= \frac{V_r}{V_i} = \frac{-i\omega U_r}{-i\omega U_i} = \frac{U_r}{U_i} = R_u \\ T_v &= \frac{V_t}{V_i} = \frac{-i\omega U_t}{-i\omega U_i} = \frac{U_t}{U_i} = T_u. \end{aligned} \tag{D.38}$$

Equations (D.31) and (D.32) show that $\tau = \rho c^2 \, \partial u / \partial x$ is valid for either plane P-waves or S-waves in a solid if we use the appropriate τ , c and u in this relationship. Similarly, for a fluid we have $p = -\rho c^2 \partial u / \partial x$. As mentioned previously, we combined these relations with the relationship between displacement and velocity, $v = \partial u / \partial t$ to obtain the various plane wave amplitude relationships given by Eqs. (D.28) and (D.29). For a plane wave

traveling in the + x-direction with a stress amplitude, T, and velocity amplitude, V, we found $T = -\rho cV$. For a pressure amplitude, P, we found $P = \rho cV$. Obviously, we can use these relations for the incident and transmitted waves since they are both traveling in the + x-direction. However, because we placed the minus sign on the reflected wave in Eq. (D.33), we can also use these same relations for the reflected wave as well. Thus, if we define, for example, reflection and transmission coefficients based on stress ratios we would find (also using Eq. (D.38))

$$R_\tau = \frac{-\rho_1 c_{p1} V_r}{-\rho_1 c_{p1} V_i} = R_u = \frac{\rho_2 c_{p2} - \rho_1 c_{p1}}{\rho_1 c_{p1} + \rho_2 c_{p2}}$$
$$T_\tau = \frac{-\rho_2 c_{p2} V_t}{-\rho_1 c_{p1} V_i} = \frac{\rho_2 c_{p2}}{\rho_1 c_{p1}} T_u = \frac{2\rho_2 c_{p2}}{\rho_1 c_{p1} + \rho_2 c_{p2}} \tag{D.39}$$

which are also valid for reflection and transmission coefficients based on pressure ratios since there are then changes of signs in the coefficients shown in Eq. (D.39) in both the numerator and denominator that cancel. In the SI system the units of specific acoustic impedance are kgm/(m^2-sec). This set of units is also called a *Rayl*, i.e. 1 Rayl = 1 kgm/(m^2-sec).

For water we have $z_w^a = 1.5 \times 10^6$ kgm/(m^2 –sec) = 1.5 MRayls and for steel $z_s^a = 46.0 \times 10^6$ kgm/(m^2 –sec) = 46 MRayls, so that for a plane wave traveling in water at normal incidence to a water-steel interface R_u = –0.937, T_u = 0.06. Because of this high impedance mismatch, we see that in immersion testing most of an ultrasonic beam will be reflected back into the water at normal incidence.

D.6 Reflection/Refraction of Plane Waves – Oblique Incidence

When plane waves are incident on a plane interface at oblique incidence, there are additional aspects of the interactions that one does not see with the normal incidence case. Consider, for example, the simple problem of a plane wave at oblique incidence to a plane interface between two fluids, as shown in Fig. D.10, where ρ_1, c_{p1} are the density and compressional wave speed of medium 1 and ρ_2, c_{p2} are the corresponding density and wave speed for medium 2. Although this problem does not correspond to one we would likely see in NDE testing, most of the physics involved in more

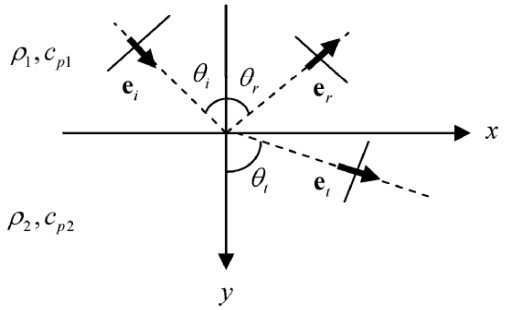

Fig. D.10. A plane wave incident on an interface between two fluids.

complicated plane wave interactions at fluid-solid and solid-solid interfaces are the same as in this problem [Fundamentals]. Here, the total pressure, p_1, due the incident and reflected waves in medium 1 and the total pressure, p_2, due to the transmitted waves in medium 2 are given by

$$\begin{aligned} p_1 &= P_i \exp\left[ik_{p1}\left(x\sin\theta_i + y\cos\theta_i\right) - i\omega t\right] \\ &\quad + P_r \exp\left[ik_{p1}\left(x\sin\theta_r - y\cos\theta_r\right) - i\omega t\right] \\ p_2 &= P_t \exp\left[ik_{p2}\left(x\sin\theta_t + y\cos\theta_t\right) - i\omega t\right]. \end{aligned} \tag{D.40}$$

From the equations of motion we have

$$-\frac{\partial p}{\partial y} = -i\omega\rho\, v_y \tag{D.41}$$

so that the total velocity, v_y, in each medium is

$$\begin{aligned} \left(v_y\right)_1 &= \frac{P_i\cos\theta_i}{\rho_1 c_{p1}} \exp\left[ik_{p1}\left(x\sin\theta_i + y\cos\theta_i\right) - i\omega t\right] \\ &\quad - \frac{P_r\cos\theta_r}{\rho_1 c_{p1}} \exp\left[ik_{p1}\left(x\sin\theta_r - y\cos\theta_r\right) - i\omega t\right] \\ \left(v_y\right)_2 &= \frac{P_t\cos\theta_t}{\rho_2 c_{p2}} \exp\left[ik_{p2}\left(x\sin\theta_t + y\cos\theta_t\right) - i\omega t\right]. \end{aligned} \tag{D.42}$$

At the interface ($y = 0$), the boundary conditions are

$$\begin{aligned} p_1 &= p_2 \\ \left(v_y\right)_1 &= \left(v_y\right)_2 \end{aligned} \tag{D.43}$$

so that we find (dividing out all common terms)

$$\begin{aligned} &P_i \exp\left(ik_{p1} x \sin\theta_i\right) + P_r \exp\left(ik_{p1} x \sin\theta_r\right) \\ &= P_t \exp\left(ik_{p2} x \sin\theta_t\right) \\ &\frac{P_i \cos\theta_i}{\rho_1 c_{p1}} \exp\left(ik_{p1} x \sin\theta_i\right) - \frac{P_r \cos\theta_r}{\rho_1 c_{p1}} \exp\left(ik_{p1} x \sin\theta_r\right) \\ &= \frac{P_t \cos\theta_t}{\rho_2 c_{p2}} \exp\left(ik_{p2} x \sin\theta_t\right). \end{aligned} \tag{D.44}$$

For these boundary conditions to be satisfied for all x along the boundary we must have the phase terms in Eq. (D.44) all match, which gives

$$k_{p1} \sin\theta_i = k_{p1} \sin\theta_r = k_{p2} \sin\theta_t. \tag{D.45}$$

The first pair of these equations gives

$$\theta_i = \theta_r \tag{D.46a}$$

while the second pair gives

$$\frac{\sin\theta_i}{c_{p1}} = \frac{\sin\theta_t}{c_{p2}}. \tag{D.46b}$$

Equation (D.46a) shows that the angle of incidence equals the angle of reflection while Eq. (D.46b) is a statement of *Snell's law* for the transmitted angle in terms of the incident angle. Applying these phase matching conditions to Eq. (D.44), we obtain

$$\begin{aligned} P_i + P_r &= P_t \\ \frac{P_i \cos\theta_i}{\rho_1 c_{p1}} - \frac{P_r \cos\theta_i}{\rho_1 c_{p1}} &= \frac{P_t \cos\theta_t}{\rho_2 c_{p2}}. \end{aligned} \tag{D.47}$$

These equations can be solved for the transmission and reflection coefficient (in terms of pressure) given by:

$$T_p = \frac{P_t}{P_i} = \frac{2\rho_2 c_{p2}\cos\theta_i}{\rho_1 c_{p1}\cos\theta_t + \rho_2 c_{p2}\cos\theta_i}$$
$$R_p = \frac{P_r}{P_i} = \frac{\rho_2 c_{p2}\cos\theta_i - \rho_1 c_{p1}\cos\theta_t}{\rho_1 c_{p1}\cos\theta_t + \rho_2 c_{p2}\cos\theta_i} \tag{D.48}$$

or, equivalently, in terms of velocity ratios (using $P = \rho c V$)

$$T_v = \frac{V_t}{V_i} = \frac{2\rho_1 c_{p1}\cos\theta_i}{\rho_1 c_{p1}\cos\theta_t + \rho_2 c_{p2}\cos\theta_i}$$
$$R_v = \frac{V_r}{V_i} = \frac{\rho_2 c_{p2}\cos\theta_i - \rho_1 c_{p1}\cos\theta_t}{\rho_1 c_{p1}\cos\theta_t + \rho_2 c_{p2}\cos\theta_i}. \tag{D.49}$$

These coefficients are functions of the acoustic impedances of the two media and the incident angle, θ_i, since by Snell's law

$$\cos\theta_t = \sqrt{1-\sin^2\theta_t} = \sqrt{1-\frac{c_{p2}^2}{c_{p1}^2}\sin^2\theta_i}\ . \tag{D.50}$$

At normal incidence we see that these results simply reduce to those found previously for that special case.

Equation (D.50) shows that when $\sin\theta_i < c_{p1}/c_{p2}$ the $\cos\theta_t$ term is real and both the reflection and transmission coefficients are merely real numbers. This condition is always true when the wave speed for the second medium is slower than that of the first medium since in that case $c_{p1}/c_{p2} > 1$. For the case when the second medium has a faster wave speed, however, the cosine term will only be real for a range of incident angles $0 \le \theta \le \theta_{cr}$, where

$$\theta_{cr} = \sin^{-1}\left(c_{p1}/c_{p2}\right) \tag{D.51}$$

is called the *critical angle*. For incident angles exceeding this critical angle, the reflection and transmission coefficients will become complex. In fact these coefficients will also become frequency dependent. To see this, consider Eq. (D.40). From that equation we see that the only exponential term affected by the critical angle is in the transmitted wave pressure term where $\cos\theta_t$ appears. That term is

$$p_2 = P_t \exp\left[i\omega\left(x\sin\theta_t + y\cos\theta_t\right)/c_{p2} - i\omega t\right]. \tag{D.52}$$

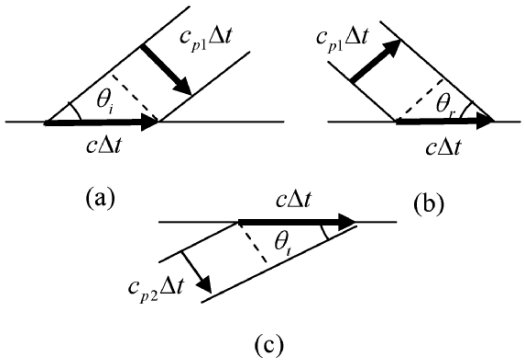

Fig. D.11. (a) The incident wave front, showing its propagation in a time Δt, and its apparent wave speed $c = c_{p1} / \sin\theta_i$ along the interface ; **(b)** the corresponding reflected wave front and its apparent wave speed $c = c_{p1} / \sin\theta_r$ along the interface; **(c)** the transmitted wave front and its apparent wave speed $c = c_{p2} / \sin\theta_t$ along the interface. By Snell's law, the wave speed, *c*, along the interface is the same for all three waves.

Beyond the critical angle we can let

$$\cos\theta_t = \pm i\sqrt{\sin^2\theta_t - 1} = \pm i\sqrt{\frac{c_{p2}^2}{c_{p1}^2}\sin^2\theta_i - 1} \tag{D.53}$$

and Eq. (D.52) becomes

$$\begin{aligned} p_2 &= P_t \exp\left[\pm\omega y\sqrt{\frac{c_{p2}^2}{c_{p1}^2}\sin^2\theta_i - 1}\right]\exp\left[i\omega x\sin\theta_t / c_{p2} - i\omega t\right] \\ &= P_t \exp\left[\pm\omega y\gamma\right]\exp\left[i\omega x / c - i\omega t\right]. \end{aligned} \tag{D.54}$$

where $\gamma = \sqrt{\frac{c_{p2}^2}{c_{p1}^2}\sin^2\theta_i - 1}$ is a real constant and $c = c_{p2} / \sin\theta_t = c_{p1} / \sin\theta_i$ is the apparent wave speed along the interface of all the waves (incident, reflected, and transmitted) as shown in Fig. D.11. From Eq. (D.54) the transmitted pressure will be a wave traveling along the interface with wave speed *c* and an amplitude that varies exponentially in *y*. However, this amplitude physically must decay to zero as *y* becomes infinitely large for all frequencies, ω, both positive and negative, so we must choose the

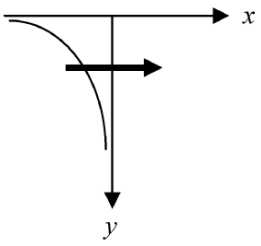

Fig. D.12. An inhomogeneous wave traveling along the interface.

positive sign in Eq. (D.54) for $\omega > 0$ and the negative sign in Eq. (D.54) for $\omega < 0$, i.e. we must let

$$\cos\theta_t = i\,\mathrm{sgn}\,\omega\sqrt{\sin^2\theta_t - 1} = i\,\mathrm{sgn}\,\omega\sqrt{\frac{c_{p2}^2}{c_{p1}^2}\sin^2\theta_i - 1} \tag{D.55}$$

where

$$\mathrm{sgn}\,\omega = \begin{cases} +1 & \omega > 0 \\ -1 & \omega < 0 \end{cases}. \tag{D.56}$$

With this choice then the transmitted pressure is given by

$$\begin{aligned} p_2 &= P_t \exp\left[-|\omega| y\gamma\right]\exp\left[i\omega x/c - i\omega t\right] \\ &= P_t \exp\left[-|\omega| y\sqrt{\frac{c_{p2}^2}{c_{p1}^2}\sin^2\theta_i - 1}\right]\exp\left[i\omega x \sin\theta_t / c_{p2} - i\omega t\right], \end{aligned} \tag{D.57}$$

which represents an *inhomogeneous wave* traveling along the interface and decaying exponentially into the second medium as shown in Fig. D.12. Beyond the critical angle, both the transmission and reflection coefficients are complex and frequency dependent because the $\cos\theta_t$ appearing in those coefficients is given by Eq. (D.55). When we consider an incident plane pulse and use these reflection and transmission coefficients and Fourier transforms to obtain the reflected and transmitted pulses at the interface, the frequency dependency in these coefficients will lead to reflected and transmitted waves that do not have the same shape as the incident waves, a phenomenon called *pulse distortion*. Note that below the critical angle, a reflected or transmitted wave pulse will have different

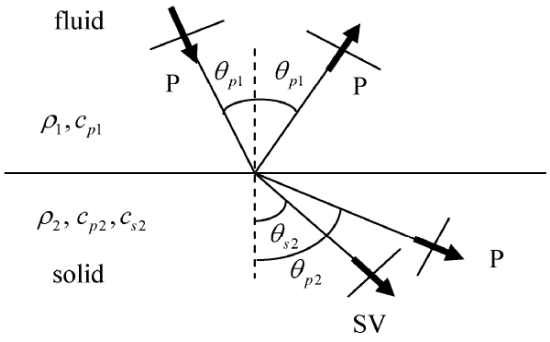

Fig. D.13. A plane wave in a fluid incident on a fluid-solid interface at oblique incidence.

amplitudes from the incident wave but will have exactly the same shape waveform as that of the incident wave.

Although we have only considered a fluid problem here, the behavior of plane waves at solid interfaces is very similar. Consider, for example, the reflection and transmission of a plane wave in a fluid at a fluid-solid interface, as would be encountered in immersion testing (Fig. D.13).The main difference between this case and the fluid-fluid case just considered is that the plane P-wave in the fluid generates both plane P- and SV-waves in the solid. The generation of a wave type by a different wave type is called *mode conversion*. The angles of each of the waves are given here by *generalized Snell's law* so that we have the angle of the reflected P-wave in the fluid equal to the incident P-wave angle, as shown in Fig. D.13, and we have

$$\frac{\sin\theta_{p1}}{c_{p1}} = \frac{\sin\theta_{p2}}{c_{p2}} = \frac{\sin\theta_{s2}}{c_{s2}}, \tag{D.58}$$

where c_{p1} is the compressional wave speed of the fluid and c_{p2}, c_{s2} are the compressional and shear wave speeds of the solid, respectively. Another difference from the fluid-fluid problem is that in this case there can be two critical angles. Above the first critical angle $\theta_{p1} = (\theta_{cr})_1 = \sin^{-1}(c_{p1}/c_{p2})$ the transmitted P-wave becomes an inhomogeneous P-wave traveling along the interface and there is only a transmitted SV-wave, as shown in Fig. D.14 (a). Such a critical angle will exist as long as the compressional

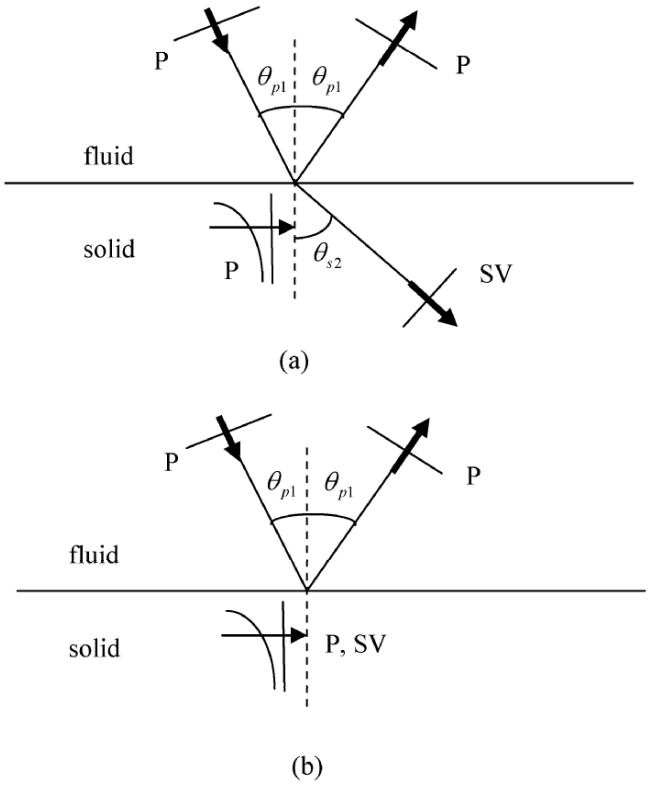

Fig. D.14. (a) The case when the incident angle is greater than the first critical angle and **(b)** the case when the incident angle is greater than the second critical angle.

wave speed of the solid is larger than the compressional wave speed of the fluid ($c_{p2} > c_{p1}$), which is satisfied for water and most structural materials. Above the second critical angle $\theta_{p1} = (\theta_{cr})_2 = \sin^{-1}(c_{p1}/c_{s2})$ the SV-wave also becomes an inhomogeneous wave as shown in Fig. D.14 (b). This critical angle will exist if the shear wave speed in the solid is larger than the compressional wave speed of the fluid ($c_{s2} > c_{p1}$), which again is normally satisfied for water and most common structural materials.

The fluid-solid interface problem can be solved in manner similar to the fluid-fluid problem to obtain the plane wave reflection and transmission

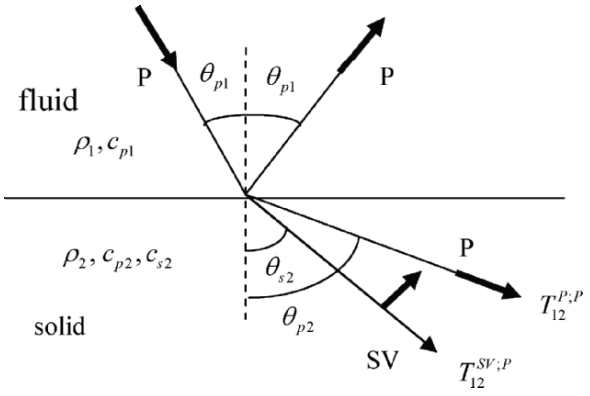

Fig. D.15. The polarization directions chosen for the reflected and transmitted waves.

coefficients. The transmission coefficients, for example, (based on velocity ratios) are given by:

$$T_{12}^{P;P} = \frac{2\cos\theta_{p1}\left[1-2\left(\sin\theta_{s2}\right)^2\right]}{\cos\theta_{p2} + \dfrac{\rho_2 c_{p2}}{\rho_1 c_{p1}}\cos\theta_{p1}\Delta}$$

$$T_{12}^{SV;P} = \frac{-4\cos\theta_{p1}\cos\theta_{p2}\sin\theta_{s2}}{\cos\theta_{p2} + \dfrac{\rho_2 c_{p2}}{\rho_1 c_{p1}}\cos\theta_{p1}\Delta} \tag{D.59a}$$

with

$$\Delta = \left[4\left(\frac{c_{s2}}{c_{p2}}\right)^2 \sin\theta_{s2}\cos\theta_{s2}\sin\theta_{p2}\cos\theta_{p2} + 1 - 4\left(\sin\theta_{s2}\cos\theta_{s2}\right)^2\right]. \tag{D59.b}$$

Both transmission coefficients are given in the form $T_{12}^{\alpha;\beta}$, which denotes a transmission from medium 1 to medium 2 of a plane wave of type α $\left(\alpha = P, SV\right)$ due to an incident plane wave of type β $\left(\beta = P\right)$. The signs of these coefficients depend on the specific choice made for the polarization

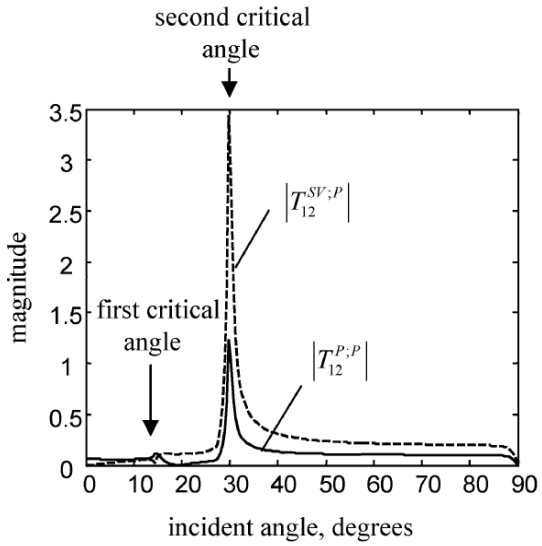

Fig. D.16. The magnitude of the plane wave transmission coefficients at a water-steel interface.

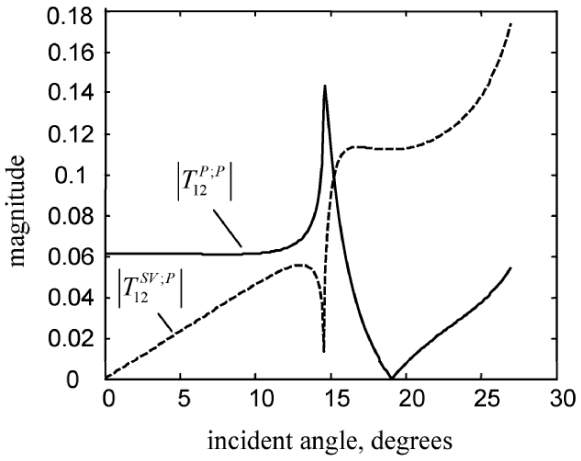

Fig. D.17. The magnitude of the plane wave transmission coefficients at a water-steel interface for incident angles below the second critical angle.

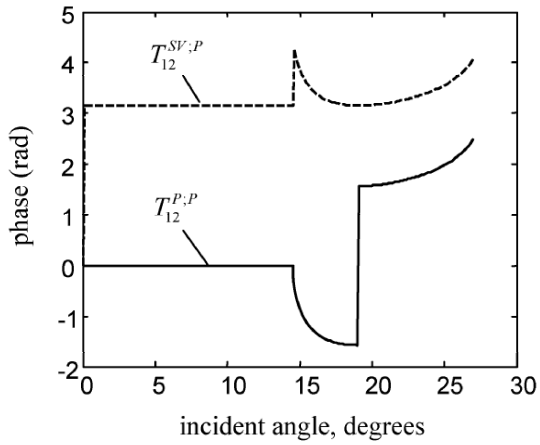

Fig. D.18. The phase (in radians) versus incident angle of the transmission coefficients at a water-steel interface.

directions of the transmitted P- and SV-waves. Here, the polarization directions are chosen as shown in Fig. D.15. When the shear wave speed $c_{s2} \to 0$, $T_{12}^{SV;P} \to 0$ and $T_{12}^{P;P}$ is the same transmission coefficient found previously for the fluid-fluid problem (see Eq. (D.49)). Figure D.16 shows a plot of the magnitude of these transmission coefficients versus the incident angle for a water-steel interface. Because of the relatively large values of these coefficients near the second critical angle, it is useful to consider only angles below that second critical angle, which is the range of most interest anyway since beyond the second critical angle there are no waves transmitted into the solid. Figure D.17 shows this expanded plot. The transmitted shear wave transmission coefficient is zero at normal incidence (incident angle = 0) where there is no mode conversion and increases almost linearly until near the first critical angle. The transmitted P-wave coefficient is small at normal incidence because of the large impedance mismatch between the water and steel and is almost constant until near the first critical angle. For angles near the first critical angle, both coefficients change rapidly in their magnitudes. Figure D.18 shows the corresponding behavior of the phase of the transmission coefficients for angles below the second critical angle. The phase of the transmitted P-wave is zero below the first critical angle because the coefficient is real. There is a phase jump of π radians at an incident angle of about 18.0 degrees (Fig. D.18) where the transmission coefficient changes sign.

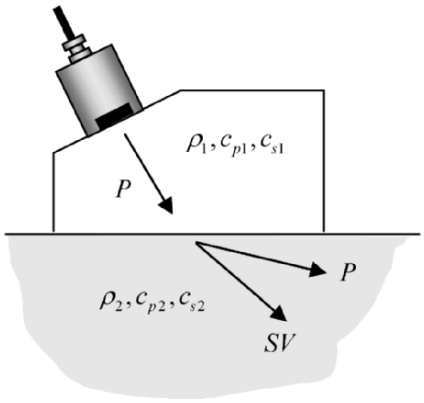

Fig. D.19. An angle beam transducer setup.

The phase of the transmitted SV-wave is π radians below the critical angle because the transmission coefficient is real but negative, i.e. the velocity of the transmitted wave is opposite to the assumed polarization direction shown in Fig. D.15.

As discussed in Appendix E, in angle beam testing a P-wave transducer is placed on a solid wedge which in turn is in contact with a solid that is to be inspected (see Fig. D.19). In this case a thin fluid couplant layer exists between the wedge and the underlying solid to guarantee that there is a good acoustic coupling between the wedge and the solid. If we neglect the thickness of the couplant layer then we can model this setup as two elastic solids in "smooth" and direct contact with each other where the shear stress must vanish at the wedge-solid boundary. In this case the transmission coefficients are given by [Fundamentals]

$$T_{12}^{P;P} = \frac{2\cos\theta_{p1}\left(1-2\sin^2\theta_{s2}\right)\left(1-2\sin^2\theta_{s1}\right)}{\Delta_1+\Delta_2}$$
$$T_{12}^{SV;P} = \frac{-4\sin\theta_{s2}\cos\theta_{p1}\cos\theta_{p2}\left(1-2\sin^2\theta_{s1}\right)}{\Delta_1+\Delta_2} \tag{D.60}$$

where

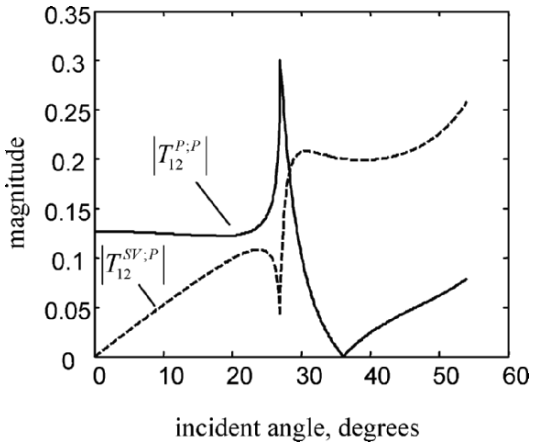

Fig. D.20. The plane wave transmission coefficients for a Lucite-steel interface where $\rho_1 = 1.18\ gm/cm^3$, $\rho_2 = 7.9\ gm/cm^3$, $c_{p1} = 2670\ m/\sec$, $c_{s1} = 1120\ m/\sec$, $c_{p2} = 5900\ m/\sec$, $c_{s2} = 3200\ m/\sec$.

$$\Delta_1 = \cos\theta_{p2}\Big[1 - 4\sin^2\theta_{s1}\cos^2\theta_{s1} + 4\frac{c_{s1}^2}{c_{p1}^2}\sin\theta_{s1}\cos\theta_{s1}\sin\theta_{p1}\cos\theta_{p1}\Big] \tag{D.61a}$$

and

$$\Delta_2 = \frac{\rho_2 c_{p2}}{\rho_1 c_{p1}}\cos\theta_{p1}\Big[1 - 4\sin^2\theta_{s2}\cos^2\theta_{s2} + 4\frac{c_{s2}^2}{c_{p2}^2}\sin\theta_{s2}\cos\theta_{s2}\sin\theta_{p2}\cos\theta_{p2}\Big]. \tag{D.61b}$$

Again, these transmission coefficients are based on velocity ratios and the polarization directions are the same as shown in Fig. D.15. If we let the shear wave speed in the wedge (c_{s1}) go to zero in these expressions, then these transmission coefficients simply reduce to those for fluid-solid case. The magnitudes of these coefficients are plotted versus angle of incidence in Fig. D.20 for a Lucite (plexiglass) wedge in smooth contact with steel.

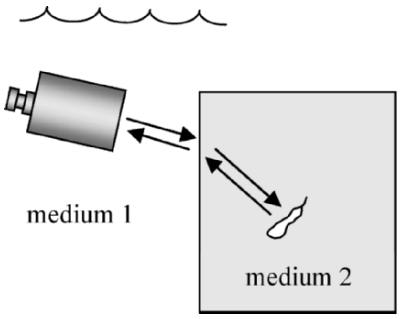

Fig. D.21. Pulse-echo immersion testing showing the transmission and reception of sound from a flaw along a completely reversed path through an interface.

Comparing Figs. D.17 and D.20 we see that the absolute magnitudes and critical angles are different in the two cases because of the wave speed differences but the overall behavior of the curves are very similar.

All the transmission and reflection coefficients discussed so far have been based on amplitude ratios. It is also possible to define similar coefficients that use energy intensity ratios instead. It can be shown that the *wave intensity*, *I*, which is defined as the average power flux (power/unit area) in a harmonic pressure wave in a fluid (where the average is carried out over one complete cycle of the wave) is given by [Fundamentals]

$$I = \frac{P^2}{2\rho c_p} = \frac{\rho c_p V^2}{2}, \tag{D.62}$$

where ρ is the density of the fluid, c_p is the compressional wave speed and P, V are the pressure and velocity amplitudes, respectively. Similarly, for harmonic plane waves in a solid we have for P-waves

$$I = \frac{T_{nn}^2}{2\rho c_p} = \frac{\rho c_p V_n^2}{2}, \tag{D.63}$$

where T_{nn}, V_n are the normal stress and velocity amplitudes, respectively, and c_p is the P-wave speed. For shear waves

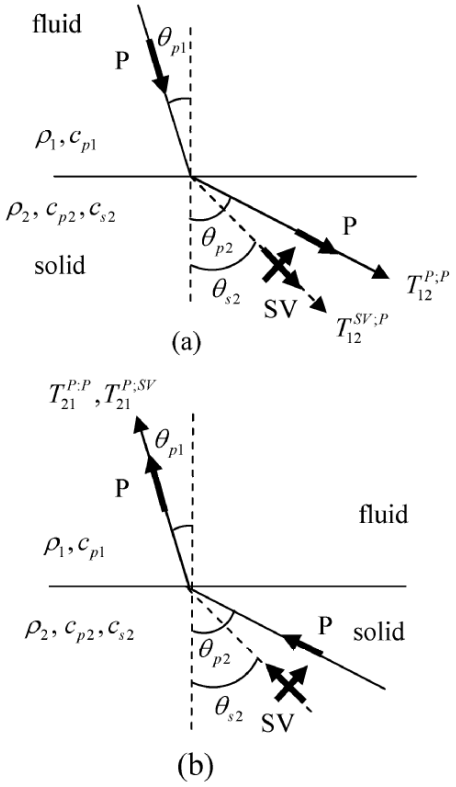

Fig. D.22. (a) Transmission coefficients when going from a fluid to a solid, and **(b)** the corresponding transmission coefficients for a completely reversed path going from the solid to the fluid.

$$I = \frac{T_{ns}^2}{2\rho c_s} = \frac{\rho c_s V_s^2}{2}, \tag{D.64}$$

where T_{ns}, V_s are shear stress and velocity amplitudes, respectively, and c_s is the shear wave speed.

In pulse-echo NDE immersion testing the same transducer is used as both a transmitter of sound and a receiver, as shown in Fig. D.21. In an ultrasonic flaw measurement, for example, if the waves transmitted to a flaw involve a transmission coefficient $T_{12}^{\alpha;P}\ (\alpha = P, SV)$ going from medium 1 (the fluid) to medium 2 (the flawed solid), the received waves

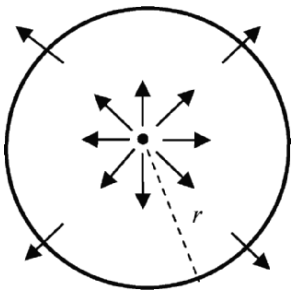

Fig. D.23. A spherical wave arising from a symmetrical point source in a fluid.

from the flaw will involve a transmission coefficient $T_{21}^{P;\alpha}$ going from medium 2 back to medium 1 along a completely reversed path, as shown. These transmission coefficients, however, are related to each other through *Stokes' relations* [Fundamentals], which are (see Fig. D.22):

$$\begin{aligned} T_{21}^{P;P} &= \frac{\rho_1 c_{p1} \cos\theta_{p2}}{\rho_2 c_{p2} \cos\theta_{p1}} T_{12}^{P;P} \\ T_{21}^{P;SV} &= \frac{\rho_1 c_{p1} \cos\theta_{s2}}{\rho_2 c_{s2} \cos\theta_{p1}} T_{12}^{SV;P}. \end{aligned} \tag{D.65}$$

D.7 Spherical Waves

A spherical wave, like a plane wave, is a special wave type that is very useful for describing the scattering properties of flaws and for constructing more general waves, including the waves generated from ultrasonic transducers [Fundamentals]. First, examine a spherical wave in a fluid. If we consider harmonic waves where the pressure, p, and velocity $\mathbf{v}$, are given by

$$\begin{aligned} p(\mathbf{x},t) &= p(\mathbf{x},\omega)\exp(-i\omega t) \\ \mathbf{v}(\mathbf{x},t) &= v(\mathbf{x},\omega)\exp(-i\omega t) \end{aligned} \tag{D.66}$$

then the equation of motion for the fluid (recall Eq. (D.3)) is

$$\nabla p(\mathbf{x},\omega) = i\omega \mathbf{v}(\mathbf{x},\omega) \tag{D.67}$$

and the wave equation for the pressure becomes the *Helmholtz equation*

$$\nabla^2 p(\mathbf{x},\omega) + k_p^2 p(\mathbf{x},\omega) = 0, \tag{D.68}$$

where $k_p = \omega / c_p$.

Consider a spherical wave in a fluid arising from a symmetrical point source as shown in Fig. D.23. Because of the symmetry, the equations of motion and the Helmholtz equation in spherical coordinates that describe this spherical wave are given by

$$\frac{\partial p}{\partial r} = i\omega\rho v_r \tag{D.69}$$

and

$$\frac{\partial^2 p}{\partial r^2} + \frac{2}{r}\frac{\partial p}{\partial r} + \frac{\omega^2}{c^2} p = 0, \tag{D.70}$$

where v_r is the radial velocity. There are two solutions of Eq. (D.70) given by

$$p = P_1 \frac{r_0}{r}\exp(ik_p r) + P_2 \frac{r_0}{r}\exp(-ik_p r), \tag{D.71}$$

where P_1, P_2 are pressure amplitudes and r_0 is a constant reference radius.

The first of these solutions represents a wave moving outwards from the source while the second moves toward the source. Since the source only generates outward-going waves we must set $P_2 = 0$. Letting $P_1 = P$ we find the pressure and velocity (using Eq. (D.69)) are

$$\begin{aligned} p &= P\frac{r_0}{r}\exp(ik_p r) \\ v_r &= \frac{Pr_0}{\rho c_p}\left[1 - \frac{1}{ik_p r}\right]\frac{\exp(ik_p r)}{r} = V\frac{r_0}{r}\exp(ik_p r). \end{aligned} \tag{D.72}$$

Unlike plane waves we see from Eq. (D.72) that the pressure amplitude, *P*, and velocity amplitude, *V*, of spherical waves are not just proportional to each other. However, at high frequencies (i.e. $k_p r >> 1$), we have approximately

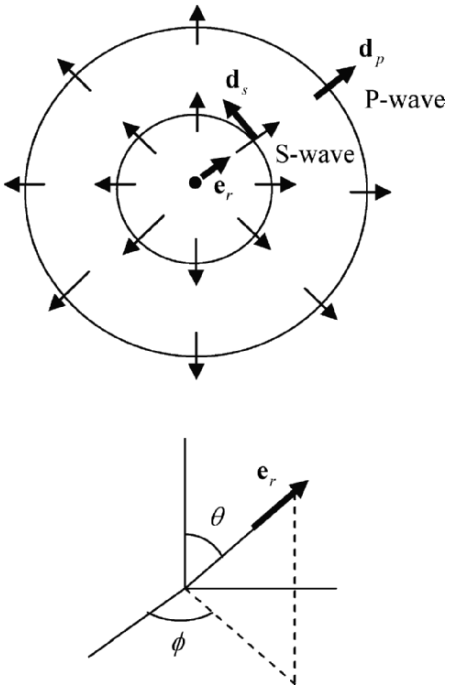

Fig. D.24. Spherical P- and S-waves from a point source in an elastic solid.

$$p = Pr_0 \frac{\exp\left(ik_p r\right)}{r}$$
$$v_r = \frac{Pr_0}{\rho c_p} \frac{\exp\left(ik_p r\right)}{r} = Vr_0 \frac{\exp\left(ik_p r\right)}{r} \tag{D.73}$$

so that P and V do just satisfy the plane wave relation $P = \rho c_p V$. In many ultrasonic NDE problems the frequencies and distances are large enough so that this high frequency approximation is valid.

In elastic solids one can also look for point source solutions to Navier's equations. The details are much more complicated than the fluid case because the sources of interest are usually not symmetric and there can be spherically spreading P-waves and S-waves that are coupled [Fundamentals]. However, at high frequencies, one can treat the waves from a source in a solid as separate traveling spherical waves, as shown in

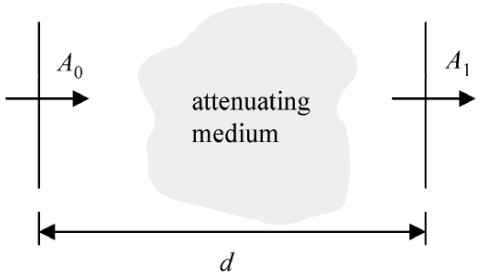

Fig. D.25. Propagation of a plane wave in an attenuating medium.

Fig. D.24 where the polarization of the P-wave, $\mathbf{d}_p$, is in the direction of propagation of the wave and the polarization, $\mathbf{d}_s$, of the shear wave is in a plane perpendicular to the propagation direction.

The displacement $\mathbf{u}(\mathbf{x},t) = \mathbf{u}(\mathbf{x},\omega)\exp(-i\omega t)$ in the solid is then given by

$$\mathbf{u}(\mathbf{x},\omega) = U_p \mathbf{d}_p r_0 \frac{\exp(ik_p r)}{r} + U_s \mathbf{d}_s r_0 \frac{\exp(ik_s r)}{r}, \tag{D.74}$$

where in general $U_p = U_p(\mathbf{e}_r(\theta,\phi),\omega), U_s = U_s(\mathbf{e}_r(\theta,\phi),\omega)$, i.e. the amplitudes are angular dependent, where θ,ϕ are the spherical coordinates defining a radial unit vector, $\mathbf{e}_r$, pointing in the direction of propagation as shown in Fig. D.24.

D.8 Ultrasonic Attenuation

All of the wave propagation models discussed in this Appendix have been for ideal, lossless media. At ultrasonic frequencies, however, there are material dependent losses that cause waves to attenuate as they propagate. Generally, the sources of the attenuation can be very complex. In metals, for example, attenuation can be due to scattering of the wave from the grain structure of the solid. One can use models to describe in some detail those scattering processes, but in most cases one can characterize the attenuation losses in a simpler, ad hoc fashion [Fundamentals]. Consider, for example, a plane wave traveling through an attenuating medium as shown in Fig. D.25. The amplitude of this wave will change as it propagates

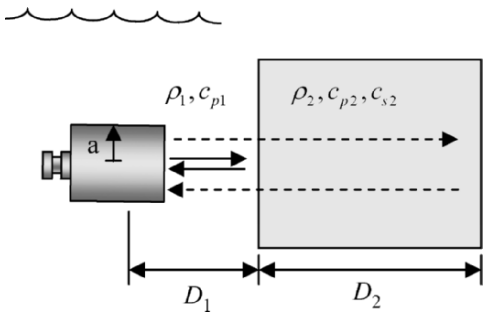

Fig. D.26. A measurement setup for determining the attenuation of P-waves in the solid block.

agates. We will model the effects of attenuation by an exponential factor that contains a frequency dependent attenuation coefficient, $\alpha(f)$, and express the amplitude changes in the form

$$\frac{A_1}{A_0} = \exp\left[-\alpha(f)d\right], \tag{D.75}$$

where d is the distance traveled in the medium. This attenuation coefficient is measured in Nepers/unit length (Np/l), where a Neper (Np) is a dimensionless quantity. It is also common to express the attenuation in terms of decibels/unit length (dB/l). To convert from Np/l to dB/l we have the relationship

$$\alpha_{dB/l} = 8.686\,\alpha_{Np/l}. \tag{D.76}$$

The attenuation of water as a function of temperature has been measured. At room temperature, the attenuation of water is [Fundamentals]

$$\alpha_w(f) = 25.3\times10^{-3} f^2 \quad Np/m, \tag{D.77}$$

where f is the frequency in MHz. Equation (D.77) is convenient to use to characterize the attenuation in the water tank of immersion studies. However, for other materials, such as metals, the attenuation is highly dependent on the material processing the metal has undergone so that tabulated values are generally not available and the attenuation must be measured. A convenient setup for making attenuation measurements is one

of the calibration setups discussed in Chapter 5 and shown in Fig. D.26. A planar transducer is used in a pulse-echo immersion arrangement to measure the waves reflected at normal incidence from both the front surface and back surface of a solid block whose P-wave attenuation is to be determined. As shown in Chapter 7 the frequency components of the received voltage from the front surface, $V_{fs}(\omega)$, and the frequency components of the voltage received from the back surface, $V_{bs}(\omega)$, can be expressed in the form

$$\begin{aligned} V_{fs}(\omega) &= s(\omega) t_A^{fs}(\omega) \\ V_{bs}(\omega) &= s(\omega) t_A^{bs}(\omega) \end{aligned} \tag{D.78}$$

where $s(\omega)$ is the system function of the measurement system that accounts for all the electrical and electromechanical components (pulser/receiver, cabling, transducer) and $t_A^{fs}(\omega), t_A^{bs}(\omega)$ are the acoustic/elastic transfer functions that account for all the wave processes, including attenuation, between the sending and receiving transducer. If both front and back surface measurements are done with the same components and at the same system settings, the system function is the same for both measurements, as indicated in Eq. (D.78).

The front surface transfer function is given in Chapter 5. We write this transfer function as

$$t_A^{fs}(\omega) = \tilde{t}_A^{fs}(\omega) \exp\left[-2\alpha_w(\omega) D_1\right], \tag{D.79}$$

where $\alpha_w(\omega)$ is the attenuation of the water and $\tilde{t}_A^{fs}(\omega)$ is the acoustic/elastic transfer function for the waves in the water without attenuation, given by (see Eq. (5.20)):

$$\tilde{t}_A^{fs}(\omega) = \tilde{D}_p\left(k_{p1} a^2 / 2D_1\right) R_{12} \exp\left(2ik_{p1} D_1\right), \tag{D.80}$$

where R_{12} is the plane wave reflection coefficient (Eq. (5.17)) for the fluid-solid interface. The $\tilde{D}_p$ coefficient is a diffraction correction (Eq. (5.20)) that accounts for the deviation of the waves in this setup from plane waves. In a similar manner, we can write the acoustic/elastic transfer function for the waves reflected from the back surface of the block as a transfer function for ideal materials, $\tilde{t}_A^{bs}(\omega)$, multiplied by an attenuation term to account for the attenuation of the waves in both the water and the solid [Fundamentals]:

$$t_A^{bs}(\omega) = \tilde{t}_A^{bs}(\omega)\exp\left[-2\alpha_w(\omega)D_1 - 2\alpha_{p2}(\omega)D_2\right] \tag{D.81}$$

with a loss free transfer function given by

$$\tilde{t}_A^{bs}(\omega) = \tilde{D}_p\left(k_{p1}a^2/2\bar{D}\right)T_{12}R_{21}T_{21}\exp\left(2ik_{p1}D_1 + 2ik_{p2}D_2\right), \tag{D.82}$$

where $\alpha_{p2}(\omega)$ is the attenuation coefficient for P-waves in the solid, R_{21} is the reflection coefficient from the back face (solid-fluid interface) of the block, T_{12} is the plane wave transmission coefficient at normal incidence (based on a pressure ratio) in going from the fluid to the solid, and T_{21} is the corresponding transmission coefficient in going from the solid to the fluid. The distance, $\bar{D}$, is given by

$$\bar{D} = D_1 + \frac{c_{p2}}{c_{p1}}D_2 \tag{D.83}$$

and c_{p1}, c_{p2} are the P-wave speeds of the fluid and the solid. It follows from Eqs. (D.78), (D.79) and (D.81) that

$$\left|\frac{V_{bs}(\omega)}{V_{fs}(\omega)}\right| = \left|\frac{\tilde{t}_A^{bs}(\omega)}{\tilde{t}_A^{fs}(\omega)}\right|\exp\left[2\alpha_{p2}(\omega)D_2\right] \tag{D.84}$$

or, equivalently

$$\exp\left[2\alpha_{p2}(\omega)D_2\right] = \left|\frac{V_{bs}(\omega)}{V_{fs}(\omega)}\right|\left|\frac{\tilde{t}_A^{fs}(\omega)}{\tilde{t}_A^{bs}(\omega)}\right|. \tag{D.85}$$

By measuring the received voltages for the front and back surface reflections from the block and using the known acoustic/elastic transfer functions in Eq. (D.85), one can solve for the attenuation coefficient as a function of frequency. Notice that the attenuation of the water is not needed as the water attenuation term is the same for both the front and back surface responses. So it cancels out in Eq. (D.85). Similarly, one does not need the system function since it also cancels out. Normally, the attenuation coefficient is fitted to a simple polynomial function (in frequency) over the bandwidth of the measurement. If the attenuation is needed over a wider range of frequencies, measurements with other transducers are needed. The setup of Fig. D.26 is suitable for measuring the attenuation of P-waves in the solid. However, in order to determine the

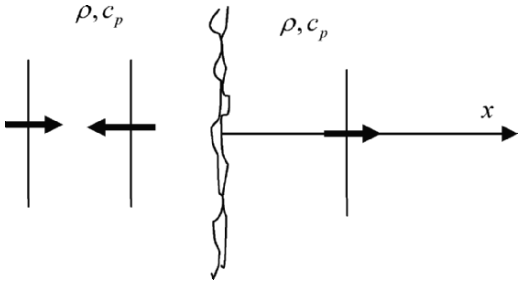

Fig. D.27. A plane P-wave incident on a rough interface.

attenuation of S-waves in the solid would require a different setup involving shear-wave transducers.

Introducing attenuation in this ad-hoc manner works well in describing attenuation effects when the attenuation is not too severe. For highly attenuating materials, however, the wave speed as well as the amplitude of the waves is affected by the attenuation, leading to *material dispersion e*ffects where this simple method of characterizing the attenuation is inadequate.

D.9 References

D.1 Cheeke JDN (2002) Fundamentals and applications of ultrasonic waves. CRC Press, Boca Raton, FL
D.2 Rose JL (1999) Ultrasonic waves in solid media. Cambridge University Press, Cambridge, UK
D.3 Harker AH (1988) Elastic waves in solids. Adam Hilger, Bristol, UK

D.10 Exercises

1. Consider the case where a solid is split along a rough planar interface which lies in the plane $x = 0$ as shown in Fig. D.27. The two parts of the solid are in contact over some places on the interface and are not in contact at other places. Where the two sides touch the stress τ_{xx} is continuous, and where the sides do not touch $\tau_{xx} = 0$ (on both sides) so again the stress is continuous. Where the sides touch the displacement u_x is continuous but where the sides do not touch there can be a displacement of one side

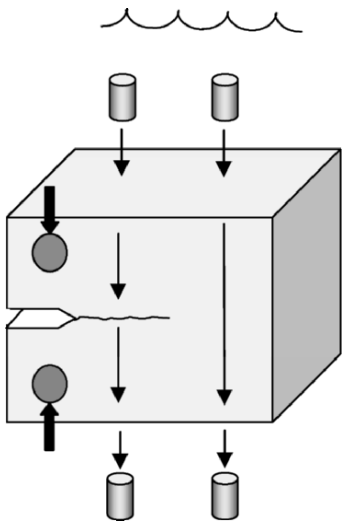

Fig. D.28. A measurement setup for ultrasonically examining a partially closed crack. Note that the crack extends across the entire width of the block.

relative to another. It is reasonable to expect that the amount of this relative displacement is proportional to the stress at the interface. Thus, under these conditions, we could expect that we might specify boundary conditions on the interface as:

continuity of stress:

$$\tau_{xx}\left(x=0^{-},t\right)=\tau_{xx}\left(x=0^{+},t\right)$$

stress proportional to the relative displacement:

$$\tau_{xx}\left(x=0,t\right)=\kappa_{s}\left[u_{x}\left(x=0^{+},t\right)-u_{x}\left(x=0^{-},t\right)\right].$$

The constant κ_s determines the relative "springiness" of the interface. The case $\kappa_s = 0$ corresponds to a stress free interface (no transmission) while $\kappa_s \to \infty$ means that the displacement is also continuous so that we have perfect contact and complete transmission (no reflection).

(a) Determine the reflection and transmission coefficients (based on stress ratios) for a P-wave at normal incidence to this rough interface

and plot the magnitude and phase of these coefficients versus frequency from 0-20 MHz for steel with $\kappa_s = 150$ MPa/μm.

(b) The magnitude of transmission coefficient, *T*, you obtain in part (a) should be of the form, $|T(f)| = 1/\sqrt{1+C^2 f^2}$, where f is the frequency and the constant C is related to κ_s and ρc_p. We could use this transmission coefficient to try to estimate the effects of crack closure of a rough crack as follows. Figure D.28 shows a compact tension specimen which is used to grow a through-thickness crack from a starter notch. If the compact tension specimen is then loaded, the sides of this rough crack will touch at some points and not at others, so the crack surface will look like two rough surfaces in partial contact, the same problem as shown in Fig. D.27. Suppose we now examine this crack with a through-transmission immersion ultrasonic experiment, as shown in Fig. D.28, and also do a reference experiment where we move the transducers laterally so that they are not over the crack. Let $V_c(f)$ be the frequency components of the measured voltage for the case when we are over the crack, and let $V_r(f)$ be the frequency components of the measured voltage for the reference experiment, Since the only difference between two setups is the transmission coefficient at the crack, we expect that the voltages to satisfy $V_c(f) = T(f)V_r(f)$. The MATLAB function rough_crack gives the sampled received voltage versus time, vc, for the case when the transducers are placed over the crack, the sampled voltage versus time, vr, for the reference setup, and the sampled time values, t. The function call is:

```
>> [ vc, vr, t] =rough_crack
```

Using this function, obtain the measured transmission coefficient, $T(f)$, versus frequency [Note: if you want to use a Wiener filter here, the numerical round off "noise" is extremely small so choose a small constant value such as $\varepsilon = 0.001$ or smaller]. Using this transmission coefficient, determine a best fit value of *C*, and the corresponding value of κ_s (in MPa/μm), which is a measure of how closed the crack is. Assume the compact tension specimen is made of steel whose specific plane wave impedance is $z^a = 46\text{x}10^6$ kg/(m^2-sec).

2. A 6 mm thick aluminum plate is immersed in water and an immersion transducer is placed in the water at normal incidence to this plate. The

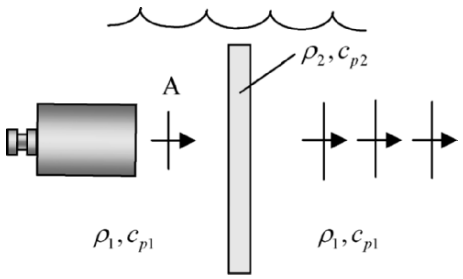

Fig. D.29. A transducer sending multiple pulses through an aluminum plate.

pulse generated from the transducer will pass through the plate and also be multiply reflected within the plate many times, causing a series of transmitted pulses to appear on the other side of the plate (see Fig. D.29). If we assume that the transducer beam incident on the plate acts as if it were a plane wave of pressure amplitude A, what would be the pressure amplitudes of the first three transmitted pulses (in terms of A) and what would be the time separation between them? For the water take $\rho_1 = 1$ gm/cm^3 , c_{p1}= 1480 m/sec and for the aluminum take ρ_2= 2.7 gm/cm^3, c_{p2}= 6420 m/sec.

3. The stress-strain (constitutive) relations for an isotropic elastic solid can be written as:

$$\tau_{xx} = \frac{E}{(1+\nu)(1-2\nu)}\left[(1-\nu)e_{xx} + \nu\left(e_{yy} + e_{zz}\right)\right]$$

$$\tau_{yy} = \frac{E}{(1+\nu)(1-2\nu)}\left[(1-\nu)e_{yy} + \nu\left(e_{xx} + e_{zz}\right)\right]$$

$$\tau_{zz} = \frac{E}{(1+\nu)(1-2\nu)}\left[(1-\nu)e_{zz} + \nu\left(e_{xx} + e_{yy}\right)\right]$$

$$\tau_{xy} = \mu\gamma_{xy}$$

$$\tau_{xz} = \mu\gamma_{xz}$$

$$\tau_{yz} = \mu\gamma_{yz}$$

where $\mu = E/2(1+\nu)$ and the strains are given by

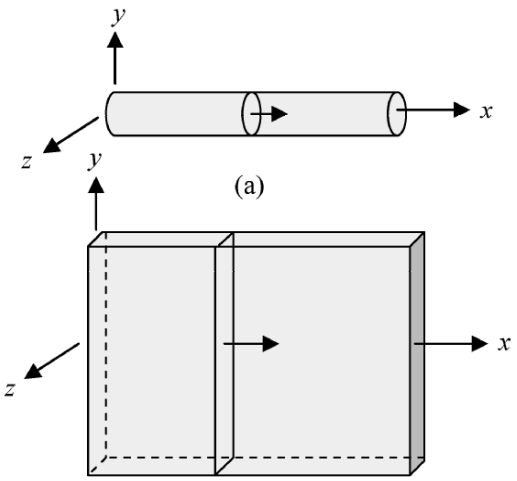

Fig. D.30. A compressional wave traveling in **(a)** a rod and **(b)** a plate.

$$e_{xx} = \frac{\partial u_x}{\partial x}, \quad e_{yy} = \frac{\partial u_y}{\partial y}, \quad e_{zz} = \frac{\partial u_z}{\partial z}$$

$$\gamma_{xy} = \frac{\partial u_x}{\partial y} + \frac{\partial u_y}{\partial x}, \quad \gamma_{xz} = \frac{\partial u_x}{\partial z} + \frac{\partial u_z}{\partial x}, \quad \gamma_{yz} = \frac{\partial u_y}{\partial z} + \frac{\partial u_z}{\partial y}.$$

(a) If we consider a compressional wave propagating along a long slender rod as shown in Fig. D.30 (a), it is reasonable to assume that $u_x = u_x(x,t)$ and that the only non-zero stress is τ_{xx} ($\tau_{yy} = \tau_{zz} = \tau_{xy} = \tau_{xz} = \tau_{yz} = 0$). The equations of motion in this case become simply

$$\frac{\partial \tau_{xx}}{\partial x} = \rho \frac{\partial^2 u_x}{\partial t^2}.$$

Use the stress-strain relations and the conditions $\tau_{yy} = \tau_{zz} = 0$ to determine the relationship between τ_{xx} and $e_{xx} = \partial u_x / \partial x$ for this case. What is the wave speed for compressional waves in the rod?

(b) Now consider a compressional wave traveling in a plate as shown in Fig. D.30 (b). In this case it is reasonable to assume $\tau_{zz} = \tau_{xy} = \tau_{xz} = \tau_{yz} = 0$ and $e_{yy} = 0$. If again we assume $u_x = u_x(x,t)$ the equation of motion for the plate is the same as for part (a). Use the stress-strain relations and the conditions $\tau_{zz} = e_{yy} = 0$ to again determine the relationship between τ_{xx} and $e_{xx} = \partial u_x / \partial x$ for this case. What is the wave speed for compressional waves in the plate? For steel (take E = 210 GPa, ν = 0.3, ρ = 7.9x10^3 kgm/m^3) how does the compressional rod wave speed and plate wave speed compare to the wave speed for bulk compressional waves?

4. A plane wave travels 100 mm in a material to a point where its amplitude is P_1. After the wave travels through an additional 100 mm of material its amplitude is reduced to $P_2 = 0.45P_1$. What is the average attenuation of this material in dB/m?

5. A transducer beam spreads as it propagates. In the far-field of the transducer this spreading is just like that of a spherical wave, i.e. the amplitude varies as 1/*r* where *r* is the distance from the transducer. At a distance of 100 mm from the transducer the amplitude of the pressure is P_1. After the beam has propagated another 100 mm the amplitude is reduced to $P_2 = 0.45P_1$. What is the average attenuation of the material in dB/m, assuming that at both of these distances we are in the transducer far-field?

6. Consider a harmonic plane P-wave traveling in water at room temperature. Determine an expression for the distance (as a function of the frequency, f) that this wave must travel (in meters) to reduce its amplitude by 10% due to attenuation. Plot this function from f = 1 MHz to f = 20 MHz.

7. The reflection and transmission coefficients (based on stress ratios) for a plane P-wave wave at normal incidence to a plane interface between two elastic solids were given by Eq. (D.39). Determine the corresponding transmission and reflection coefficients based on ratios of the energy intensities (see Eq. (D.63)). Plot these intensity-based coefficients versus the impedance ratio of the two solids, as done in Fig. D.9.What is the sum of these intensity-based reflection and transmission coefficients?

E Waves Used in Nondestructive Evaluation

Bulk P-waves and S- waves are the types of waves most frequently used in NDE testing. Thus, the wave propagation models developed in Appendix D and in Chapters 8-12 are all bulk wave models. In this Appendix we discuss some of the issues associated with the generation of bulk S-waves in solids and briefly describe surface (Rayleigh) and plate waves since these wave types also have important NDE applications.

E.1 Shear Waves

Many ultrasonic nondestructive evaluation inspections are performed with P-wave transducers operating either in a contact mode or in immersion testing. It is also possible to have a piezoelectric crystal generate a shearing motion when it is excited by a voltage pulse and use that shearing motion to launch a shear wave into a solid component in a contact setup as shown in Fig. E.1. In order to couple the motion of the crystal to the solid, however, the shear wave transducer must be attached to the solid in a permanent or semi-permanent fashion. Highly viscous shear wave couplants or glues can be used for this purpose, but the transducer is then not able to be scanned along the surface which greatly limits the usefulness of such a shear wave setup. As a consequence, most shear waves are instead generated through the process of mode conversion from a P-wave to an SV-wave at oblique incidence to an interface. This is the basic mechanism used in an *angle beam shear wave transducer*, as shown in Fig. E.2. An ordinary P-wave type of crystal and backing is placed on a plastic wedge. The P-wave this crystal generates strikes the interface between the wedge and the solid to be inspected at oblique incidence. If the incident angle in the wedge is chosen so that the first critical angle in the solid is exceeded, then only a transmitted SV-wave propagates into the solid as shown in Fig. E.2. The angle of propagation of the shear wave in the solid is determined by generalized Snell's law so that

$$\theta_{s2} = \sin^{-1}\left[c_{s2} \sin\theta_{p1} / c_{p1} \right] \tag{E.1}$$

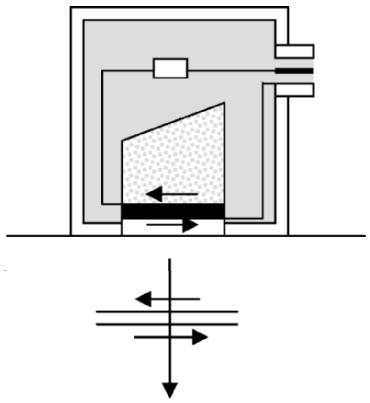

Fig. E.1. A contact shear wave transducer on the free surface of a solid showing the shear motion of the piezoelectric and the corresponding shear wave that is generated.

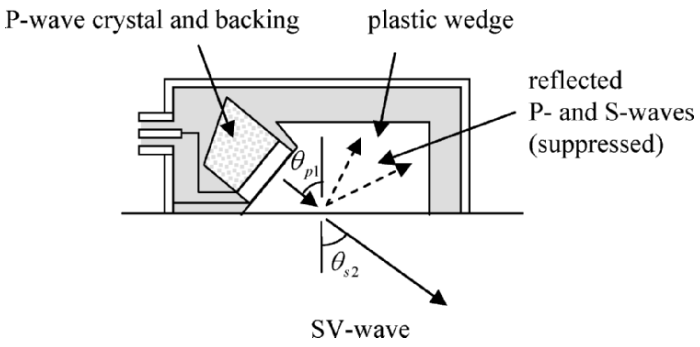

Fig. E.2. An angle beam shear wave transducer on the free surface of an elastic solid.

where c_{p1} is the P-wave speed in the wedge, c_{s2} is the shear wave speed in the solid, and θ_{p1} is the angle that the P-wave in the wedge makes with the normal to the surface. Some refracted shear wave angles that are commonly used in practice are: $\theta_{s2} = 45^\circ, 60^\circ, 70^\circ$. The angle beam shear wave transducer, like an ordinary P-wave contact transducer, can be coupled to the solid by a thin fluid layer so that it can be scanned along the surface. Angle beam shear wave transducers are often used for weld inspection

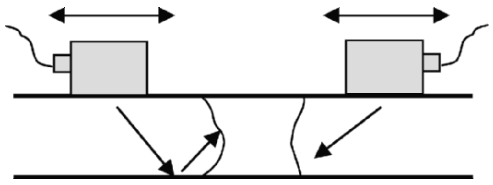

Fig. E.3. An angle beam shear wave inspection of a welded plate geometry using a directly generated SV-wave as shown on the right side of the weld or a SV-wave reflected from a back surface as shown on the left side.

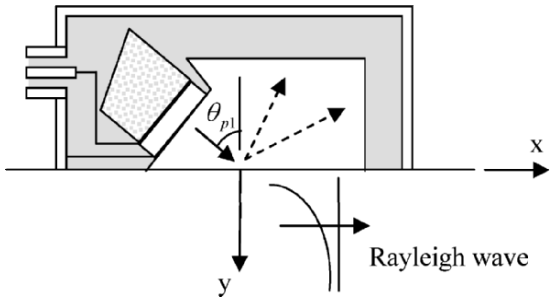

Fig. E.4. A Rayleigh wave transducer on the free surface of an elastic solid.

problems as shown in Fig. E.3, where the entire weld zone can be probed by scanning the transducer along the surface and using either the SV-wave directly or a wave reflected from a back surface. Models of angle beam shear wave inspections are discussed in Chapter 13.

E.2 Rayleigh Waves

A transducer arrangement very similar to the angle beam shear wave case can also be used to generate Rayleigh surface waves, as shown in Fig. E.4 [E.1]. In this case the angle of the incident P-waves in the wedge must be slightly larger than the second critical angle. Specifically,

$$\theta_{p1} = \sin^{-1}\left[c_{p1} / c_{r2} \right], \tag{E.2}$$

where c_{r2} is the wave speed for Rayleigh waves in the solid. Typically the Rayleigh wave speed is about 90 per cent the shear wave speed. At this angle, there are only inhomogeneous P- and SV-waves generated in the solid which combine to form the Rayleigh wave mode. The Rayleigh wave travels along the stress free surface of the solid and decays in depth from the surface. Lord Rayleigh first discovered these waves by choosing P- and SV-wave potentials given by [Fundamentals]

$$\begin{aligned} \phi &= A\exp\left[-\alpha y\right]\exp\left[ik\left(x-ct\right)\right] \\ \psi &= B\exp\left[-\beta y\right]\exp\left[ik\left(x-ct\right)\right] \end{aligned} \tag{E.3}$$

which represent inhomogeneous waves propagating along the surface with the common wave speed , *c*. These waves must satisfy the wave equations

$$\begin{aligned} \nabla^2\phi - \frac{1}{c_{p2}^2}\frac{\partial^2\phi}{\partial t^2} &= 0 \\ \nabla^2\psi - \frac{1}{c_{s2}^2}\frac{\partial^2\psi}{\partial t^2} &= 0, \end{aligned} \tag{E.4}$$

where c_{p2} and c_{s2} are the wave speeds for compressional and shear waves in the solid, respectively. Also, these waves must satisfy the free surface (zero stress) boundary conditions which are $\tau_{yy} = \tau_{xy} = 0$ on $y = 0$. Rayleigh showed that potentials of the form given in Eq. (E.3) could be found that satisfy both the wave equations and the boundary conditions if

$$\begin{aligned} \alpha &= \left|\omega / c\right|\sqrt{1 - c^2 / c_{p2}^2} \\ \beta &= \left|\omega / c\right|\sqrt{1 - c^2 / c_{s2}^2} \end{aligned} \tag{E.5}$$

and the wave speed , *c*, is a root of the equation

$$\left(2 - c^2 / c_{s2}^2\right)^2 - 4\sqrt{1 - c^2 / c_{p2}^2}\sqrt{1 - c^2 / c_{s2}^2} = 0. \tag{E.6}$$

Equation (E.6) is called the *Rayleigh equation*. It can be shown [E.3] that for an isotropic elastic solid there is always one real root of Eq. (E.5) $c = c_{r2}$, where $c_{r2} < c_{s2}$, called the *Rayleigh wave speed*. Eq. (E.5) then shows that α and β are both real so that the Rayleigh wave potentials

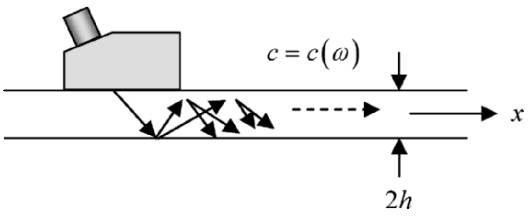

Fig. E.5. An angle beam transducer on a thin plate generating a series of reflected and mode-converted waves that combine to form a dispersive (frequency dependent) plate wave traveling with the wave speed $c = c(\omega)$.

have an exponential decay in distance from the surface. A simple approximate expression for the Rayleigh wave speed is given by

$$c_{r2} \cong \frac{0.862 + 1.14\nu}{1+\nu} c_{s2}, \tag{E.7}$$

where ν is Poisson's ratio.

If one examines the displacements and stresses in the Rayleigh wave, one finds that like the potentials they also decay in depth from the interface but the decay is not a simple exponential behavior as given in Eq. (E.3). However, at high frequencies, these quantities are all confined near the surface while at lower frequencies they have deeper penetration. Thus, in an inspection with Rayleigh waves one can adjust the depth of the region one is interrogating by adjusting the frequency. Since they are confined to the surface Rayleigh waves are very useful for inspecting for surface flaws or near-surface flaws. Also, since Rayleigh waves travel and spread out in two-dimensions on the surface whereas bulk waves spread out in three-dimensions as they propagate through the volume of a material the amplitudes of Rayleigh waves do not decay as fast as bulk waves and they can travel long distances.

E.3 Plate (Lamb) Waves

If an angle beam shear wave transducer is placed on a thin plate, as shown in Fig. E.5, a series of reflected and mode converted waves are generated in the plate and these combine to form a new wave mode traveling with a wave speed, c, in the x-direction called a plate (or Lamb) wave [E.2].

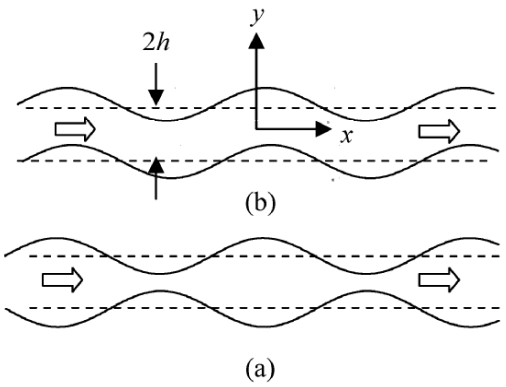

Fig. E.6. (a) An extensional plate wave traveling in the *x*-direction in a thin plate and **(b)** a flexural plate wave traveling in the *x*-direction. The type of deformation present in each of these wave types is shown.

Unlike bulk waves or Rayleigh waves whose wave speeds are just a function of material constants, $c = c(\omega)$ i.e. the wave speed of a plate wave is generally frequency dependent, a phenomenon called *geometric dispersion*. Actually as we will see there are many different plate waves that can be generated, each with a different frequency dependency.

Plate waves are solutions of the wave equations for the potentials where we assume

$$\begin{aligned} \phi &= f(y)\exp\left[ik(x-ct)\right] \\ \psi &= g(y)\exp\left[ik(x-ct)\right]. \end{aligned} \tag{E.8}$$

In this case, we find that

$$\begin{aligned} f &= A\cosh(\alpha y) \\ g &= B\sinh(\beta y) \end{aligned} \tag{E.9}$$

or

$$\begin{aligned} f &= A'\sinh(\alpha y) \\ g &= B'\cosh(\beta y), \end{aligned} \tag{E.10}$$

where α and β are again given by Eq. (E.5). Solutions of the form given by Eq. (E.9) are *extensional plate waves*, while those given by Eq. (E.10)

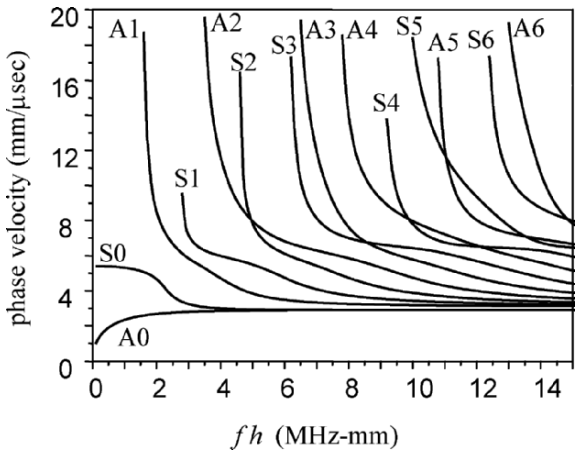

Fig. E.7. The phase velocity versus non-dimensional frequency (dispersion) curves. Extensional wave modes are labeled An and flexural modes are labeled Sn (n = 0, 1, 2…).

are *flexural plate waves*. In general, we may have both types of waves generated. The extensional plate waves are waves with the symmetric thickness variations shown in Fig. E.6 (a) while the flexural plate waves generate a bending deformation of the plate as they propagate, as shown in Fig. E.6 (b).

Both types of these plate waves must satisfy the boundary conditions $\tau_{yy} = \tau_{xy} = 0$ on $y = \pm h$ which yields the Rayleigh-Lamb equations

$$\frac{\tanh(\beta h)}{\tanh(\alpha h)} = \left[\frac{4\omega^2 \alpha\beta}{c^2\left(\omega^2/c^2 + \beta^2\right)^2} \right]^{\pm 1}, \tag{E.11}$$

where the plus sign is for extensional waves and the negative sign for flexural waves. Solutions of Eq. (E.11) for the frequency dependent wave speed $c = c(\omega)$ are rather complex and generally must be determined numerically. Plots of the wave speed versus frequency are shown in Fig. E.7 for a number of extensional and flexural wave modes.

We can obtain some information on the behavior of these waves by noting that for sufficiently high frequencies we have $\tanh(\alpha h) = 1$,

$\tanh(\beta h) = 1$ and the Rayleigh-Lamb equations for both extensional and flexural waves reduce to just our equation for Rayleigh waves, Eq. (E.6). This is a reasonable result since at very high frequencies the two sides of the plate appear very far away from each other and the waves can propagate independently on each side (as Rayleigh waves) as if the other side did not exist. Thus, all the curves in Fig. E.7 asymptote to the Rayleigh wave speed at sufficiently high frequencies.

At low frequencies, one can also extract some explicit results from the Rayleigh-Lamb equation. For the lowest order extensional wave mode (see Fig. E.7), one finds [Fundamentals]

$$c \cong \sqrt{\frac{E}{\rho\left(1-\nu^2\right)}} \tag{E.12}$$

which is the non-dispersive wave speed for extensional plate waves found from elementary plate theory. In contrast, the lowest order flexural mode at low frequencies produces a wave speed [Fundamentals]

$$c \cong \left(\frac{D_p}{2\rho h}\right)\sqrt{\omega}, \tag{E.13}$$

where $D_p = \dfrac{8\mu(\lambda+\mu)h^3}{3(\lambda+2\mu)}$ is the flexural rigidity of the plate. In this case we see the flexural waves remain dispersive even at low frequencies.

Plate waves are good candidates for inspecting thin plates and pipes and are frequently used in those applications [E.2]. The inherent dispersive nature of plate waves and the fact that one often simultaneously generates many different modes often makes inspections with these waves challenging from a data interpretation standpoint.

E.4 References

E.1 Uberall H (1973) Surface waves in acoustics. In: Mason WP, Thurston, RN (eds) Physical acoustics, vol. X. Academic Press, New York, NY

E.2 Rose JL (1999) Ultrasonic waves in solid media. Cambridge Univ. Press, Cambridge, UK

E.3 Achenbach JD (1973) Wave propagation in elastic solids. Am. Elsevier Publishing Co., New York, NY

F Gaussian Beam Fundamentals

A Gaussian beam is a very important type of propagating wave since it is an elementary wave that can be used as an efficient building block for constructing the more complex wave fields present in NDE inspections. Chapter 9 develops in detail the propagation and transmission/reflection laws for Gaussian beams in fluid and solid media. That Chapter also describes how a multi-Gaussian beam model of circular and rectangular piston NDE transducers can be constructed by superimposing only 10-15 Gaussian beams. The Gaussian beam discussions and derivations given in Chapter 9, however, are inherently rather complex since they involve the types of Gaussian beams and beam interactions that are needed to model general NDE testing situations. In this Appendix we will discuss Gaussian beams in a much more restricted context in order to illustrate some of the important properties of this type of wave in as simple a manner as possible. Specifically, we will examine the propagation of a circularly symmetrical Gaussian beam in a fluid medium along a single coordinate direction and describe the interactions of that beam with spherical or planar interfaces that are normal to the propagation direction. Special cases of this type are commonly encountered when using Gaussian beams to represent the fields present in lasers, so we will also use a notation that is consistent with many references found in the laser science literature.

F.1 Gaussian Beams and the Paraxial Wave Equation

Let the pressure, p, of a propagating harmonic wave (of $\exp(-i\omega t)$ time dependency) be written in cylindrical coordinates (ρ, z) in the form of a *quasi-plane wave* propagating in the z-direction, i.e.

$$p = P(\rho, z, \omega)\exp(ikz - i\omega t). \tag{F.1}$$

This is called a quasi-plane wave because the amplitude, P, has variations in (ρ, z) while in a true plane wave P would be constant. Placing Eq. (F.1) into the wave equation (see Eq. (D.8)) then shows that P must satisfy

$$\frac{1}{\rho}\frac{\partial}{\partial\rho}\left(\rho\frac{\partial P}{\partial\rho}\right)+\frac{\partial^2 P}{\partial z^2}+2ik_p\frac{\partial P}{\partial z}=0, \tag{F.2}$$

where $k_p=\omega/c_p$ is the wave number. Note that this is an axially symmetrical wave since there are no angular variations in the plane perpendicular to the z-axis. As discussed in Chapter 9 if Eq. (F.1) represents a wave disturbance propagating primarily in the z-direction we can assume that the $\partial^2 P/\partial z^2$ term in Eq. (F.2) will be smaller than the other terms in that equation, leading to the *paraxial wave equation* for P given by [F.1], [F.2]

$$\frac{1}{\rho}\frac{\partial}{\partial\rho}\left(\rho\frac{\partial P}{\partial\rho}\right)+2ik_p\frac{\partial P}{\partial z}=0. \tag{F.3}$$

The paraxial wave equation assumes that

$$\left|\frac{\partial^2 P}{\partial z^2}\right| << \left|2ik_p\frac{\partial P}{\partial z}\right|, \left|\frac{1}{\rho}\frac{\partial}{\partial\rho}\left(\rho\frac{\partial P}{\partial\rho}\right)\right|, \tag{F.4}$$

but since the magnitudes of both terms on the right side of Eq. (F.4) are always equal by virtue of the paraxial wave equation, it is sufficient to require only that

$$\left|\frac{\partial^2 P}{\partial z^2}\right| << \left|2ik_p\frac{\partial P}{\partial z}\right|. \tag{F.5}$$

We will discuss the consequences of this inequality shortly. Now consider a Gaussian beam solution of Eq. (F.3) in the form

$$P=\tilde{P}\exp\left(ik_p\rho^2/2q\right), \tag{F.6}$$

where $\tilde{P}=\tilde{P}(z)$ and $q=q(z)$ can both be complex-valued functions. Placing Eq. (F.6) into Eq. (F.3) gives

$$2ik_p\left(\frac{\tilde{P}}{q}+\frac{d\tilde{P}}{dz}\right)+\frac{k_p^2\rho^2\tilde{P}}{q^2}\left(\frac{dq}{dz}-1\right)=0. \tag{F.7}$$

Since we must satisfy Eq. (F.7) for all ρ we have

$$\frac{dq}{dz} = 1 \tag{F.8a}$$

and

$$\frac{d\tilde{P}}{dz} + \frac{\tilde{P}}{q} = 0. \tag{F.8b}$$

The solution of Eq. (F.8a) is just the propagation law

$$q(z) = z + q_0 \tag{F.9}$$

where q_0 is a complex constant (that can also depend on the frequency, ω). Placing this solution into Eq. (F.8b) then also gives

$$\tilde{P}(z) = \frac{P_0}{z + q_0} = \frac{P_0}{q(z)}. \tag{F.10}$$

Thus, we see that a propagating Gaussian beam is given by

$$\begin{aligned} p &= \frac{P_0}{q(z)} \exp\left[ik_p z\right] \exp\left[\frac{ik_p \rho^2}{2q(z)}\right] \\ &= \frac{P_0}{z + q_0} \exp\left[ik_p z\right] \exp\left[\frac{ik_p \rho^2}{2(z + q_0)}\right] \end{aligned} \tag{F.11}$$

(where we have omitted writing explicitly the $\exp(-i\omega t)$ term, a convention we will follow throughout the remainder of this Appendix). To put this beam expression in a more understandable form, let the constant q_0 be represented in the form

$$q_0 = -\left(z_0 + \frac{i\pi w_0^2}{\lambda_p}\right), \tag{F.12}$$

where (z_0, w_0) have the dimensions of a length and $\lambda_p = 2\pi / k_p$ is the wavelength. The distance $z_c = \pi w_0^2 / \lambda_p$ is called the *confocal distance* (or *confocal parameter*). In terms of these parameters, therefore, the Gaussian beam is given by

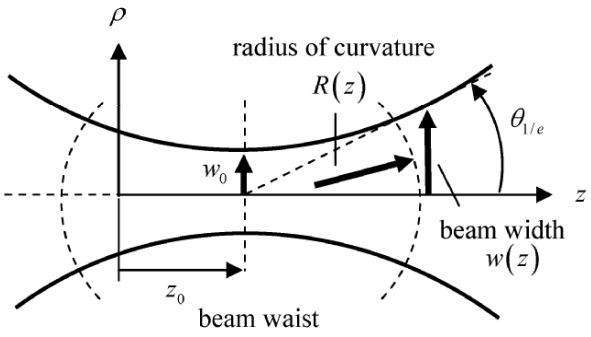

Fig. F.1. A Gaussian beam of circular cross-section propagating in the z-direction, showing the wave front curvature and the beam width. The beam waist is located at $z = z_0$ where the beam width is w_0. The half angle divergence of the beam at a large distance from the beam waist is defined by the angle $\theta_{1/e}$.

$$p = \frac{P_0}{(z - z_0) - iz_c} \exp\left[ik_p z\right] \cdot \exp\left[\frac{ik_p \rho^2 (z - z_0)/2}{(z - z_0)^2 + (z_c)^2} - \frac{\rho^2 (z_c / w_0)^2}{(z - z_0)^2 + (z_c)^2}\right]. \tag{F.13}$$

Now, define a *beam width* parameter, $w(z)$, and a *beam wave front curvature* parameter, $R(z)$, as

$$\frac{1}{\left[w(z)\right]^2} = \frac{(z_c / w_0)^2}{(z - z_0)^2 + (z_c)^2}$$
$$\frac{1}{R(z)} = \frac{(z - z_0)}{(z - z_0)^2 + (z_c)^2}. \tag{F.14}$$

Then the Gaussian beam becomes

$$p = \frac{P_0}{(z - z_0) - iz_c} \exp\left[ik_p z\right] \exp\left[\frac{ik_p \rho^2}{2R(z)} - \frac{\rho^2}{\left(w(z)\right)^2}\right]. \tag{F.15}$$

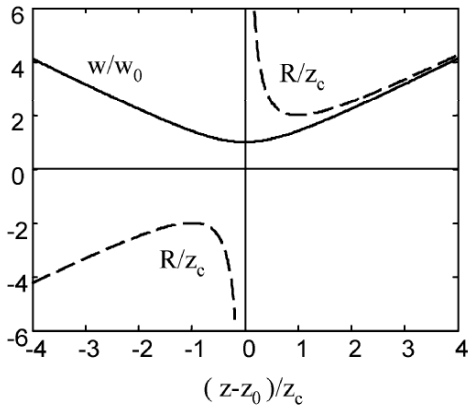

Fig. F.2. A plot of the normalized beam width, w/w_0, and the normalized radius of curvature, R/z_c, versus the normalized distance, $(z-z_0)/z_c$.

Figure F.1 shows a side view of the Gaussian beam represented by Eq. (F.15) and Fig. F.2 shows a plot of both the normalized beam width and normalized curvature parameters. We see that the beam wave front curvature, $R(z)$, is infinite at the location $z=z_0$. Therefore at that location the wave front of the Gaussian beam is planar. For $z>z_0$ the curvature is positive and the Gaussian beam is a diverging beam while for $z<z_0$ the beam is a converging beam. From Eq. (F.15) we see that the amplitude of the Gaussian beam in the ρ-direction is a Gaussian function whose width is $w(z)$, where the width is defined as the radial distance to which the beam amplitude drops by a factor e^{-1} from its on-axis value. Figures F.1 and F.2 show that the minimum beam width also occurs at $z=z_0$ which is called the location of the *beam waist*. At the beam waist from Eq. (F.14) it follows that $w(z_0)=w_0$.

Physically, the confocal parameter $z_c=\pi w_0^2/\lambda_p$ is the axial distance from the beam waist to where the Gaussian beam remains reasonably well collimated (i.e. where the beam width is approximately a constant) [F.2]. This can be seen from Eq. (F.14) where at $z-z_0=z_c$ we find $w=1.414w_0$ so that the beam width is only 40% larger than at the waist. However, at larger distances from the beam waist the beam width

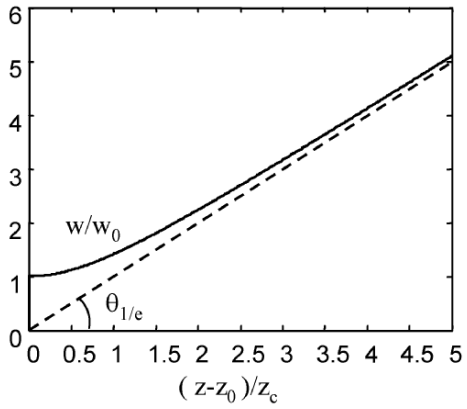

Fig. F.3. The normalized beam width versus normalized distance, $(z-z_0)/z_c$ and the corresponding asymptotic beam growth angle.

grows considerably wider as the beam diverges. If we compute the half angle to the e^{-1} width point in the beam, $\theta_{1/e}$, (see Figs. F.1 and F.3) where

$$\theta_{1/e} = \lim_{z\to\infty}\left\{\tan^{-1}\left[\frac{w(z)}{(z-z_0)}\right]\right\} = \tan^{-1}\left(\frac{\lambda_p}{\pi w_0}\right) = \tan^{-1}\left(\sqrt{\frac{\lambda_p}{\pi z_c}}\right) \qquad \text{(F.16)}$$

we see that if the wavelength, λ, is much smaller than the beam width, w_0, then the *asymptotic beam growth angle*, $\theta_{1/e}$, is very small. For example, if we consider a Gaussian beam with a waist size $w_0 = 3$ mm radiating into water at 5 MHz, then the wavelength $\lambda_p = 0.3$ mm and $\theta_{1/e} = 1.8$ degrees. This shows that a Gaussian beam of roughly the same size as an ultrasonic NDE transducer that propagates at MHz frequencies will be highly collimated. A typical NDE transducer beam at these frequencies also is highly collimated (see, for example, Fig. 8.3). It is this fact that makes it possible to take a relatively few Gaussian beams of different widths and waist locations and accurately synthesize the wave field of an NDE transducer, as shown in Chapter 9. In contrast, it takes a superposition of many more spherical waves or plane waves to model a transducer wave field since neither of those wave types are collimated beams like the Gaussian beam.

It is interesting to compare Eq. (F.15) with the paraxial approximation for the propagation of a spherical wave in the neighborhood of the z-axis. This case is examined in Chapter 9 as part of the discussion of the paraxial approximation. For such a spherical wave we have (see Eq. (9.6))

$$p = \frac{A}{z}\exp\left[ik_p z\right]\exp\left(\frac{ik_p\rho^2}{2z}\right). \tag{F.17}$$

Both Eq. (F.15) and (F.17) have a varying "amplitude" term, a plane wave propagation term, $\exp\left(ik_p z\right)$, and a phase term that is quadratic in the radial distance, ρ, from the propagation axis. In fact, we can view the Gaussian beam as representing a spherical wave propagating from a complex source point in the paraxial approximation [F.3]. Such complex point sources can be used as a means of forming wave solutions that do not rely on the paraxial approximation, but we will not discuss those solutions here. Note that if we let $q_0 = 0$ in the Gaussian beam it reduces exactly to the spherical wave of Eq. (F.17).

Whereas the amplitude of a spherical wave becomes infinite at the source location $z = 0$ (see Eq. (F.17), the Gaussian beam (see Eq. (F.15)) remains well behaved everywhere. In fact, as shown in Chapter 9, a Gaussian beam is never singular, even after propagation and reflection/refraction in multiple media. The same is not true for spherical or plane waves which at high frequencies can become singular at focal points or caustics after either of those wave types interact with curved interfaces. This non-singular behavior of Gaussian beams is also a feature of this wave type that makes it a better building block than spherical or plane waves to generate more complex wave fields.

F.2 Quasi-Plane Wave Conditions and the Paraxial Approximation

If the pressure is given by Eq. (F.11) then the velocity, v_z, in the direction of the propagating Gaussian beam is given by

$$\begin{aligned} v_z &= \frac{1}{i\omega\rho}\frac{\partial p}{\partial z} \\ &= \frac{1}{i\omega\rho}\left[ik_p - \frac{q'}{q} - \frac{ik_p\rho^2}{2}\left(\frac{q'}{q^2}\right)\right]p, \end{aligned} \tag{F.18}$$

where $q' = dq/dz = 1$. We will now consider the conditions under which the magnitude of the first term on the right side of Eq. (F.18) is much larger than the other two terms. First consider the condition

$$\left|\frac{q'}{q}\right| << k_p. \tag{F.19}$$

This condition is equivalent to requiring that

$$k_p|q| = k_p\left|(z - z_0) - iz_c\right| >> 1. \tag{F.20}$$

Because $|q| \geq z_c$ Eq. (F.20) will certainly be satisfied if we require the stronger condition $k_p|z_c| >> 1$ which gives

$$2\pi^2\left(\frac{w_0}{\lambda_p}\right)^2 >> 1. \tag{F.21}$$

Now consider the second condition

$$\frac{k_p\rho^2}{2}\left|\frac{q'}{q^2}\right| << k_p. \tag{F.22}$$

Since most of the energy in a Gaussian beam is contained within a beam width, w, Eq. (F.22) will be satisfied for all ρ within that distance if we set $\rho = w$ in Eq. (F.22) and require

$$\frac{w^2}{2}\left|\frac{1}{q^2}\right| << 1. \tag{F.23}$$

But since $w \geq w_0$ Eq. (F.23) implies

$$\frac{w_0^2}{2}\left|\frac{1}{q^2}\right| << 1 \qquad \text{or, equivalently,} \qquad \frac{2|q^2|}{w_0^2} >> 1.$$

Again, since $|q| \geq z_c$ the above inequality will certainly be satisfied if we require the stronger condition

$$2\left(\frac{z_c}{w_0}\right)^2 = 2\pi^2\left(\frac{w_0}{\lambda_p}\right)^2 >> 1 \tag{F.24}$$

This is just the same result as obtained in Eq. (F.21). Thus, we see that as long as the beam waist size is much larger than a wavelength, the velocity, v_z, in the Gaussian beam given by Eq. (F.18) reduces to

$$v_z = \frac{p}{\rho c_p}, \tag{F.25}$$

which is a relationship also true for plane waves (see Appendix D). Thus, in terms of the pressure-velocity relationship we can view a Gaussian beam as behaving like a quasi-plane wave.

These results are also useful for examining the requirement given by Eq. (F.5) for the paraxial approximation to be valid for a Gaussian beam. Since we have

$$P = \frac{P_0}{q}\exp\left[ik_p\rho^2/2q\right] \tag{F.26}$$

it follows that

$$\frac{dP}{dz} = -\left(\frac{q'}{q} + \frac{ik\rho^2}{2}\frac{q'}{q^2}\right)P. \tag{F.27}$$

But the terms appearing in the brackets in Eq. (F.27) are the same terms we have just analyzed, so under the same condition given by either Eq. (F.21) or Eq. (F.24) we have

$$\left|\frac{dP}{dz}\right| << \left|2k_pP\right|. \tag{F.28}$$

Using Eq. (F.28) we see that Eq. (F.5) can also be written as

$$\left|\frac{\partial^2 P}{\partial z^2}\right| << \left|4k_p^2P\right|. \tag{F.29}$$

If we differentiate Eq. (F.27) once more and assume that again Eq. (F.19) and (F.22) are satisfied for the terms of those forms that appear in the

expression for d^2P/dz^2, then Eq. (F.29) will be satisfied if for the one remaining term we have

$$\left|\frac{k_p^2\rho^4}{4}\left(\frac{q'}{q^2}\right)^2 P\right| << 4k_p^2|P|. \tag{F.30}$$

[The details are not given here as they are very similar to those just presented for proving Eq. (F.25)]. Thus, the paraxial condition of Eq. (F.29) becomes

$$\left|\left(\frac{\rho^2}{2}\frac{q'}{q^2}\right)^2\right| << 4 \tag{F.31}$$

which is certainly satisfied if we require

$$\left(\frac{\rho^2}{2}\left|\frac{q'}{q^2}\right|\right)^2 << 1. \tag{F.32}$$

But if we take the square root of both sides of Eq. (F.32) we obtain Eq. (F.22) again so that the condition for the paraxial approximation to be valid for a Gaussian beam is once more either Eq . (F.21) or Eq. (F.24).

We can also view the conditions of Eqs. (F.21), (F.24) in terms of the asymptotic beam growth angle. Placing this paraxial approximation condition into Eq. (F.16) gives

$$\theta_{1/e} = \tan^{-1}\left(\frac{\lambda_p}{\pi w_0}\right) << \tan^{-1}\left(\sqrt{2}\right)$$

which is satisfied if $\theta_{1/e} << 54.7^{\circ}$. If we keep the beam growth angle to about half this angle ($\theta_{1/e} \cong 30^{\circ}$) we might expect the propagating Gaussian beam will not violate significantly the paraxial condition. Angular values of this size are consistent with the angular limits on the paraxial approximation discussed in Chapter 9 using plane waves and spherical waves.

F.3 Transmission/Reflection of a Gaussian Beam

As shown previously a circularly symmetrical Gaussian beam is completely determined by the amplitude, $\tilde{P}(z) = P_0/q(z)$, and the phase parameter,

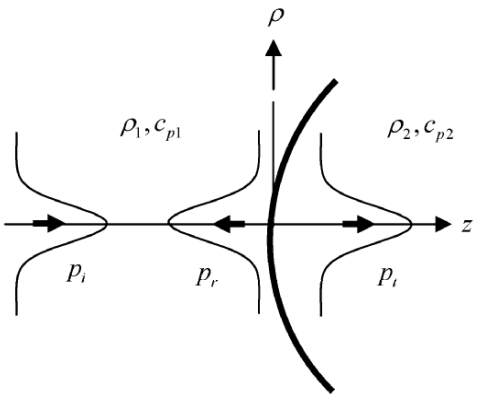

Fig. F.4. Transmission and reflection of a circular cross-section compressional wave Gaussian beam at a spherically curved interface between two media.

$q(z)$. The *propagation law* of Eq. (F.9) describes how both these amplitude and phase terms change as this Gaussian beam propagates. Here we want to define the corresponding *transmission and reflection laws* when the symmetric Gaussian beam strikes a spherically curved interface of radius, R_0, at normal incidence, as shown in Fig. F.4. In this case, both axially symmetric transmitted and reflected Gaussian beams are generated. The incident, transmitted, and reflected Gaussian beams can all be written in general as

$$\begin{aligned} p_i &= \tilde{P}_i(z)\exp\left[ik_{p1}z + i\omega t_0\right]\exp\left[\frac{ik_{p1}\rho^2}{2q_i(z)}\right] \\ p_r &= \tilde{P}_r(z_2)\exp\left[ik_{p1}z_2 + i\omega t_0\right]\exp\left[\frac{ik_{p1}\rho^2}{2q_r(z_2)}\right] \\ p_t &= \tilde{P}_t(z)\exp\left[ik_{p2}z + i\omega t_0\right]\exp\left[\frac{ik_{p2}\rho^2}{2q_t(z)}\right], \end{aligned} \tag{F.33}$$

where (p_i, p_r, p_t) are the incident, reflected and transmitted wave pressures and $k_{pm} = \omega / c_{pm}$ (m = 1,2) are the wave numbers for the first and second media, respectively, as shown in Fig. F.4.The z-coordinate here is taken with its origin at the interface (see Fig. F.4). Both the incident and transmitted waves are propagating in the + z direction, but the reflected wave is propagating in the $z_2 = -z$ direction. Typically, the incident

Gaussian beam will have started out from some fixed position at time $t = 0$ located at a distance, *D*, from the interface in medium one so that the term, $t_0 = D/c_{p1}$, which appears in all the beams of Eq. (F.33) simply represents the common time delay for all these waves.

At the curved interface, Σ, the boundary conditions require that pressure, *p*, and the normal velocity, v_z, must be continuous so that we have

$$\begin{aligned} p_i(\Sigma) + p_r(\Sigma) &= p_t(\Sigma) \\ v_{iz}(\Sigma) + v_{rz}(\Sigma) &= v_{tz}(\Sigma). \end{aligned} \tag{F.34}$$

Because we showed in the paraxial approximation the pressure and velocity in the Gaussian beams must satisfy Eq. (F.25), the boundary conditions of Eq. (F.34) can be re-written as

$$\begin{aligned} p_i(\Sigma) + p_r(\Sigma) &= p_t(\Sigma) \\ \frac{p_i(\Sigma)}{\rho_1 c_{p1}} - \frac{p_r(\Sigma)}{\rho_1 c_{p1}} &= \frac{p_t(\Sigma)}{\rho_2 c_{p2}}, \end{aligned} \tag{F.35}$$

where the minus sign arises in Eq. (F.35) since $p_r = \rho_1 c_{p1} v_{z_2} = -\rho_1 c_{p1} v_z$. We will not attempt to satisfy the boundary conditions of Eq. (F.35) exactly, but consistent with the paraxial approximation where all these Gaussian beams are considered as quasi-plane waves confined to a region near the *z*-axis, we will match the amplitude ($\tilde{P}$) terms in Eq. (F.34) only at the point *z* = 0 and the phase terms to second order in the distance, ρ, from the *z*-axis. Thus, the boundary conditions of Eq. (F.35) for the amplitude terms become

$$\begin{aligned} \tilde{P}_i(0) + \tilde{P}_r(0) &= \tilde{P}_t(0) \\ \frac{\tilde{P}_i(0)}{\rho_1 c_{p1}} - \frac{\tilde{P}_r(0)}{\rho_1 c_{p1}} &= \frac{\tilde{P}_t(0)}{\rho_2 c_{p2}} \end{aligned} \tag{F.36}$$

(where we can cancel all the phase terms in Eq. (F.36) since they will all be made common in the following discussion). Solving these equations we find

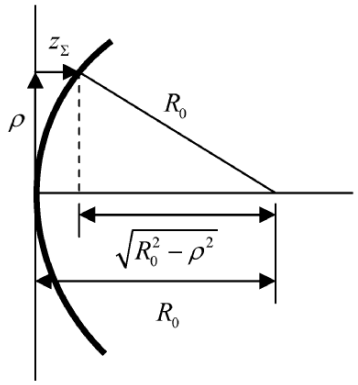

Fig. F.5. The geometry of the spherical interface.

$$\begin{aligned}\tilde{P}_r(0) &= \frac{\rho_2 c_{p2} - \rho_1 c_{p1}}{\rho_1 c_{p1} + \rho_2 c_{p2}} \tilde{P}_i(0) = R_p \tilde{P}_i(0) \\ \tilde{P}_t(0) &= \frac{2\rho_2 c_{p2}}{\rho_1 c_{p1} + \rho_2 c_{p2}} \tilde{P}_i(0) = T_p \tilde{P}_i(0),\end{aligned} \tag{F.37}$$

where (R_p, T_p) are the plane wave reflection and transmission coefficients (based on pressure ratios – see Appendix D).

Now consider the matching of the phase terms of Eq. (F.35). On the interface, Σ, from Fig. F.5 we see that

$$\begin{aligned}z_\Sigma &= R_0 - \sqrt{R_0^2 - \rho^2} \\ &\cong R_0 - R_0\left[1 - \frac{\rho^2}{2R_0^2} + \ldots\right] \\ &= \frac{\rho^2}{2R_0}\end{aligned} \tag{F.38}$$

so matching the incident and transmitted Gaussian beam phase terms to second order we have from Eq. (F.33)

$$\frac{ik_{p1}\rho^2}{2R_0} + \frac{ik_{p1}\rho^2}{2q_i(0)} + i\omega t_0 = \frac{ik_{p2}\rho^2}{2R_0} + \frac{ik_{p2}\rho^2}{2q_t(0)} + i\omega t_0, \tag{F.39}$$

which gives the *transmission law*

$$\frac{1}{q_t(0)} = \left(\frac{c_{p2}}{c_{p1}} - 1\right)\frac{1}{R_0} + \frac{c_{p2}}{c_{p1}}\frac{1}{q_i(0)}. \tag{F.40}$$

Similarly, matching the incident and reflected Gaussian beam phase terms in Eq. (F.33) we find

$$\frac{ik_{p1}\rho^2}{2R_0} + \frac{ik_{p1}\rho^2}{2q_i(0)} + i\omega t_0 = -\frac{ik_{p1}\rho^2}{2R_0} + \frac{ik_{p1}\rho^2}{2q_r(0)} + i\omega t_0 \tag{F.41}$$

to obtain the *reflection law*

$$\frac{1}{q_r(0)} = \frac{2}{R_0} + \frac{1}{q_i(0)}. \tag{F.42}$$

If we let $\left(R_i(0), w_i(0)\right)$ be the wave front curvature and beam width of the incident Gaussian beam at the interface, respectively and similarly define $\left(R_t(0), w_t(0)\right)$ and $\left(R_r(0), w_r(0)\right)$ for the transmitted and reflected beams, since

$$\frac{1}{q_m(0)} = \frac{1}{R_m(0)} + \frac{i\lambda_m}{\pi\left[w_m(0)\right]^2} \qquad m = (i,t,r) \tag{F.43}$$

taking the real and imaginary parts of the transmission and reflection laws show that

$$w_t(0) = w_r(0) = w_i(0) \tag{F.44}$$

i.e. the widths of all the beams at the interface are the same and also

$$\begin{aligned} \frac{1}{R_t(0)} &= \left(\frac{c_{p2}}{c_{p1}} - 1\right)\frac{1}{R_0} + \frac{c_{p2}}{c_{p1}}\frac{1}{R_i(0)} \\ \frac{1}{R_r(0)} &= \frac{2}{R_0} + \frac{1}{R_i(0)} \end{aligned} \tag{F.45}$$

showing how the wave front curvatures of the incident and transmitted/ reflected Gaussian beams are related at the interface. For a planar interface, these relations simply reduce to

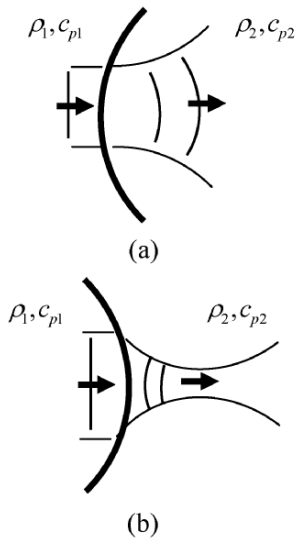

Fig. F.6. A Gaussian beam incident on a curved interface where the waist of the incident beam is located at the interface and the corresponding transmitted Gaussian beam and its wave front curvature is shown for **(a)** $c_{p2} > c_{p1}$ and $R_0 > 0$, **(b)** $c_{p2} > c_{p1}$ and $R_0 < 0$.

$$\frac{1}{R_t(0)} = \frac{c_{p2}}{c_{p1}} \frac{1}{R_i(0)}$$
$$\frac{1}{R_r(0)} = \frac{1}{R_i(0)}. \tag{F.46}$$

From Eq. (F.45) we can gain some understanding of the effects of the curvature of the interface (and the wave speeds) on the transmitted wave if we consider the case where the waist of the incident beam occurs at the interface so that $1/R_i(0) = 0$. Then if we have $c_{p2} > c_{p1}$ and $R_0 > 0$ we see from Eq. (F.45) that $R_t(0) > 0$. In this case the transmitted Gaussian beam is a diverging beam as shown in Fig. F.6 (a). This type of interface is therefore a *defocusing interface* for the transmitted wave. If instead we have $c_{p2} > c_{p1}$ and $R_0 < 0$ we find $R_t(0) < 0$ and the transmitted Gaussian beam is a converging beam as shown in Fig. F.6 (b). In this case the interface acts as a *focusing interface* for the transmitted wave. But for

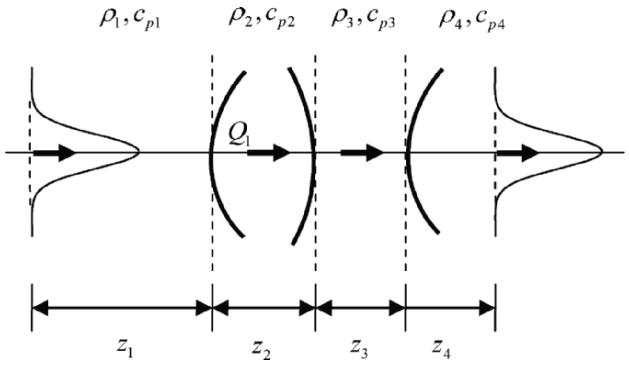

Fig. F.7. The transmission of a circularly symmetric Gaussian beam across multiple spherically curved interfaces.

$c_{p2} < c_{p1}$ the interfaces shown in Fig. F.6 (a), (b) are instead focusing and defocusing interfaces, respectively, for the transmitted wave. These same focusing or defocusing characteristics of curved interfaces were also discussed in Chapter 8, section 8.12. If we again let $1/R_i(0) = 0$ and examine the reflected wave, Eq. (F.45) shows that regardless of the wave speeds we have $R_r(0) > 0$ if $R_0 > 0$ and $R_r(0) < 0$ if $R_0 < 0$, which results in a diverging (defocused) and converging (focused) reflected Gaussian beam, respectively.

F.4 Gaussian Beams at Multiple Interfaces and ABCD Matrices

In the last section we developed the transmission/reflection laws for a symmetrical Gaussian beam at normal incidence to a spherically curved interface. We also have previously obtained the propagation law for a Gaussian beam (Eq. (F.9)). If an axially symmetrical Gaussian beam interacts with multiple spherically curved interfaces at normal incidence we can use those laws and the plane wave transmission/reflection coefficients to obtain the final form of the Gaussian beam (see Fig. F.7, where the beam is shown in undergoing multiple transmissions only, but we will also consider here multiple reflections as well). For example, if a

Gaussian beam starts at $z = 0$ with a pressure amplitude $\tilde{P}(0)$ and phase parameter $q_1(0)$, then after propagation through a distance z_1 we have:

$$p = \tilde{P}(0)\frac{q_1(0)}{q_1(z_1)}\exp(ik_{p1}z_1)\exp\left[\frac{ik_{p1}}{2}\frac{\rho^2}{q_1(z_1)}\right]. \tag{F.47}$$

If this beam then is transmitted across an interface at a point Q_1 (see Fig. F.7) where $z = z_1$ and propagates from Q_1 a distance z_2 in a second medium we have

$$\begin{aligned} p(z_2,\omega) = \tilde{P}(0)&\frac{q_2(Q_1)}{q_2(z_2)}T_{12}\frac{q_1(0)}{q_1(Q_1)} \\ &\cdot\exp(ik_{p1}z_1 + ik_{p2}z_2)\exp\left[\frac{ik_{p2}}{2}\frac{\rho^2}{q_2(z_2)}\right], \end{aligned} \tag{F.48}$$

where $q_m(z)$ is the q-parameter for the mth media and we will take the z-coordinate for each medium to have as its origin the starting point for the Gaussian beam in that medium. Since point Q_1 is both the ending point for the beam in medium one and the starting point for the beam in medium two we have $q_1(Q_1) = q(z_1)$, $q_2(Q_1) = q_2(0)$ so we can also write Eq. (F.48) as

$$\begin{aligned} p(z_2,\omega) = \tilde{P}(0)&\frac{q_2(0)}{q_2(z_2)}T_{12}\frac{q_1(0)}{q_1(z_1)} \\ &\cdot\exp(ik_{p1}z_1 + ik_{p2}z_2)\exp\left[\frac{ik_{p2}}{2}\frac{\rho^2}{q_2(z_2)}\right]. \end{aligned} \tag{F.49}$$

Obviously this same process can be continued for additional transmissions (or reflections). After the interaction with M interfaces, for example, we could write the beam in medium M+1 as

$$\begin{aligned} p(z_{M+1},\omega) = \tilde{P}(0)&\frac{q_{M+1}(0)}{q_{M+1}(z_{M+1})}\prod_{m=1}^{M}\tilde{T}_{m\,m+1}\frac{q_m(0)}{q_m(z_m)} \\ &\cdot\exp\left[i\sum_{m=1}^{M+1}k_{pm}z_m\right]\exp\left[\frac{ik_{pM+1}}{2}\frac{\rho^2}{q_{M+1}(z_{M+1})}\right], \end{aligned} \tag{F.50}$$

where $\tilde{T}_{m\,m+1}$ is either a transmission or reflection coefficient depending on whether we are considering a transmitted or reflected wave at the mth interface between medium m and m+1. The propagation and transmission/ reflection laws developed previously then can be written for all M +1 media as

Propagation laws: (for M +1 media)

$$q_m(z_m) = q_m(0) + z_m \qquad (m = 1, M+1) \tag{F.51}$$

Transmission laws: (for M interfaces)

$$q_{m+1}(Q_m) = \frac{q_m(Q_m)}{\left(\frac{c_{p\,m+1}}{c_{p\,m}} - 1\right)\frac{q_m(Q_m)}{(R_0)_m} + \frac{c_{p\,m+1}}{c_{p\,m}}} \qquad (m = 1, M) \tag{F.52}$$

Reflection laws: (for M interfaces)

$$q_{m+1}(Q_m) = \frac{q_m(Q_m)}{\frac{2}{(R_o)_m} q_m(Q_m) + 1} \qquad (m = 1, M) \tag{F.53}$$

If we let a final value of q after propagation/transmission/reflection be q_f and an initial value before propagation/transmission/reflection be q_i, then all these laws can be written in the form [F.1], [F.2]

$$q_f = \frac{Aq_i + B}{Cq_i + D} \tag{F.54}$$

or, equivalently,

$$\frac{1}{q_f} = \frac{D(1/q_i) + C}{B(1/q_i) + A}, \tag{F.55}$$

and the ABCD parameters can be placed in an ABCD matrix that defines each law:

Propagation laws:

$$\begin{bmatrix} A^d & B^d \\ C^d & D^d \end{bmatrix} = \begin{bmatrix} 1 & z_m \\ 0 & 1 \end{bmatrix} \tag{F.56}$$

Transmission laws:

$$\begin{bmatrix} A^t & B^t \\ C^t & D^t \end{bmatrix} = \begin{bmatrix} 1 & 0 \\ \dfrac{\left(c_{p\,m+1}/c_{p\,m}-1\right)}{\left(R_0\right)_m} & \dfrac{c_{p\,m+1}}{c_{p\,m}} \end{bmatrix} \tag{F.57}$$

Reflection laws:

$$\begin{bmatrix} A^r & B^r \\ C^r & D^r \end{bmatrix} = \begin{bmatrix} 1 & 0 \\ \dfrac{2}{\left(R_0\right)_m} & 1 \end{bmatrix} \tag{F.58}$$

A remarkable feature of writing the laws in this fashion is that even after multiple propagations and transmissions/reflections the final and starting q-values can still be related in the forms of Eq. (F.54) and Eq. (F.55) as

$$q_f = \frac{A^G q_i + B^G}{C^G q_i + D^G} \tag{F.59}$$

and

$$\frac{1}{q_f} = \frac{D^G\left(1/q_i\right) + C^G}{B^G\left(1/q_i\right) + A^G}, \tag{F.60}$$

where the "global" ABCD matrix components appearing in Eq. (F.59) and Eq. (F.60) can be obtained from a matrix multiplication of all the individual propagation, transmission, and reflection ABCD matrices that define a particular set of beam propagations or interface interactions. One can easily prove this fact by merely placing Eq. (F.54) for one ABCD matrix into Eq. (F.54) involving a second ABCD matrix and showing that the resulting equation again is in the same form of Eq. (F.54) but with ABCD elements corresponding to the matrix multiplication of the original two matrices. For example, after propagation of a beam in medium one followed by a transmission across an interface we would have

$$\begin{bmatrix} A^G & B^G \\ C^G & D^G \end{bmatrix} = \begin{bmatrix} A^t & B^t \\ C^t & D^t \end{bmatrix} \begin{bmatrix} A^d & B^d \\ C^d & D^d \end{bmatrix} \tag{F.61}$$

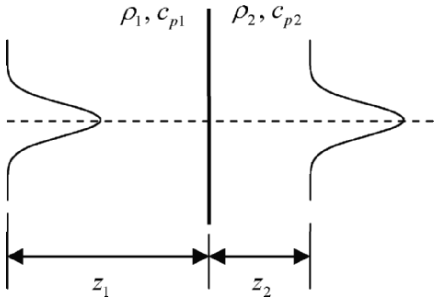

Fig. F.8. Propagation of a Gaussian beam across a plane interface.

and this same process can be continued for any number of interactions [Note: the order of the matrix multiplications is important. In the above example propagation occurs first, followed by transmission, but in multiplying the ABCD matrices this order is reversed]. Using ABCD matrices in this fashion makes it very easy to follow a Gaussian beam through multiple interfaces and similar ABCD matrices are commonly used in the laser science field to describe the interaction a Gaussian laser beam with multiple optical elements such as lenses, mirrors, etc. As a simple example, consider the propagation of a Gaussian beam through a distance z_1 in medium one followed by transmission across a plane interface, and then propagation through a distance z_2 in medium two (see Fig. F.8). In this case we have

$$\begin{aligned}\begin{bmatrix} A^G & B^G \\ C^G & D^G \end{bmatrix} &= \begin{bmatrix} 1 & z_2 \\ 0 & 1 \end{bmatrix}\begin{bmatrix} 1 & 0 \\ 0 & c_{p2}/c_{p1} \end{bmatrix}\begin{bmatrix} 1 & z_1 \\ 0 & 1 \end{bmatrix} \\ &= \begin{bmatrix} 1 & z_1 + \left(c_{p2}/c_{p1}\right) z_2 \\ 0 & \left(c_{p2}/c_{p1}\right) \end{bmatrix}\end{aligned} \tag{F.62}$$

so that Eq. (F.59) yields

$$q_2\left(z_2\right) = \frac{c_{p1}}{c_{p2}}\left[q_1\left(0\right) + z_1 + \frac{c_{p2}}{c_{p1}} z_2 \right]. \tag{F.63}$$

This shows that the phase terms of the incident beam propagating, which is given by:

$$\frac{ik_{p1}}{2}\frac{\rho^2}{q_1(0)+z_1} \tag{F.64}$$

becomes for the transmitted beam

$$\frac{ik_{p1}}{2}\frac{\rho^2}{q_1(0)+\left(z_1+\left(c_{p2}/c_{p1}\right)z_2\right)}, \tag{F.65}$$

which looks exactly like the incident beam term with the replacement $z_1 \to z_1+\left(c_{p2}/c_{p1}\right)z_2$. This same behavior is discussed in Chapter 8, section 8.5 when examining the on-axis pressure for a circular piston transducer in the paraxial approximation.

In a single medium problem the phase term in the Gaussian beam can be written as

$$\frac{ik_{p1}}{2}\frac{\rho^2}{q_1(z_1)}=\frac{ik_{p1}}{2}\frac{\rho^2}{\left[\dfrac{A_1^d q_1(0)+B_1^d}{C_1^d q_1(0)+D_1^d}\right]}, \tag{F.66}$$

where the propagation ABCD matrix components for medium one are $A_1^d=D_1^d=1, B_1^d=z_1, C_1^d=0$. By using the global ABCD matrix formed from the individual ABCD matrices for a multiple medium problem, the phase term in Eq. (F.50) can also be written in the same form where

$$\frac{ik_{pM+1}}{2}\frac{\rho^2}{q_{M+1}(z_{M+1})}=\frac{ik_{pM+1}}{2}\frac{\rho^2}{\left[\dfrac{A^G q_1(0)+B^G}{C^G q_1(0)+D^G}\right]}. \tag{F.67}$$

In a single medium case the amplitude coefficient of the Gaussian beam contains the term

$$\frac{q_1(0)}{q_1(z_1)}=\frac{q_1(0)}{\left[A_1^d q_1(0)+B_1^d\right]}. \tag{F.68}$$

The similar part of the amplitude coefficient in Eq. (F.50) for a multiple medium problem contains a series of products of the same form given on the left side of Eq. (F.68). Consider, for example, the first two products given by:

$$\frac{q_2(0)}{q_2(z_2)}\frac{q_1(0)}{q_1(z_1)} \tag{F.69}$$

and the global ABCD matrix corresponding to propagation in medium one, transmission across the first interface, and propagation in medium two:

$$\begin{bmatrix} A^G & B^G \\ C^G & D^G \end{bmatrix} = \begin{bmatrix} A_2^d & B_2^d \\ C_2^d & D_2^d \end{bmatrix}\begin{bmatrix} A_1^t & B_1^t \\ C_1^t & D_1^t \end{bmatrix}\begin{bmatrix} A_1^d & B_1^d \\ C_1^d & D_1^d \end{bmatrix}, \tag{F.70}$$

where $\left(A_m^d, B_m^d, C_m^d, D_m^d\right)$ are the ABCD matrix components for propagation in medium m, and $\left(A_m^t, B_m^t, C_m^t, D_m^t\right)$ are the ABCD components for transmission across the mth interface. We have

$$\begin{aligned} \frac{1}{q_2(z_2)} &= \frac{1}{A_2^d q_2(0) + B_2^d} \\ q_2(0) &= \frac{q_1(z_1)}{C_1^t q_1(z_1) + D_1^t} \end{aligned} \tag{F.71}$$

so combining these two relations we find

$$\frac{1}{q_2(z_2)} = \frac{C_1^t q_1(z_1) + D_1^t}{A' q_1(z_1) + B'} = \frac{\left[q_1(z_1)/q_2(0)\right]}{A' q_1(z_1) + B'}, \tag{F.72}$$

where

$$\begin{aligned} \begin{bmatrix} A' & B' \\ C' & D' \end{bmatrix} &= \begin{bmatrix} A_2^d & B_2^d \\ C_2^d & D_2^d \end{bmatrix}\begin{bmatrix} A_1^t & B_1^t \\ C_1^t & D_1^t \end{bmatrix} \\ &= \begin{bmatrix} A_2^d & B_2^d \\ C_2^d & D_2^d \end{bmatrix}\begin{bmatrix} 1 & 0 \\ C_1^t & D_1^t \end{bmatrix}. \end{aligned} \tag{F.73}$$

We then can substitute $q_1(z_1) = A_1^d q_1(0) + B_1^d$ into $A' q_1(z_1) + B'$ to obtain

$$A' q_1(z_1) + B' = A^G q_1(0) + B^G \tag{F.74}$$

in terms of the global matrix elements $A^G = A' A_1^d$, $B^G = A' A_1^d + B'$. This also follows by writing Eq. (F.70) as

$$\begin{aligned}\begin{bmatrix} A^G & B^G \\ C^G & D^G \end{bmatrix} &= \begin{bmatrix} A' & B' \\ C' & D' \end{bmatrix}\begin{bmatrix} A_1^d & B_1^d \\ C_1^d & D_1^d \end{bmatrix} \\ &= \begin{bmatrix} A' & B' \\ C' & D' \end{bmatrix}\begin{bmatrix} A_1^d & B_1^d \\ 0 & 1 \end{bmatrix}.\end{aligned} \tag{F.75}$$

Thus, from Eqs. (F.72) and (F.74) we can write

$$\frac{q_2(0)}{q_2(z_2)}\frac{q_1(0)}{q_1(z_1)} = \frac{q_1(0)}{A^G q_1(0) + B^G}, \tag{F.76}$$

which has exactly the same form as for the single medium case (Eq. (F.68)). We can continue this process and consider all the other pairs of amplitude terms in Eq. (F.50) in exactly the same manner and so obtain

$$\frac{q_{M+1}(0)}{q_{M+1}(z_{M+1})}\prod_{m=1}^{M}\frac{q_m(0)}{q_m(z_m)} = \frac{q_1(0)}{A^G q_1(0) + B^G}, \tag{F.77}$$

where now $\left(A^G, B^G\right)$ are elements of the global ABCD matrix for all the media and interfaces involved in going from medium one to medium M+1.

We can also define a global transmission/reflection coefficient, $\mathcal{T} = \prod_{m=1}^{M}\tilde{T}_{m\,m+1}$ and a propagation delay term $t_0 = \sum_{m=1}^{M+1} z_m / c_{pm}$ and write Eq. (F.50) as

$$\begin{aligned} p(z_{M+1},\omega) &= \mathcal{T}\tilde{P}(0)\frac{q_1(0)}{A^G q_1(0) + B^G} \\ &\cdot\exp[i\omega t_0]\exp\left[\frac{ik_{p\,M+1}}{2}\frac{\rho^2}{\dfrac{A^G q_1(0) + B^G}{C^G q_1(0) + D^G}}\right], \end{aligned} \tag{F.78}$$

which is in exactly the same form as for the propagation of a Gaussian beam in a single medium where using the same notation we have:

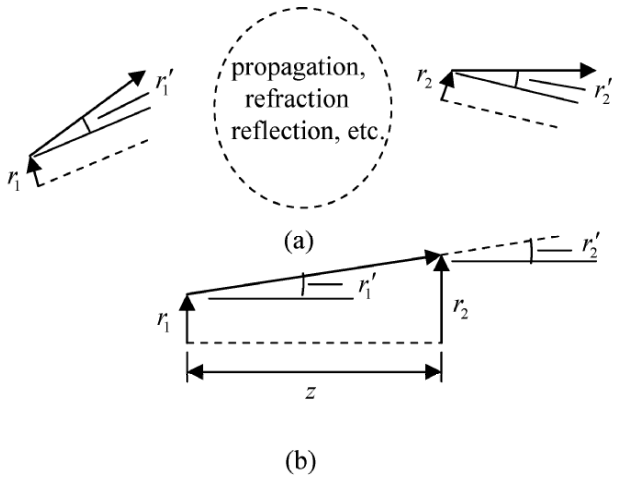

Fig. F.9. (a) A paraxial geometrical ray before and after a general ray interaction, and **(b)** the special case of propagation of the ray over a distance, z. The central ray is the dashed line and the paraxial ray is assumed to have a small distance from the central ray and a small slope relative to the central ray.

$$p(z_1,\omega)=\tilde{P}(0)\frac{q_1(0)}{A_1^d q_1(0)+B_1^d} \cdot\exp\left[ik_{p1}z_1\right]\exp\left[\frac{ik_{p1}}{2}\frac{\rho^2}{\dfrac{A_1^d q_1(0)+B_1^d}{C_1^d q_1(0)+D_1^d}}\right]. \tag{F.79}$$

In Chapter 9 it is shown that even in more general Gaussian beam problems one can use ABCD matrices, but for those cases the scalar (A,B,C,D) components are replaced by 2x2 matrices $(\mathbf{A},\mathbf{B},\mathbf{C},\mathbf{D})$.

The ABCD matrices used here for our Gaussian beam problems are closely related to the same ABCD matrices used in geometrical optics to facilitate the tracing of paraxial rays through optical elements [F.1], [F.2]. Consider, for example a central ray before and after a given interaction (such as propagation through a lens or reflection from a mirror, etc.) as shown in Fig. F.9 (a) and a nearby (paraxial) ray. Let (r_1,r_1') be the

displacement and slope of the paraxial ray from the central ray before an interaction and let (r_2, r_2') be the same quantities for the paraxial ray after an interaction (see Fig. F.9 (a)). For a paraxial ray that is close to the central ray and at a small slope to that ray it is reasonable to assume that these quantities are linearly related to one another, i.e.

$$\begin{pmatrix} r_2 \\ r_2' \end{pmatrix} = \begin{bmatrix} A & B \\ C & D \end{bmatrix} \begin{pmatrix} r_1 \\ r_1' \end{pmatrix}. \tag{F.80}$$

However, if we define curvatures $R_1 = r_1 / r_1', R_2 = r_2 / r_2'$ we find

$$R_2 = \frac{AR_1 + B}{CR_1 + D}, \tag{F.81}$$

which is of the same form as Eq. (F.59) for the *q*- parameter in a Gaussian beam. This is perhaps not surprising since the wave front curvature of the Gaussian beam, $R(z)$, is related to $q(z)$ through

$$\mathrm{Re}\left(\frac{1}{q(z)}\right) = \frac{1}{R(z)} \tag{F.82}$$

(where Re denotes "real part of") so that we can view the use of the ABCD matrices for Gaussian beam problems as the extension of the geometrical optics relations for real ray curvatures to corresponding complex *q*-values that define the Gaussian beam. To demonstrate in a simple case that the geometrical optics ABCD matrices are indeed the same as our Gaussian beam matrices, consider the ABCD matrix for propagation of a ray through a distance, *z*, as shown in Fig. F.9 (b).Then since $r_2' = r_1'$ and $r_2 = r_1 + r_1' z$ (for small slopes) we have

$$\begin{pmatrix} r_2 \\ r_2' \end{pmatrix} = \begin{bmatrix} 1 & z \\ 0 & 1 \end{bmatrix} \begin{pmatrix} r_1 \\ r_1' \end{pmatrix}, \tag{F.83}$$

which is identical to the propagation ABCD matrix of Eq. (F.56). In Chapter 9, this same example is discussed in a more general context (see section 9.4).

F.5 Multi-Gaussian Beam Modeling

In 1988 Wen and Breazeale [F.4] showed that by the superposition of only 10 Gaussian beams, one could generate an accurate model of the radiated wave field of a circular planar piston transducer. Since commercial ultrasonic NDE transducers can often be modeled as piston transducers, this multi-Gaussian beam model is a very effective tool for simulating the sound beams generated in NDE tests. Here we will briefly outline Wen and Breazeale's multi-Gaussian beam model and relate it to our previous Gaussian beam discussions. Chapter 9 also gives many more details of multi-Gaussian beam models.

At $z = 0$ for a single Gaussian beam the pressure is given by (see Eq. (F.11))

$$p = \frac{P_0}{q_0} \exp\left[\frac{ik_p \rho^2}{2q_0}\right]. \tag{F.84}$$

Wen and Breazeale wrote Eq. (F.81) instead as

$$\frac{p}{\rho c_p v_0} = A \exp\left[-B\rho^2 / a^2\right] \tag{F.85}$$

and used a non-linear least squares optimization procedure to determine a set of 10 complex A and B coefficients that produced a constant velocity, v_0, on the face of a circular piston transducer of radius a located at $z = 0$, as discussed in more detail in Chapter 9. The wave field generated by the superposition of 10 Gaussian beams with the starting forms of Eq. (F.81) is shown in Chapter 9 to match well the exact wave field of the piston transducer except close to the transducer face. Note that these A, B coefficients represent Gaussian beams of different waist locations, widths and amplitudes since

$$\begin{aligned} A &= \frac{-P_0 / \rho c_p v_0}{z_0 + iz_c} \\ B &= \frac{ik_p a^2}{2\left(z_0 + iz_c\right)} \end{aligned} \tag{F.86}$$

from which it follows that

$$-q_0 = z_0 + iz_c = \frac{ik_p a^2/2}{B}$$
$$\frac{P_0}{\rho c_p v_0} = -A\frac{ik_p a^2/2}{B}. \tag{F.87}$$

A multi-Gaussian beam model of a transducer uses the A, B coefficients directly to synthesize the transducer wave field so there is no advantage in expressing the wave field in terms of Gaussian waist locations and width parameters, as is commonly done in the laser science literature. Instead, using Eq. (F.87) we can write the propagating Gaussian beam in a single medium (see Eq. (F.11)) in terms of A and B directly:

$$p = \frac{\rho c_p v_0 A}{1 + iBz/D_R}\exp\left[ik_p z\right]\exp\left[\frac{ik_p\rho^2}{2}\frac{\left(iB/D_R\right)}{\left(1+iBz/D_R\right)}\right], \tag{F.88}$$

where $D_R = k_p a^2/2$ is called the *Rayleigh distance* for the piston transducer, a quantity that is analogous to the confocal parameter for a Gaussian beam. Using the ten A, B coefficients of Wen and Breazeale then yields a multi-Gaussian transducer beam model for a single medium given by

$$p = \sum_{n=1}^{10}\frac{\rho c_p v_0 A_n}{1 + iB_n z/D_R}\exp\left[ik_p z\right]\exp\left[\frac{ik_p\rho^2}{2}\frac{\left(iB_n/D_R\right)}{\left(1+iB_n z/D_R\right)}\right], \tag{F.89}$$

which is the form used in Chapter 9 (see Eq. (9.134)). If we define starting values for each of the Gaussian beams in Eq. (F.89) as

$$\left[q_1(0)\right]_n = \frac{-ik_p a^2/2}{B_n}$$
$$\tilde{P}_n(0) = \rho c_p v_0 A_n \tag{F.90}$$

then using Eq. (F.78) we have a very simple model for the field of a piston transducer after multiple transmissions or reflections:

$$p\left(z_{M+1},\omega\right)=\sum_{n=1}^{10}\mathcal{T}\tilde{P}_n\left(0\right)\frac{\left[q_1\left(0\right)\right]_n}{A^G\left[q_1\left(0\right)\right]_n+B^G}$$
$$\cdot\exp\left[i\omega t_0\right]\exp\left[\frac{ik_{p\,M+1}}{2}\frac{\rho^2}{\dfrac{A^G\left[q_1\left(0\right)\right]_n+B^G}{C^G\left[q_1\left(0\right)\right]_n+D^G}}\right]. \tag{F.91}$$

In Chapter 9, use is made of the Wen and Breazeale coefficients and the corresponding $\left(\mathbf{A},\mathbf{B},\mathbf{C},\mathbf{D}\right)$ matrices in this same manner to obtain transducer wave fields much more complex multiple media problems.

F.6 References

F.1 Goldsmith PF (1998) Quasi-optical systems. IEEE Press, Piscataway, NJ
F.2 Siegman AE (1986) Lasers. University Science Books, Mill Valley, CA
F.3 Heyman E, Felsen LB (2001) Gaussian beam and pulsed-beam dynamics: complex-source and complex-spectrum formulations within and beyond paraxial asymptotics. J. Opt. Soc. Am. 18: 1588-1611
F.4 Wen JJ, Breazeale MA (1988) A diffraction beam field expressed as the superposition of Gaussian beams. J. Acoust. Soc. Am. 83: 1752-1756
F.5 Huang D, Breazeale MA (1999) A Gaussian finite-element method for description of sound diffraction. J. Acoust. Soc. Am. 106: 1771-1781

F.7 Exercises

1. Consider the propagation of a central ray and a paraxial ray at oblique incidence across a plane interface where the paraxial ray lies in the *x*-*z* plane (see Fig. F.10). Relate the distances $\left(x_1,x_2\right)$ to each other to first order in terms of the angles $\left(\theta_1,\theta_2\right)$ directly from the geometry. Also, using Snell's law, which must be satisfied for both the central ray and the paraxial ray, relate the slopes $\left(x_1',x_2'\right)$ to each other to first order in terms of $\left(\theta_1,\theta_2\right)$ and $\left(c_{p1},c_{p2}\right)$. Combining these results, obtain the ABCD matrix for this case, where

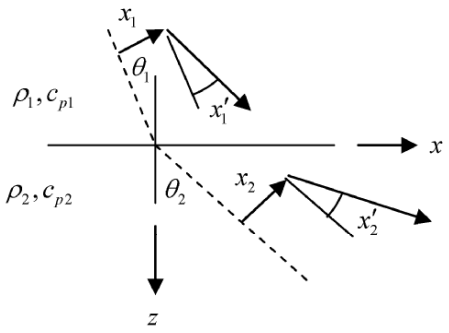

Fig. F.10. A central ray (dashed line) and a nearby paraxial ray (arrows) being transmitted at oblique incidence across a planar interface.

$$\begin{Bmatrix} x_2 \\ x_2' \end{Bmatrix} = \begin{bmatrix} A_x & B_x \\ C_x & D_x \end{bmatrix} \begin{Bmatrix} x_1 \\ x_1' \end{Bmatrix}$$

Since there is no change in direction for the central ray in the *y*-direction, the values (y_2, y_2') and (y_1, y_1') for the paraxial ray are related by a corresponding ABCD matrix valid near normal incidence. From your previous results let $\theta_1, \theta_2 \to 0$ to show that in this case

$$\begin{Bmatrix} y_2 \\ y_2' \end{Bmatrix} = \begin{bmatrix} A_y & B_y \\ C_y & D_y \end{bmatrix} \begin{Bmatrix} y_1 \\ y_1' \end{Bmatrix} = \begin{bmatrix} 1 & 0 \\ 0 & c_{p2}/c_{p1} \end{bmatrix} \begin{Bmatrix} y_1 \\ y_1' \end{Bmatrix}$$

Because there are different ABCD matrices in the *x*- and *y*-directions, an incident Gaussian beam of circular cross-section, where the phase term is given at the interface by

$$\exp\left[\frac{ik_{p1}}{2}\frac{\rho^2}{q_i}\right] = \exp\left[\frac{ik_{p1}}{2}\frac{\left(x^2+y^2\right)}{q_i}\right]$$

will be changed, upon transmission through the interface into a Gaussian beam of elliptical cross section, where the phase term is:

$$\exp\left[\frac{ik_{p2}}{2}\left(\frac{x^2}{\dfrac{A_x q_i + B_x}{C_x q_i + D_x}} + \frac{y^2}{\dfrac{c_{p1} q_i}{c_{p2}}}\right)\right]$$

Thus, for oblique incidence problems we can no longer consider only circular cross-section Gaussian beam solutions of the paraxial wave equation but must treat more general solutions for elliptical cross-section Gaussian beams. For oblique incidence on curved interfaces the transmitted Gaussian beam can also be rotated, resulting in Gaussian beams with phase terms containing both quadratic and mixed products of the coordinates, i.e. $\left(x^2, xy, y^2\right)$. Chapter 9 treats these more general cases by seeking Gaussian beam solutions to the paraxial wave equation given by

$$p = P(z)\exp\left(ik_{p1}z\right)\exp\left(\frac{i\omega}{2}\mathbf{X}^T\mathbf{M}_p(z)\mathbf{X}\right)$$

where $\mathbf{X} = [x, y]^T$ and $\mathbf{M}_p$ is a 2x2 symmetrical matrix. For a circular cross-section Gaussian beam then we have

$$\mathbf{M}_p(z) = \begin{bmatrix} \dfrac{1}{c_{p1}q(z)} & 0 \\ 0 & \dfrac{1}{c_{p1}q(z)} \end{bmatrix}$$

2. Wen and Breazeale also defined 15 Gaussian beam coefficients $\left(A_n, B_n\right)$ that improve on the modeling of a circular planar piston transducer in comparison to their original 10 coefficients [F.5]. Use the MATLAB function gauss_c15 that returns those 15 coefficients and write a MATLAB script that obtains the normalized pressure field, $p/\rho_1 c_{p1} v_0$, for a 6.35 mm radius piston transducer radiating through spherically curved water-steel interface ($R_0 = 76$ mm) at a frequency of 5 MHz (see Fig. F.11) and plots the magnitude of the on-axis normalized pressure versus the distance z_2 in the steel from $z_2 = 0$ to $z_2 = 50$ mm. Modify the script and consider the same case but where $R_0 = -76$ mm.

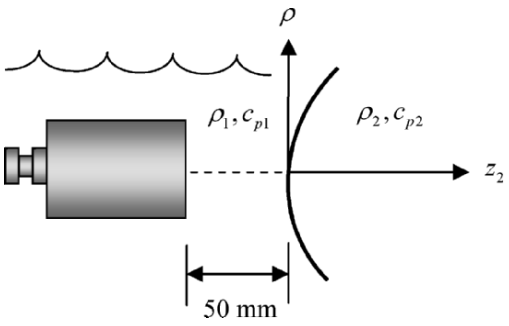

Fig. F.11. A circular planar piston transducer radiating a sound beam through a spherically curved fluid-solid interface.

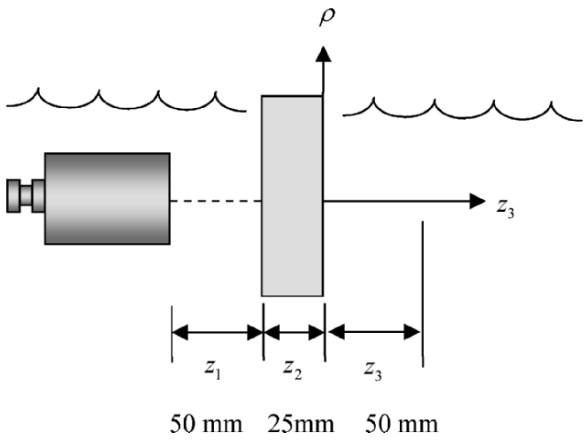

Fig. F.12. Radiation of an immersion transducer through an aluminum plate.

3. Rewrite the scripts of problem 2 so that they display a 2-D image of the magnitude of the normalized pressure (i.e. normalized pressure versus (ρ, z_2)) in the steel for both the defocusing and focusing interfaces considered there.

4. Use the ABCD matrices and the 15 coefficients of Wen and Breazeale contained in the MATLAB function gauss_c15 to write a MATLAB script that obtains the normalized pressure, $p/\rho_1 c_{p1} v_0$, in a sound beam that is directly transmitted (with no reflections) from a 10 MHz, 6.35 mm radius planar piston transducer through the aluminum plate shown in Fig. F.12. The script should plot the magnitude of the normalized pressure versus ρ at $z_3 = 50$ mm.

5. Modify the script of problem 4 so that the normalized pressure transmitted through the plate is evaluated at many frequencies for $\rho = 0$, $z_3 = 50$ mm and is multiplied at each frequency by the MATLAB function spectrum1 written for exercise 1 in Appendix A, where the center frequency fc = 10 MHz and the bandwidth bw = 4 MHz. Evaluate this product at 1024 positive frequencies ranging from zero to 100 MHz and use the Fourier transform IFourierT defined in Appendix A to obtain a time-domain pulse. Plot that pulse versus time. In evaluating the normalized pressure, ignore the $\exp\left[ik_{p1} z_1 + ik_{p2} z_2 + ik_{p3} z_3 \right]$ propagation term which simply produces a time delay.

G MATLAB Functions and Scripts

A number of MATLAB functions and scripts are described in the text. The MATLAB code listings for all these functions/scripts are available on the web at www.springer.com/978-0-387-49061-8. The web site also has the MAT-files that contain the experimental data used in various model/ experimental comparisons. In this Appendix we will summarize the MATLAB functions and scripts discussed in the text and give code listings for those functions which are not explicitly defined elsewhere. Note that a number of the MATLAB functions used in the exercises are not given here, but they can be found on the web site. In some cases those MATLAB functions are given in p-code form instead of ordinary open text m-files so that they can be used by students as unknown "black boxes" in some of the exercise problems given at the end of the Chapters. Those p-code functions were generated in MATLAB release 7.0 so that they will not work with earlier versions of MATLAB. If this poses a problem, there are alternate p-code versions of the same functions on the web that were generated in release 6.5 and are identified by having a "65" in their function name.

G.1 Fourier Analysis Functions

```
Vf = FourierT(vt , dt);
vt = IFourierT(Vf , dt);
y = s_space(a, b, M);
y = c_shift(vt, N);
y = t_shift(t, N);
y = Wiener_filter(O, I, e);
Vf =lp_filter(f, fstart, fend);
y = system_f (f, amp, fc, bw);
```

The functions Fourier_T(vt, dt) and IFourierT(Vf, dt) perform the Fast Fourier transform and its inverse on a set of sampled values in the time and frequency domains, respectively. Besides those sampled values the sampling interval in the time domain, dt, is the only other input parameter

to these functions. These discrete Fourier transforms implement the Fourier transform and its inverse as defined in Appendix A. Code listings of both these functions can be found in Appendix A.

The function s_space(a, b, M) is a utility function that produces a set of M evenly spaced sampled values from a to (b − dx), where dx = (b − a)/M is the sample spacing. These are precisely the sampled values that are used in Fourier analysis so that this function is used primarily to generate the time and frequency axes to use in conjunction with FourierT and IFourierT. This function is discussed in Chapter 12 and the code listing for the function can be found in section G.8.

The function c_shift(vt, N) moves the last N components of the vector vt into the first N component places and shifts the remaining components of vt to follow those N components. This type of shift is called a circular shift. This shift is sometimes needed since IFourierT always generates a set of sampled time domain values over the time interval [0, T), where T = 1/df is the length of the total time window and df is the sample interval in the frequency domain. However, if the sampled time domain function values are non-zero before time t = 0, these sampled values at negative times will appear in the upper half of the window and the function will appear to be "split". This splitting can be removed by applying c_shift to the sampled values with a large enough value for N. For example, consider the following eight function values:

```
>> f= [ 1 1 0 0 0 0 2 2];
```

If we apply c_shift to this function with N = 2 we obtain

```
>> fs =c_shift(f,2)

fs =

    2    2    1    1    0    0    0    0
```

The use of c_shift on a sampled time-domain signal will also mean that the corresponding sampling times will be incorrect. In some cases this is not significant, but if one wants to also change the time axis appropriately to preserve the original time values then the function t_shift(t, N) can also be used in conjunction with c_shift. As a simple example of the action of t_shift, consider the following eight time domain values:

```
>> t = [ 0  0.1  0.2  0.3  0.4  0.5  0.6  0.7];
```

Now, apply t_shift to this sampled time axis with N = 2:

```
>> t_shift(t, 2)

ans =

  -0.2000   -0.1000         0    0.1000    0.2000    0.3000    0.4000
0.5000
```

In most cases t_shift is used in conjunction with c_shift in plotting a sampled function. For example, the MATLAB command plot(t_shift(t, N), c_shift(V, N)) will do a circular shift of the last N sampled values contained in the vector V and also modify the sampled values of the time axis contained in the vector t appropriately so that the original time origin is changed appropriately in the resulting plot. The code listings for both c_shift and t_shift are given in section G.8.

The function Wiener_filter(O, I, e) is described in Appendix C where its code listing is also given. This function takes the sampled frequency domain values contained in vectors O and I and performs a deconvolution. A direct deconvolution would simply be an element by element division, i.e. in MATLAB we would compute

```
>> G = O./ I ;
```

The Wiener filter function modifies this division process and desensitizes it to noise, as discussed in Appendix C. The constant, e, which is the other input to this function, is used in the Wiener filter to represent the noise level present. Generally, small values such as e = 0.01 to 0.05 work well in many ultrasonic NDE problems.

The function lp_filter(f, fstart, fend) generates a low-pass filter that is unity below a frequency value, fstart, and smoothly goes to zero at the value, fend. Above fend the function is zero. Multiplying a model-based function (that is defined in the frequency domain) by this low-pass filter will remove the high frequency content and allow one to perform an inverse FFT on the product as long as fend is chosen below the Nyquist frequency. The code listing for this function is given in section G.8.

The function system_f (f, amp, fc, bw) models the behavior of a system function in the frequency domain with a Gaussian that is defined by its amplitude, center frequency, and bandwidth. The code listing for this function is given in section G.8.

G.2 Setup Functions

```
setup = setup_maker;
display_setup;
```

The function setup_maker provides a way of storing all the input parameters needed to generate the ultrasonic measurement models described in Chapter 12. The function places a default set of values for all these parameters in a MATLAB structure called setup which then can be modified by the user to produce any set of parameters needed to describe a particular ultrasonic system configuration. When modifying the setup structure, it is convenient to be able to examine its contents to check that the proper parameters are present. This can be easily done with the function display_setup which lists all the current setup parameters. There are no input arguments for either of these functions. The code listings for both setup_maker and display_setup are given in Chapter 12.

G.3 Ultrasonic Beam Modeling Functions

```
[A, B] = gauss_c15;
T = fluid_solid(setup);
T =smooth_solid(setup);
V = init_z(setup);
[Vf, setup] = MGbeam(setup);
[Vi, setup] = I_MGbeam(setup);
```

The multi-Gaussian beam model described in Chapter 9 and implemented in software in Chapter 12 uses a set 15 complex-valued amplitude and phase coefficients (A,B) to model the sound beam generated by an ultrasonic transducer. Those 15 coefficients are returned by the function gauss_c15. There are no input arguments for gauss_c15. The code listing for gauss_c15 is given in Chapter 12.

When a sound beam passes through an interface, changes in the amplitude of the beam are controlled by the plane wave transmission coefficient as discussed in Chapter 9. The expressions for the plane wave transmission coefficients for a fluid-solid interface are obtained in Appendix D and those expressions are coded in the MATLAB function fluid_solid, whose code listing is given in Chapter 12. The only input argument of the function fluid_solid is the setup structure. This function extracts the necessary material and geometry parameters needed from that structure

and returns the appropriate plane wave transmission coefficient for the incident and transmitted wave types specified in setup.

In pulse-echo angle beam testing a P-wave transducer is placed on a solid wedge instead of being in a fluid. This wedge is then placed in "smooth" contact with the surface of the component being tested, as described in Appendix D. The expressions for the transmission coefficients for such a setup are given in Appendix D. The function smooth_solid, whose code listing is given in section G.8, performs identically to the fluid_solid function but returns instead the appropriate transmission coefficient for the angle beam testing setup.

In performing ultrasonic beam modeling studies, one may want to perform beam calculations at a single frequency for multiple locations in the beam field or synthesize a pulse by performing beam field calculations at many frequencies for a single location or multiple locations. Thus, the setup parameters setup.f, setup.geom.z1, setup.geom.z2, setup.geom.x2, and setup.geom.y2 may be scalars, vectors, or matrices depending on the type of study one wants to perform. The function init_z(setup) decides what the largest size of matrix is present for these parameters and simply outputs an empty array of values of that size. That empty array is then filled with beam field (velocity) values when the actual beam model calculations are performed by a beam model function. This pre-allocation of an empty array is done for efficiency. The code listing for the init_z function is given in Chapter 12.

The function MGbeam(setup) uses the multi-Gaussian beam theory described in Chapter 9 and the specific implementation described in Chapter12 to return the complex-valued velocity amplitude of the transducer sound field generated in a pulse-echo immersion test with input parameters as specified in the setup structure. In performing these calculations MG_beam also uses the functions gauss_c15, fluid_solid, and init_z described previously. The only input argument to the MGbeam function is the setup structure. The outputs of MGBeam are the beam velocity amplitude and a new setup structure that contains updated values for setup.wave.c1, setup.wave.c2, and setup.wave.T12 parameters (see Chapter 12). The code listing for MGbeam is given in Chapter 12.

The function I_MGbeam(setup) uses all the same inputs and functions as MGbeam but instead of the velocity amplitude returned by MGbeam, this function returns a spatial integral of the square of the velocity amplitude, as required by the measurement model for long cylindrical reflectors such as a side-drilled hole (see Chapter 12). Like MGbeam, I_MGbeam also returns a new setup structure that contains updated values for setup.wave.c1, setup.wave.c2, and setup.wave.T12 parameters. The code listing for I_MGbeam is given in Chapter12.

G.4 Flaw Scattering Functions

```
A = A_void(setup);
A = A_crack(setup);
A = A_SDH(setup);
A = A_void_Psep(setup);
A = A_void_Ssep(setup);
A = A_SDH_Psep(setup);
A = A_SDH_Ssep(setup);
A = A_unity(setup);
```

As discussed in Chapters 10, 11 and 12 a component of the vector far-field scattering amplitude of a flaw is a quantity that can be used to characterize the flaw response. This quantity appears explicitly as part of an ultrasonic measurement model when the beam variations over the flaw surface are negligible. The functions A_void(setup), A_crack(setup), and A_SDH(setup) return the pulse-echo far-field scattering amplitude component for a void, crack, and a side-drilled hole, respectively, using the Kirchhoff approximation. The incident waves can either be P-waves or S-waves. Code listings for all three of these functions are given in Chapter 12.

Spherical and cylindrical shaped flaws are the only two geometries where one can obtain exact separation of variables solutions for the far- field scattering amplitude of a flaw in a solid. The functions A_void_Psep(setup) and A_void_Ssep(setup) return the pulse-echo scattering amplitudes for a spherical void for incident P-waves or SV-waves, respectively, using the method of separation of variables. The functions A_SDH_Psep(setup) and A_SDH_Ssep(setup) return the pulse-echo scattering amplitudes for a cylindrical void (side-drilled hole) for P-waves and SV-waves, respectively, when the incident wave direction is perpendicular to the axis of the hole. These two functions use a 2-D separation of variables solution for the hole and convert it to a 3-D scattering amplitude normalized by the length of the hole using the relationship described in Chapter 10. The code listings for all four functions that implement these separation of variables solutions are given in section G.8.

When determining the far-field scattering amplitude of a flaw experimentally, one needs to deconvolve a measured flaw response with all those terms in the measurement model except the far-field scattering amplitude term, as discussed in Chapter 13. Those terms can be generated by measurement model function with the far-field scattering amplitude

response set equal to one at all frequencies. The function A_unity(setup) simply returns these needed values of unity. The code listing for this function is given in Chapter 13.

G.5 Ultrasonic Measurement Modeling Functions

```
y = attenuate(setup);
s = systf(setup);
s = exp_systf(setup);
[Vf, setup] = TG_PE_MM(setup);
[Vi, setup] = SDH_PE_MM(setup);
```

An ultrasonic measurement model requires an ultrasonic beam model and flaw scattering model to account for the beam propagation and scattering effects present in an ultrasonic measurement. Since the beam model functions MGbeam and I_MGbeam predict the beam amplitudes in ideal (lossless) media, material attenuation effects must be included separately. The function attenuate(setup) returns a frequency dependent attenuation factor that allows us to include these losses based on measured attenuation coefficients placed in the setup structure. The code listing for this function is given in Chapter 12.

An ultrasonic measurement model also requires a specification of the system function that characterizes all the electrical and electromechanical components present in the measurement system. For simulation studies, one can use a model-based system function that mimics the behavior of a real (measured) system function. The function systf(setup) is such a function that returns a purely model-based system function determined by specified amplitude, center frequency, and bandwidth parameters in the setup structure. In contrast, the function exp_systf (setup) uses the measured voltage in a reference experiment to determine the system function experimentally. This sampled voltage and the corresponding sampled time axis must be contained in a MAT-file whose name is contained in the setup structure. The function exp_systf then uses these measured values in combination with other parameters of the reference setup contained in the setup structure to return the system function. Code listings for systf and exp_systf are given in Chapter 12.

The function TG_PE_MM(setup) generates the pulse-echo response of a flaw in an immersion setup, as described in Chapter 12, using the Thompson-Gray measurement model. This measurement model is suitable for modeling the response of a flaw when the beam variations over the

flaw surface are negligible, as discussed in Chapter 11. This function returns the output voltage (in the frequency domain) and a new setup structure that contains updated values for setup.wave.c1, setup.wave.c2, and setup.wave.T12 parameters. The code listing for this function is given in Chapter 12.

The function SDH_PE_MM(setup) similarly returns the pulse-echo output voltage (in the frequency domain) for a side-drilled hole in a an immersion setup, as discussed in Chapter 12. This measurement model assumes the beam variations are negligible over the cross-sectional area of the side-drilled hole but accounts for the beam variations over the entire length of the hole. This function also returns a new setup structure that contains updated values for setup.wave.c1, setup.wave.c2, and setup.wave. T12 parameters. The code listing for this function is given in Chapter 12.

G.6 Miscellaneous Functions

```
y= pulserVT(V0, t0, a1, a2, t) ;
y =fresnel_int(x) ;
```

The function pulserVT implements Eq. (2.3) of Chapter 2 which uses the four parameters (V0, t0, a1, a2) to model the open-circuit output voltage of a spike pulser or square wave pulser versus time. The code listing for this function is given in section G.8.The function fresnel_int computes the Fresnel integral, where the argument, x, is the upper limit of that integral. As shown in Chapter 8, this integral appears in modeling rectangular transducers. The code listing for this function is given in section G.8.

G.7 MATLAB Script Examples

```
TG_sphere_example1
TG_sphere_example2
TG_sphere_example3
FBH_example1
SDH_example1
SDH_deconvolve1
```

In Chapters 12 and 13 scripts that implement a number of measurement model examples are given. The script TG_sphere_example1, for example,

uses the Thompson-Gray measurement model to calculate the time domain pulse-echo P-wave response of an on-axis spherical pore interrogated by a 12.7 mm diameter, 5 MHz planar probe through a fluid-solid interface at normal incidence. The code for this script is given in Code Listing 12.11. In this case, a model-based system function is used in the calculations. The script TG_sphere_example2 models the same spherical pore considered in TG_sphere_example1 but uses an experimentally determined system function instead to synthesize the time-domain signal. The code for this script is given in Code Listing 12.13. The script TG_sphere_example3 also calculates the time domain response of the same pore contained in the previous two scripts but replaces the planar probe with a 12.46 mm diameter, 172.9 mm focal length focused probe (both of which values are measured effective parameters) and uses an experimentally determined system function for this probe. The modeled response is then compared to a measured signal. The code for this script is given in Code Listing 12.14.

FBH_example1 is a script that illustrates an example of a measurement model calculation where the beam variations over the face of the flaw must be accounted for. In this case the script calculates the time domain pulse-echo P-wave response of an on-axis #8 flat-bottom hole interrogated by a 12.7 mm diameter, 5 MHz planar probe through a fluid-solid interface at normal incidence and compares the modeled response to an experimentally measured signal. The code for this script is given in Code Listing 12.15.

The script SDH_example1 calculates the pulse-echo P-wave time domain response of an on-axis 1 mm diameter side-drilled hole interrogated by a 12.7 mm diameter, 5 MHz planar probe through a fluid-solid interface at normal incidence. The script uses an experimentally determined system function and compares the modeled response to an experimentally measured signal. The code for the script is given in Code Listing 12.19.

In Chapter 13, the script SDH_deconvolve1 demonstrates how a model-based approach can be used to extract the scattering amplitude of a side-drilled hole from a measured signal. This script uses the side-drilled hole measurement model and the measured pulse-echo P-wave time-domain response of an on-axis 1 mm diameter side-drilled hole interrogated by a 12.7 mm diameter, 5 MHz planar probe through a fluid-solid interface at normal incidence to obtain an experimental far field scattering amplitude for the hole by deconvolution.

This experimental result is plotted versus frequency and compared to the theoretical scattering amplitude calculated by the method of separation of variables. The code for this script is given in Code Listing 13.2.

G.8 Code Listings of Some Supporting Functions

Many of the MATLAB functions that implement the examples discussed in this book are given in the Chapters and Appendices. The previous sections describe where those functions can be found. This section gives MATLAB code listings for functions that are not given elsewhere in the text. All of the MATLAB functions, scripts, and experimental data files are on the web at www.springer.com/978-0-387-49061-8.

Code Listing G.1. The MATLAB function s_space for generating sampled values for use in Fourier analysis.

```
function  y = s_space(xstart, xend, num)
% S_SPACE(XSTART,XEND, NUM) generates num evenly spaced sampled
% values from xstart to (xend - dx), where dx is the sample
% spacing. This is useful in FFT analysis where we generate
% sampled periodic functions. Example: generate 1000
% sampled frequencies from 0 to 100MHz via f =s_space(0,100,1000);
% In this case the last value of f will be 99.9 MHz and the
% sampling interval will be 100/1000 =0.1 MHz.
%
ye =linspace(xstart, xend, num+1);
y=ye(1:num);
```

Code Listing G.2. A circular shift function to use with FFT operations

```
function y = c_shift(x, n)
% C_SHIFT moves the last n components of the vector x
% into the first n component places and shifts the
% remaining components of x to follow those n components,
% i.e. this is a circular shift.  Note: x must be row or column vector
%
[nr,nc]= size(x);
if nr == 1
   len = nc;
   y = [x(len-n+1 : end), x(1:len -n)];
elseif nc == 1
   len = nr;
   y = [x(len-n+1 : end); x(1:len -n)];
```

```
else
   error(' c_shift only works with vectors')
end
```

Code Listing G.3. A time shift function to be used with c_shift to preserve the appropriate time axis values.

```
function  y = t_shift(x, n)
% T-SHIFT is used with the C_SHIFT function to change the time axis
% values appropriately so that the time axis is shifted along with the
% function.
% Example use:  plot(t_shift(t, 100), c_shift(fun, 100))
[nr,nc]= size(x);
dx = x(2) -x(1);
if nr = = 1
   len = nc;
   y = [x(len-n+1 : end)-x(end)-dx+x(1), x(1:len -n)];
elseif nc = = 1
   len = nr;
   y = [x(len-n+1 : end)-x(end)-dx+x(1); x(1:len -n)];
else
   error(' t_shift only works with vectors')
end
```

Code Listing G.4. A low-pass filter for use in Fourier analysis where we have to remove the frequencies above a certain value.

```
function  Vf =lp_filter(f, fstart, fend)
% LP_FILTER(f, fstart, fend) generates a low-pass filter
% which has a value of 1.0 below the frequency value
% fstart and tapers to zero at frequencies above the
% value fend with a cosine function.
% The calling sequence is:
% Vf = lp_filter(f, fstart, fend)

if fend > f(end)
   error( 'fend exceeds max frequency')
end
if fend < fstart
```

```
   error(' fend must be greater than fstart')
end
const = ones(size(f)).*(f < fstart);
taper = cos(pi.*(f-fstart)./(2*(fend-fstart))).*(f >= fstart & f <= fend);
Vf = const + taper;
```

Code Listing G.5. A function that simulates the band-limited behavior of a system function, i.e. where the frequency response is maximum at a particular frequency and has an extent in the frequency domain defined by a bandwidth parameter.

```
function y = system_f (f, amp, fc, bw)
% SYSTEM_F(f, amp, fc, bw) returns the system function as modeled by a
% Gaussian window function of amplitude amp
% centered at frequency fc and with a bandwidth bw defined to
% be the spread in frequency at the half amplitude point in the Gaussian.
% The Gaussian is tapered to zero at frequencies below fc with a
% sine function to guarantee the dc value is always zero.
% For small fc and large bw, this tapering will distort the Gaussian
% The calling sequence for this function is: y =system_f(f, amp, fc, bw);

% compute the 'a' parameter and define system function above and below the
% center frequency
a = sqrt(log(2))/(pi*bw);
s1 = exp(-(2*a*pi*(f - fc)).^2).*(f > fc);
s2 = exp(-(2*a*pi*(f - fc)).^2).*sin(pi*f/(2*fc)).*(f <= fc);
% combine terms to obtain total system function
y = amp*(s1 + s2);
```

Code Listing G.6. A function for calculating the transmission coefficient for refracted P-waves or S-waves at the interface between two solids in smooth (shear stress free) contact. The incident wave must be a P-wave.

```
function T12 = smooth_solid(setup)
% SMOOTH_SOLID(SETUP) computes the P-P (tpp)
% and P-S (tps) transmission coefficients based on velocity ratios
% for two solids in smooth contact. It obtains the necessary input
% parameters from the setup structure and then returns the
% appropriate transmission coefficient
```

```
% Note: If setup.matl.cs1 = 0 the values returned are for a fluid-solid interface.

% get setup parameters
type1 =setup.type1;
type2 =setup.type2;
inc= setup.geom.i_ang;
d1 = setup.matl.d1;
d2 =setup.matl.d2;
cp1 = setup.matl.cp1;
cs1 =setup.matl.cs1;
cp2 =setup.matl.cp2;
cs2 =setup.matl.cs2;

% consistency check (if incident wave in medium 1 is an S-wave
% then can't use this fluid-solid trans. coefficient)

if strcmp(type1, 's')
   error('wrong wave type for medium 1')
end
iang = (inc.*pi)./180;  %change degrees to radians

%calculate sines and cosines of all incident and refracted angles
sinp1 = sin(iang);
cosp1 = sqrt(1-sinp1.^2);
sins1 = (cs1/cp1)*sin(iang);
coss1= sqrt(1-sins1.^2);
sinp2 = (cp2/cp1)*sin(iang);
sins2 =(cs2/cp1)*sin(iang);
   % take into account cosines of refracted angles may be imaginary beyond
   % critical angles
cosp2= (i*sqrt(sinp2.^2 - 1)).*(sinp2 >= 1) + ...
   (sqrt(1 - sinp2.^2)).*(sinp2 < 1);
coss2 = (i*sqrt(sins2.^2 - 1)).*(sins2 >= 1) + ...
   (sqrt(1 - sins2.^2)).*(sins2 < 1);

%calculate transmission coefficients
denom1 = (cp1/cp2).*(cosp2./cosp1).*...
   (4.*((cs1/cp1)^2).*(sins1.*coss1.*sinp1.*cosp1) + ...
   1 - 4.*(sins1.^2).*(coss1.^2));
denom2 = (d2/d1).*(4.*((cs2/cp2)^2).*(sins2.*coss2.*sinp2.*cosp2) ...
                        + 1 - 4.*(sins2.^2).*(coss2.^2));
   denom = denom1 + denom2;

tpp = ((2*cp1/cp2).*(1-2*sins1.^2).*(1-2*sins2.^2))./denom;
tps = -((4*cp1*cs2/(cp2^2)).*sinp2.*cosp2.*(1-2*sins1.^2))./denom;
%select appropriate coefficient
```

```
if strcmp(type2, 'p')
   T12 = tpp;
elseif strcmp(type2, 's')
   T12 = tps;
else
   error('wrong wave type specification')
end
```

Code Listing G.7. A function that uses the separation of variables method to calculate the far field pulse-echo P-wave scattering of a spherical void.

```
function Aout = A_void_Psep(setup)
% A_VOID_PSEP  computes the far field P-wave scattering amplitude, Aout ,
% for a spherical void of radius b in an elastic solid (pulse echo)
% using the method of separation of variables. the only input parameter is
% the setup structure. The complex scattering amplitude, Aout,
% is returned (in mm).
% The calling sequence is:
% Aout = A_void_Psep(setup)

% get input parameters
f=setup.f;
b =setup.flaw.b;
cp = setup.matl.cp2;
cs =setup.matl.cs2;

cr = cp/cs;                % ratio of P- and S- wave speeds
kp = 2000*pi*b*f./cp;      % non-dimensional wave number, P-waves
kp = kp + .0001*(kp == 0);

% break P-wave wave number into two regions: kp < 2 and kp >= 2
indc = find(kp < 2.);
kpd =kp(indc);
ind2 =find(kp >= 2.);
kpu = kp(ind2);
% S-wave wave numbers over same ranges
ksd =cr*kpd;
ksu =cr*kpu;

% use relatively small, fixed number of terms for kp <2
num = 10;
% compute scattering amplitude over kp <2 for sphere of radius b
```

```
A1 =sca(kpd, ksd, num, b);

% use much larger number of terms for kp >= 2
num2= 10 + round(kpu(end));
% compute scattering amplitude over kp >= 2 for sphere of radius b
A2 = sca(kpu,ksu, num2, b);

% combine two ranges
Aout= [A1  A2];
% force zero frequency scattering amplitude to zero exactly
Aout(1) =0;

% subfunction for calculating scattering amplitude with a given number
% of terms in the series. Generally, ten terms should be adequate
% for kp < 2 and a number of terms that is proportional to the max
% kp-value should be adequate for large kp values. However, if the
% max kp-value is very large, the number of terms used here based on this
% value may be too large for the values just above kp =2, resulting in the
% round-offs that cause the function to return NaNs at those lower
% frequencies. This function has been tested up to kp = 90 without problems
% of this sort.

function A = sca(xp,xs, numb, b)
An = zeros(size(xp));       % initialize array of zeros

% First compute the normalized scattering amplitude A/b.

% xp = P- wave number, xs = S- wave number, k is an integer.
% Uses spherical Bessel functions and spherical Hankel functions
% of order k defined by sphJ(k,x), sphH(k, x)

for k = 0:numb
e3 = (2.*k+1).*((k.^2 - k - xs.^2./2).*sphJ(k, xp) +2.*xp.*sphJ(k+1,xp));
e4 = (2.*k+1).*((k-1).*sphJ(k, xp) - xp.*sphJ(k+1, xp));
e32 = -k.*(k+1).*((k-1).*sphH(k, xs) - xs.*sphH(k+1, xs));
e31 = (k.^2 - k - xs.^2./2).*sphH(k, xp) + 2.*xp.*sphH(k+1, xp);
e41 = (k - 1).*sphH(k, xp) -xp.*sphH(k+1, xp);
e42 = -(k.^2 -1 - xs.^2./2).*sphH(k, xs) - xs.*sphH(k+1, xs);
if k == 0
   c = e3./e31;
else
c = (e3.*e42 - e4.*e32)./(e31.*e42 - e41.*e32);
end
An = An + ((-1.)^k)*c;
end
% Now, put the b factor back, insert i/kp term which multiplies entire result
```

```
A = i*b*An./xp;
```

Code Listing G.8. A function that uses the separation of variables method to calculate the far field pulse-echo S-wave scattering of a spherical void.

```
function Aout = A_void_Ssep(setup)
% A_VOID_SSEP  computes the far field SV-wave scattering amplitude, Aout ,
% for a spherical void of radius b in an elastic solid (pulse echo)
% using the method of separation of variables. the only input parameter is
% the setup structure. The complex scattering amplitude, Aout,
% is returned (in mm).
% The calling sequence is:
% Aout = A_void_Ssep(setup)

% get input parameters
f=setup.f;
b =setup.flaw.b;
cp = setup.matl.cp2;
cs =setup.matl.cs2;

cr = cp/cs;                    % ratio of P- and S- wave speeds
ks = 2000*pi*b*f./cs;      % non-dimensional wave number, S-waves
ks = ks + .001*(ks == 0);

% break S-wave wave number into two regions: ks < 5 and ks >= 5
indc = find(ks < 5);
ksd =ks(indc);
ind2 =find(ks >= 5);
ksu = ks(ind2);
% P-wave wave numbers over same ranges
kpd =ksd./cr;
kpu =ksu./cr;

% use relatively small, fixed number of terms for ks <5
num = 10;
% compute scattering amplitude over ks < 5 for sphere of radius b
A1 =sca(kpd, ksd, num, b);

% use much larger number of terms for ks >= 5
num2= 10 + round(ksu(end));
% compute scattering amplitude over ks >= 5 for sphere of radius b
A2 = sca(kpu,ksu, num2, b);
```

```
% combine two ranges
Aout= [A1  A2];
% force zero frequency scattering amplitude to zero exactly
Aout(1) =0;

% subfunction for calculating scattering amplitude with a given number
% of terms in the series. Generally, ten terms should be adequate
% for ks < 5 and a number of terms that is proportional to the max
% ks-value should be adequate for large ks values. However, if the
% max ks-value is very large, the number of terms used here based on this
% value may be too large for the values just above ks=5, resulting in the
% round-offs that cause the function to return NaNs at those lower
% frequencies. this function has been tested up to ks = 50 without problems
% of this sort.

function A = sca(xp,xs, numb, b)
An = zeros(size(xp));       % initialize array of zeros

% First compute the normalized scattering amplitude A/b.

% xp = P- wave number, xs = S- wave number, k is an integer.
% Uses spherical Bessel functions and spherical Hankel functions
% of order k defined by sphJ(k,x), sphH(k, x)

for k = 1:numb
j12 = k.*(k+1).*((k-1).*sphJ(k, xs)-xs.*sphJ(k+1,xs));
h12 = k.*(k+1).*((k-1).*sphH(k, xs) -xs.*sphH(k+1,xs));
h13 =((k.^2-k-xs.^2./2).*sphH(k,xp) +2.*xp.*sphH(k+1, xp));
j41 =((k-1).*sphJ(k, xs) -xs.*sphJ(k+1, xs))./2;
h41 = ((k-1).*sphH(k, xs) -xs.*sphH(k+1, xs))./2;
j42 = (k.^2 -1 -xs.^2./2).*sphJ(k, xs) + xs.*sphJ(k+1, xs);
h42 =((k.^2 -1 -xs.^2./2).*sphH(k, xs) + xs.*sphH(k+1, xs));
h43 = ((k-1).*sphH(k, xp) - xp.*sphH(k+1, xp));

c = (h13.*j42 -j12.*h43 )./(h13.*h42 -h12.*h43) -j41./h41;

An = An + (-1)^k.*((2.*k+1)./2).*c./(-i.*xs);
end

% Now, put the b factor back
A = b*An;
```

Code Listing G.9. A function that uses the separation of variables method to calculate the normalized 3-D far field pulse-echo P-wave scattering amplitude of a cylindrical void, $A_{3D}\left(\mathbf{e}_i^p;-\mathbf{e}_i^p\right)/L$.

```
function Ascatt = A_SDH_Psep(setup)
% A_SDH_PSEP computes the separation of variables solution
% for the 3-D non-dimensional pulse-echo P-wave
% scattering amplitude, Ascatt, for a side-drilled hole
% of radius b (in mm).
% The function returns the scattering amplitude, A, divided
% by the length, L, i.e. Ascatt = A/L so that a value for L
% does not need to be specified. The only input to the function
% is the setup structure. The calling sequence is:
% Ascatt =A_SDH_Psep(setup);

% get setup parameters
f =setup.f;
b = setup.flaw.b;
cp =setup.matl.cp2;
cs = setup.matl.cs2;
%
cr = cp/cs;                % ratio of P- and S- wave speeds
kp = 2000*pi*b*f./cp;      % non-dimensional wave number, P-waves
kp = kp + .0001*(kp == 0);

% break P-wave wave number into two regions: kp < 2 and kp >= 2
indc = find(kp < 2.);
kpd =kp(indc);
ind2 =find(kp >= 2.);
kpu = kp(ind2);
% S-wave wave numbers over same ranges
ksd =cr*kpd;
ksu =cr*kpu;

% use relatively small, fixed number of terms for kp <2
num = 10;
% compute normalized scattering amplitude over kp <2 for sphere of radius b
A1 =sca(kpd, ksd, num);

% use much larger number of terms for kp >= 2
num2= 10 + round(kpu(end));
% compute normalized scattering amplitude over kp >= 2 for sphere of radius b
A2 = sca(kpu,ksu, num2);
% combine two ranges
```

```
Ascatt= [A1  A2];
% force zero frequency normalized scattering amplitude to zero exactly
Ascatt(1) =0;

% subfunction for calculating normalized scattering amplitude for a
% side- drilled hole with a given number of terms in the series.
% Generally, ten terms should be adequate
% for kp < 2 and a number of terms that is proportional to the max
% kp-value should be adequate for large kp values. However, if the
% max kp-value is very large, the number of terms used here based on this
% value may be too large for the values just above kp =2, resulting in the
% round-offs that cause the function to return NaNs at those lower
% frequencies. This function has been tested up to kp = 90 without problems
% of this sort.
% This function uses Hankel functions of type m, order n given by the MATLAB
% function besselh(n, m, x)

function A = sca(kp,ks, numb)
% initialize arrays
An = zeros(size(kp));
Ckp1 =zeros(size(kp));
Ckp2 =zeros(size(kp));
Cks1 =zeros(size(kp));
Dkp1 =zeros(size(kp));
Dkp2 =zeros(size(kp));
Dks1 =zeros(size(kp));
c =zeros(size(kp));

%calculate the series
for n = 0:numb

Ckp1 =(n^2 +n -(ks.^2/2)).*besselh(n, 1,kp) -((2*n).*besselh(n,1,kp)...
 -kp.*besselh(n+1,1,kp));
Ckp2 =(n^2 +n -(ks.^2/2)).*besselh(n, 2,kp) -((2*n).*besselh(n,2,kp)...
 -kp.*besselh(n+1,2,kp));
Cks1 =(n^2 +n -(ks.^2/2)).*besselh(n, 1,ks) -((2*n).*besselh(n,1,ks)...
 -ks.*besselh(n+1,1,ks));
Dkp1 = (n^2 +n).*besselh(n,1,kp) -n*((2*n).*besselh(n,1,kp)...
 -kp.*besselh(n+1,1,kp));
Dkp2 = (n^2 +n).*besselh(n,2,kp) -n*((2*n).*besselh(n,2,kp)...
 -kp.*besselh(n+1,2,kp));
Dks1 = (n^2 +n).*besselh(n,1,ks) -n*((2*n).*besselh(n,1,ks)....
 -ks.*besselh(n+1,1,ks));

if n == 0
   c = 1+ Ckp2./Ckp1;
```

```
else
c = 2*(1+(Ckp2.*Cks1 -Dkp2.*Dks1)./(Ckp1.*Cks1 - Dkp1.*Dks1));
end
An = An + ((-1.)^n)*c;
end
% Now, put the external factor in
A = (i/(2*pi))*An;
```

Code Listing G.10. A function that uses the separation of variables method to calculate the normalized 3-D far field pulse-echo SV-wave scattering amplitude of a cylindrical void, $A_{3D}\left(\mathbf{e}_i^s;-\mathbf{e}_i^s\right)/L$.

```
function Ascatt = A_SDH_Ssep(setup)
% A_SDH_SSEP computes the separation of variables solution
% for the 3-D non-dimensional pulse-echo SV-wave
% scattering amplitude, Ascatt, for a side-drilled hole
% of radius b (in mm).
% The function returns the scattering amplitude, A, divided
% by the length, L, i.e. Ascatt = A/L so that a value for L
% does not need to be specified.The only input to the function
% is the setup structure. The calling sequence is:
% Ascatt =A_SDH_Ssep(setup);
%

% get input parameters
f=setup.f;
b =setup.flaw.b;
cp = setup.matl.cp2;
cs =setup.matl.cs2;

cr = cp/cs;                % ratio of P- and S- wave speeds
ks = 2000*pi*b*f./cs;      % non-dimensional wave number, S-waves
ks = ks + .001*(ks == 0);

% break S-wave wave number into two regions: ks < 5 and ks >= 5
indc = find(ks < 5);
ksd =ks(indc);
ind2 =find(ks >= 5);
ksu = ks(ind2);
% P-wave wave numbers over same ranges
kpd =ksd./cr;
kpu =ksu./cr;
```

```
% use relatively small, fixed number of terms for ks <5
num = 10;
% compute scattering amplitude over ks < 5 for sphere of radius b
A1 =sca(kpd, ksd, num);

% use much larger number of terms for ks >= 5
num2= 10 + round(ksu(end));
% compute scattering amplitude over ks >= 5 for sphere of radius b
A2 = sca(kpu,ksu, num2);

% combine two ranges
Ascatt= [A1  A2];
% force zero frequency scattering amplitude to zero exactly
Ascatt(1) =0;

% subfunction for calculating normalized scattering amplitude for a
% side-drilled hole with a given number of terms in the series.
% Generally, ten terms should be adequate
% for ks < 5 and a number of terms that is proportional to the max
% ks-value should be adequate for large ks values. However, if the
% max ks-value is very large, the number of terms used here based on this
% value may be too large for the values just above ks = 5, resulting in the
% round-offs that cause the function to return NaNs at those lower
% frequencies. This function has been tested up to ks = 50 without
% problems of this sort.
% This function uses Hankel functions of type m, order n defined by the
% MATLAB function besselh(n, m, x)


function A = sca(kp, ks, numb)

% initialize arrays
An = zeros(size(kp));
Cnp1 =zeros(size(kp));
Cns1 =zeros(size(kp));
Cns2 =zeros(size(kp));
Dnp1 =zeros(size(kp));
Dnp2 =zeros(size(kp));
Dns1 =zeros(size(kp));
c =zeros(size(kp));

% Calculate series
for n = 0:numb

Cnp1 =(n^2 +n -(ks.^2/2)).*besselh(n, 1,kp) -((2*n).*besselh(n,1,kp)...
 -kp.*besselh(n+1,1,kp));
```

```
Cns2 =(n^2 +n -(ks.^2/2)).*besselh(n, 2,ks) -((2*n).*besselh(n,2,ks)...
 -ks.*besselh(n+1,2,ks));
Cns1 =(n^2 +n -(ks.^2/2)).*besselh(n, 1,ks) -((2*n).*besselh(n,1,ks)...
 -ks.*besselh(n+1,1,ks));
Dnp1 = (n^2 +n).*besselh(n,1,kp) -n*((2*n).*besselh(n,1,kp)...
 -kp.*besselh(n+1,1,kp));
Dns2 = (n^2 +n).*besselh(n,2,ks) -n*((2*n).*besselh(n,2,ks)...
 -ks.*besselh(n+1,2,ks));
Dns1 = (n^2 +n).*besselh(n,1,ks) -n*((2*n).*besselh(n,1,ks)...
 -ks.*besselh(n+1,1,ks));

if n == 0
   c = 1+ Cns2./Cns1;
else
c = 2*(1+(Cns2.*Cnp1 -Dns2.*Dnp1)./(Cnp1.*Cns1 - Dnp1.*Dns1));
end
An = An + ((-1.)^n)*c;
end
% Now, put the external factor in
A = (i/(2*pi))*An;
```

Code Listing G.11. A function that models the open-circuit voltage output versus time of a pulser.

```
function V = pulserVT(V0, t0, a1, a2, t)
% PULSERVT(V0, t0, a1, a2, t) models the open-circuit voltage of
% a spike or square wave pulser using the four parameters V0, t0,
% a1, and a2. The parameter V0 controls the amplitude and the other
% parameters control the rise and fall characteristics of the pulse.
% The input parameter t is a set of sampled times.
t = t + eps*( t ==0);
Vinf = V0/(1-exp(-a1*t0));
V = -Vinf*(1- exp(-a1*t)).*(t <= t0) -V0*exp(-a2*(t -t0)).*(t > t0);
```

Code Listing G.12. A function that computes the Fresnel integral.

```
function y=fresnel_int(x)
%FRESNEL_INT(X) computes the Fresnel integral defined as the integral
%from t = 0 to t = x of the function exp(i*pi*t^2/2). Uses the approximate
```

```
%expressions given by Abramowitz and Stegun, Handbook of Mathematical
%Functions, Dover Publications, 1965, pp. 301-302.
%The calling sequence is: y = fresnel_int(x)

%separate arguments into positive and negative values, change sign
%of the negative values
xn =-x(x<0);
xp=x(x >=0);

%compute cosine and sine integrals of the negative values, using the
%oddness property of the cosine and sign integrals
[cn,sn] =cs_int(xn);
cn= -cn;
sn = -sn;

%compute cosine and sine integrals of the positive values

[cp, sp]=cs_int(xp);

%combine cosine and sine integrals for positive and negative
%values and return the complex Fresnel integral
ct =[cn cp];
st =[sn sp];
y=ct+i*st;

%CS_INT(XI) calculates approximations of the cosine and sine integrals
%for positive values of xi only(see Abramowitz and Segun reference above)
function [c, s]=cs_int(xi)
f =(1+0.926.*xi)./(2+1.792.*xi +3.104.*xi.^2);      % f function (see ref.)
g=1./(2+4.142.*xi+3.492.*xi.^2+6.67.*xi.^3);        % g function (see ref.)
c=0.5 +f.*sin(pi.*xi.^2./2) -g.*cos(pi.*xi.^2./2);  % cosine integral approx.
s = 0.5 -f.*cos(pi.*xi.^2./2)-g.*sin(pi.*xi.^2./2); % sine integral approx.
```

Index